University of Cincinnati

Date: 6/29/2020

I, Saeed Azad, hereby submit this original work as part of the requirements for the degree of Doctor of Philosophy in Mechanical Engineering.

It is entitled:

Combined Design and Control Optimization of Stochastic Dynamic Systems

Student's name: **Saeed Azad**

This work and its defense approved by:

Committee chair: Michael Alexander-Ramos, Ph.D.

Committee member: Kelly Cohen, Ph.D.

Committee member: Manish Kumar, Ph.D.

Committee member: David Thompson, Ph.D.

36819

Combined Design and Control Optimization of Stochastic Dynamic Systems

by

Saeed Azad

Dissertation submitted to the faculty of the University of Cincinnati in

Partial fulfillment of the requirements for the degree of

Doctor of Philosophy

in

Mechanical Engineering

Committee chair: Michael J. Alexander-Ramos, Ph.D.

Committee member: Kelly Cohen, Ph.D.

Committee member: Manish Kumar, Ph.D.

Committee member: David Thompson, Ph.D.

June 2020

Abstract

Optimization of dynamic engineering systems requires an integrated approach that accounts for the coupling between embodiment design and control system design, simultaneously. Generally known as combined design and control optimization (co-design), these methods offer superior system performance and reduced costs. Despite the widespread use of co-design techniques in the literature, extremely limited research has been done to address the issue of uncertainty in co-design problem formulations. This is problematic as all engineering models contain some level of uncertainty that might negatively affect the system's performance, if overlooked. Accounting for these uncertainties transforms the deterministic problem into a stochastic one, requiring the use of appropriate stochastic optimization approaches. Therefore, this dissertation serves as the starting point for research on stochastic co-design problems when the uncertainty is propagated into the system from random design decision variables and/or problem parameters. Specifically, a simultaneous co-design formulation within multidisciplinary dynamic system design optimization (MDSDO), along with a special class of direct methods, known as direct transcription (DT), are consistently used throughout this research as the basis for uncertainty considerations. Therefore, the stochastic co-design formulations proposed in this dissertation are tailored for the DT-variants of stochastic co-design problems.

Using techniques from robust design optimization (RDO), we develop a novel stochastic co-design formulation within MDSDO, known as robust MDSDO (R-MDSDO). This formulation enables a protective measure against uncertainties by minimizing the sensitivity of the objective function to variations in design decision variables and fixed problem parameters. The robust objective function and inequality constraints are evaluated per usual through their first-order-approximated means and variances, whereas the analysis-type (physics-based) equality constraints are evaluated deterministically at the means of random decision variables and fixed problem parameters. The R-MDSDO formulation is applied to two case studies to assess its effectiveness and implementation challenges.

While RDO techniques focus on minimizing the sensitivity of the objective function to variations in

design, reliability-based design optimization (RBDO) maintains design feasibility under uncertainty. Therefore, a more rigorous evaluation of probabilistic constraints is required to ensure reliability. In this dissertation, we develop a novel stochastic co-design approach based on the principles of RBDO. We implement the reliability analysis through a performance measure approach (PMA) and employ a double-loop most-probable-point (MPP) method, along with a first-order reliability method (FORM) to evaluate the probabilistic constraints. The analysis-type dynamic and algebraic equality constraints are satisfied at the vectors of mean-values of random decision variables, as well as their MPPs. The inner-loop reliability analysis, which is performed for every function evaluation of the outer-loop problem to find MPPs, is implemented using various methods such as advanced mean value (AMV), conjugate mean value (CMV), hybrid mean value (HMV), and general purpose optimizers. This novel formulation is known as the double-loop reliability-based MDSDO (RB-MDSDO).

A major concern in the implementation of the proposed double-loop RB-MDSDO is its high computational cost for the computationally-intensive co-design problems. Specifically, since the reliability analysis is performed for every function evaluation of the outer-loop problem, a more efficient and practical method is desired to pave the way for the widespread adoption of RB-MDSDO approaches for real-world complex systems. Therefore, we use the sequential optimization and reliability assessment (SORA) algorithm to develop a novel single-loop MPP method for RB-MDSDO. In this algorithm, the optimization and reliability assessment steps are decoupled from each other and run sequentially. Similar to the double-loop formulation, FORM is employed to approximate the probabilistic constraints, while the reliability assessment step is formulated using PMA. Due to the decoupled nature of this algorithm, the reliability assessment step entails the satisfaction of the analysis-type dynamic and algebraic equality constraints.

The effectiveness, efficiency, and scalability of the proposed RB-MDSDO formulations are assessed by solving the complex co-design problem of an automotive active-suspension system. Using a linear quarter-car model with a rough surface input, and employing high-fidelity mathematical models for a helical compression spring and a single-tube telescopic damper, we solved the double-loop and single-loop RB-MDSDO co-design problems to identify the optimal spring and damper designs, state trajectories and control trajectories, such that the multiobjective weighted function of the tire deflection, sprung mass acceleration and active control is minimized. By comparing the solutions of the double-loop and the single-loop RB-MDSDO, we concluded that the latter approach offers superior computational efficiency for stochastic co-design problems while preserving accuracy. We note that despite the smaller inner-loop MPP optimization problem in

the double-loop RB-MDSDO, and the advantages of utilizing efficient MPP solver methods such as AMV, CMV, and HMV, the decoupled nature of the single-loop algorithm is more suitable for stochastic co-design problems.

Finally, the proposed formulations are used to address the real-world complex co-design problem of hybrid-electric vehicle (HEV) powertrain under uncertainty. These uncertainties may stem from a variety of sources including imperfect manufacturing processes, measurement errors and/or uncertain operational conditions and may not only impact HEV powertrain component sizing and control strategies, but also overall vehicle performance and cost —both of which are critically-important in the fiercely competitive automotive industry. Therefore, it is important to quantify and minimize the impact of these uncertainties on the integrated system solution of HEVs. In this dissertation, we use R-MDSDO, as well as the RB-MDSDO to explicitly account for random variations within design decision variables and fixed problem parameters for a power-split HEV powertrain. Moderate-fidelity mathematical models of the major components of a power-split HEV powertrain including the engine, electric motor, generator and battery pack are used to identify the optimal plant design variables, state trajectory decision variables, and control trajectory decision variables, such that the vehicle powertrain cost is minimized under uncertainties. The impact of these uncertainties within the HEV powertrain model and problem formulation is then demonstrated by comparing the results from R-MDSDO and RB-MDSDO to those from the associated deterministic co-design problems.

To Mohammad, Shirin, and Kerry

Acknowledgments

First and foremost, I would like to thank my advisor, Dr. Michael J. Alexander-Ramos, for his valuable and constructive advice throughout this research. This dissertation would not have been successful without his enthusiastic encouragement and scientific guidance. I would also like to express my gratitude to my committee members Professor Manish Kumar, Professor David Thomson and Professor Kelly Cohen for their useful critiques of this research.

I would like to thank my colleagues at the University of Cincinnati, particularly, the members of the Integrated Vehicle Design Laboratory (IVDL) for their support. My thanks are extended to the International Partners and Leaders (IPALs) organization at UC International office as my experience at UC was tremendously improved through my involvement with this organization.

I would like to express my very great appreciation to my family, especially my parents Mohammad and Shirin, who have always supported my education and gave me their unconditional love. Finally, I am particularly grateful for the love and support given by Kerry.

Table of Contents

List of Figures

List of Tables

Chapter 1

Introduction

As dynamics—a system's state evolution through time—becomes an increasingly critical trait of engineering systems, it is essential to develop new methods to account for the bi-directional dependency of embodiment design and control system design, such that the issue of inherent uncertainties that prevail over many dynamic engineering systems is also addressed. During the last few years, the effectiveness of conventional design methodologies has been challenged by multiple novel approaches that take into account the coupling between plant design and control system design. Generally referred to as combined design and control optimization, or co-design, these methods have been proven to improve the performance of the dynamic system when the coupling between the embodiment design and control system design is significant [1, 2, 3].

However, nearly all of these approaches in the literature are limited to the co-design of deterministic dynamic systems. This is problematic because without accounting for uncertainty, the deterministic solution would be suboptimal at best, and infeasible at worst (due to the tendency for deterministic solutions to be found near the boundary of the decision space). Thus, in this dissertation, we focus on developing novel formulations that account for the synergistic interactions between plant design and control system design under uncertainty. Accounting for these uncertainties transforms the standard, deterministic co-design problem into a stochastic one, thus requiring appropriate stochastic optimization approaches for its solution. Specifically, a balanced co-design method within the multidisciplinary dynamic system design optimization (MDSDO) approach is consistently used as the basis to:

- Develop a robust co-design approach, referred to as R-MDSDO.
- Develop a reliability-based co-design approach within MDSDO, referred to as RB-MDSDO, using a double-loop MPP formulation.

- Develop a reliability-based co-design approach within MDSDO, referred to as RB-MDSDO, using the single-loop MPP formulation of the sequential optimization and reliability assessment (SORA).

These formulations are applied to a wide range of problems to assess their effectiveness and scalability. Specifically, the effectiveness of R-MDSDO is assessed through a simple, mathematical co-design problem as well as a more complex problem involving the co-design of a hang glider. Similarly, the effectiveness of the double-loop RB-MDSDO formulation is assessed using a rather complex automotive active suspension co-design problem, while the effectiveness of the SORA-based RB-MDSDO formulation is assessed using progressively complex co-design examples, starting with a Van der Pol oscillator and then moving on to the hang glider and automotive active suspension problems again. Finally, a hybrid-electric vehicle (HEV) powertrain co-design problem is used to assess the scalability of both R-MDSDO an RB-MDSDO in stochastic co-design. The remainder of this section is focused on the description of general deterministic co-design approaches and various methods used for their solution in the literature.

1.1 Deterministic Co-design Methods

Adopting an integrated approach in the optimization of dynamic engineering systems—one that accounts for the coupling between physical plant and control system disciplines—offers clear advantages. A system-level optimal solution for the optimal plant design variables, state trajectory decision variables and control trajectory decision variables can be obtained such that the overall system's performance is improved. Figure 1.1 shows various strategies that could be employed for a plant and controller optimization problem. Note that in this figure, $\mathbf{d}_p$ is the vector of plant design variables and $\mathbf{u}$ is the vector of control trajectory decision variables. Generally, these problems can be solved using sequential, iterative, nested, and simultaneous approaches [4, 5].

Sequential design approaches generally refer to the legacy design methods where the plant design is followed by the design of the control artifact. In the conventional single-loop sequential design approaches, also known as 'single pass', the plant is designed first, and then the control system is designed without any modifications to the plant design. An iterative sequential design attempts to repeatedly find an optimal design solution and an optimal controller until convergence [6, 7, 8, 9]. While these legacy design approaches are optimal with respect to every individual discipline, they cannot generate a system-level optimal solution since the synergistic interactions between plant and control disciplines are lost in the sequential iterative or

single pass procedures [1, 2, 4, 10, 11]. In the nested approach, the objective function is optimized over a set of feasible design variables in an outer loop, while an inner loop solves the optimal control problem at every given deign [2, 4, 11, 12]. Although nested optimization guarantees a system-level optimal solution, the double-loop nature of this algorithm incurs high computational cost when a closed-form optimal control solution method such as linear quadratic regulator (LQR) cannot be employed (for instance due to plant constraints [10]).

The simultaneous solution strategy optimizes the plant design, state trajectory, and control trajectory decision variables within the same optimization formulation and guarantees a system-level optimal solution. Since high computational efficiency can be achieved by employing a simultaneous approach for co-design of complex dynamic systems [13, 1, 2, 14], in this dissertation, we employ a generalized, simultaneous, optimization method that can be used to solve co-design problems.

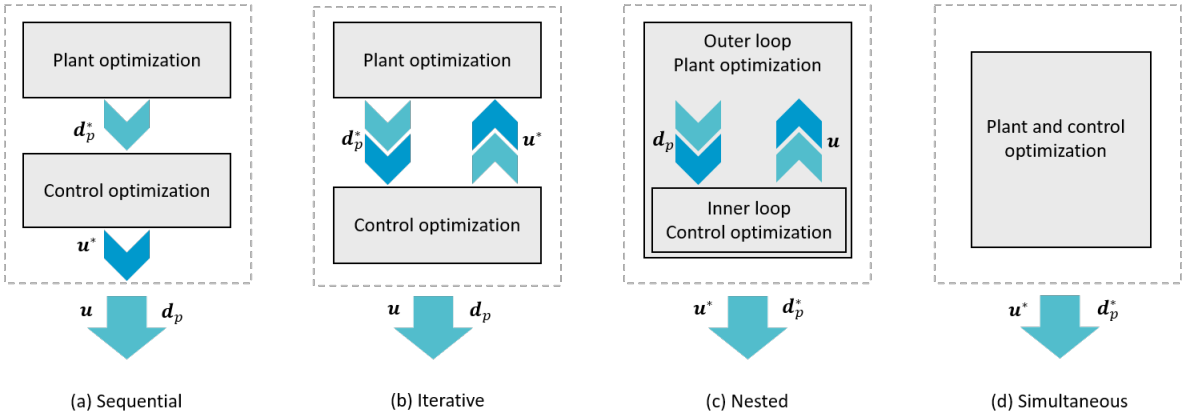

Figure 1.1: Plant and controller solution strategies, $\mathbf{d}_p$: plant design decision variable $\mathbf{u}$: control trajectory decision variable *: optimal decision variables.

1.2 Research Objectives

Deterministic co-design problem formulations have been extensively studied in the literature and their application, implementation and corresponding challenges are well-established. However, an issue that has not been addressed in the co-design literature is the impact of inherent uncertainties within a dynamic system on its integrated design solution. Therefore, as more researchers investigate the application of co-design techniques to large-scale and complex dynamic systems, it is necessary to develop formulations that account

for uncertainties within these systems. The integrated solution of stochastic co-design techniques requires formulations that (i) minimize the sensitivity of the solution to uncertainties in design decision variables and fixed problem parameters, and (ii) satisfy the probabilistic inequality constraints with a given probability of success. Therefore, in this dissertation, we initiate the research on stochastic co-design strategies. By employing a simultaneous co-design technique within the balanced formulation of MDSDO, we develop novel formulations that explicitly account for uncertainties within the system and its problem formulation. These uncertainties may be of aleatory or epistemic types. Aleatory uncertainty includes phenomena such as uncertain operating conditions or imperfect manufacturing processes, while epistemic uncertainty stems from the lack of knowledge about a system, such as simplifications in model development. The proposed formulations specifically account for aleatory uncertainties within random plant design decision variables and fixed problem parameters. Using the principles of robust design optimization (RDO) and reliability-based design optimization (RBDO), we define the main objectives of this dissertation as:

- Developing a robust MDSDO (R-MDSDO) formulation for stochastic dynamic systems.
- Developing double-loop and singe-loop reliability-based MDSDO (RB-MDSDO) formulations for co-design of stochastic dynamic systems and selecting the most efficient yet reasonably accurate approach for complex co-design problems.
- Investigating the impact and scalability of uncertainties on the real-world, complex co-design problem of a power-split HEV powertrains using the proposed R-MDSDO and RB-MDSDO.

Several implementation issues, including the high computational cost of calculating the gradient information in R-MDSDO problems, the satisfaction of the probabilistic analysis-type equality constraints under uncertainty, and the challenge of trajectory-based performance measure functions in RB-MDSDO approaches will be discussed in future chapters. The double-loop and single-loop RB-MDSDO formulations will be applied to the complex co-design problem of an automotive active-suspension system, and their efficiency and accuracy will be compared for various most-probable-point (MPP) optimization subproblems and solvers. Finally, the scalability and effectiveness of the proposed formulations will be further demonstrated by solving a power-split HEV powertrain co-design problem with moderate-fidelity mathematical models for the engine, electric motor, generator, and battery pack, using R-MDSDO and RB-MDSDO.

1.3 Summary and Overview

In this chapter, we introduced the general description of deterministic co-design problems and concluded that due to its computational efficiency for complex dynamic systems, the simultaneous co-design problem formulation is the most appropriate approach for the purposes of this study. Then, the main objectives of this dissertation were listed—focusing on the development of stochastic co-design formulations and ultimately investigating their impact and scalability on real-world co-design problems such as power-split HEV powertrain co-design. The remainder of this dissertation is organized in the following manner:

Chapter 2 briefly describes MDSDO and how to formulate a general deterministic co-design problem within this optimization framework. This chapter also discusses the traditional RDO and RBDO problem formulations for static design optimization problems, as well as their corresponding formulations in the presence of equality constraints. Chapter 3 describes how the RDO approach is integrated into the MDSDO problem formulation to introduce the novel R-MDSDO problem formulation. The proposed robust co-design formulation is then applied to two case studies including a mathematical stochastic co-design problem and a hang glider stochastic co-design problem. Chapter 4 introduces the problem formulation for the double-loop MPP implementation of RB-MDSDO. This formulation employs a FORM approximation within a performance measure approach (PMA). The proposed double-loop algorithm is then applied to solve the complex co-design problem of an automotive active-suspension, the mathematical model of which is also included in this chapter. Chapter 5 introduces a single-loop MPP formulation using the sequential optimization and reliability assessment (SORA) algorithm. A general formulation for the traditional SORA algorithm is described and then SORA is extended to account for equality constraints. The implementation challenges of the proposed single-loop RB-MDSDO are identified by solving two small-scale case studies, including a mathematical application as well as the hang glider co-design application again. In addition, the automotive active-suspension co-design problem is again solved but through the single-loop RB-MDSDO. and the results are compared with that of the double-loop RB-MDSDO to assess which algorithm is the most efficient yet reasonably accurate within RB-MDSDO. Chapter 6 describes the mathematical model for the power-split HEV powertrain, including the propulsion architecture and its major components, the cost models associated with each component, and the co-design problem formulations within the deterministic MDSDO as well as R-MDSDO and RB-MDSDO. The results from the implementation of these formulations are also described in Chapter 6. Finally, conclusions and future directions of this research are discussed

in Chapter 7.

Chapter 2

Background

Complex engineering systems involve the interaction of multiple disciplines and energy domains. Additionally, these systems are often dynamic and stochastic in nature, and so their system-level optimal solution requires an approach that accounts for the coupling between embodiment design and control system design under uncertainty. Combined design and control optimization, also known as co-design, is generally used to find the integrated system-level optimal solution of these dynamic systems. Robust design optimization (RDO) and reliability-based design optimization (RBDO), on the other hand, are generally used to find solutions for stochastic design optimization problems. Therefore, in this chapter, we first introduce a balanced co-design approach within multidisciplinary dynamic system design optimization (MDSDO). Then, general formulations for traditional RDO and RBDO problems, along with those for RDO and RBDO problems containing stochastic equality constraints, reliability-based design optimization (RBDO), and RBDO with equality constraints are introduced.

2.1 Co-design in MDSDO

Integration of plant design and control strategy decisions in optimization problem formulations, also known as co-design, has gained momentum as the inherent coupling between these disciplines has been proven to be significant [4, 7, 15, 16]. By employing techniques from multidisciplinary design optimization and optimal control theory, MDSDO integrates the physical plant design and control system design to achieve a superior system performance [10]. In its most common form, a co-design problem for an active dynamic system can be solved within MDSDO using a simultaneous approach [10]. The general simultaneous problem formulation includes vectors of design decision variables $\mathbf{d}$, state trajectory decision variables $\mathbf{x}(t)$, control trajectory decision variables $\mathbf{u}(t)$, and fixed problem parameters $\mathbf{p}$. The objective function ϕ

is minimized subject to the vector of inequality constraints $\mathbf{g}(\cdot)$, algebraic equality constraints $\mathbf{h}(\cdot)$, and dynamic system equality constraints $\dot{\mathbf{x}}(t) - \mathbf{f}(\mathbf{d}, \mathbf{x}(t), \mathbf{u}(t), t; \mathbf{p}) = \mathbf{0}$. Depending on the problem type, initial and final times and conditions (e.g. t_0, t_f, $\mathbf{x}(t_0)$, $\mathbf{x}(t_f)$) could also be decision variables. Therefore, the nominal simultaneous problem formulation can be written as [10]:

$$\begin{aligned} &\min_{\mathbf{d}, \mathbf{x}(t), \mathbf{u}(t)} && \phi(\mathbf{d}, \mathbf{x}(t), \mathbf{u}(t), t; \mathbf{p}) \\ &\text{subject to} \\ & && \mathbf{g}(\mathbf{d}, \mathbf{x}(t), \mathbf{u}(t), t; \mathbf{p}) \leq \mathbf{0} \\ & && \mathbf{h}(\mathbf{d}, \mathbf{x}(t), \mathbf{u}(t), t; \mathbf{p}) = \mathbf{0} \\ & && \dot{\mathbf{x}}(t) - \mathbf{f}(\mathbf{d}, \mathbf{x}(t), \mathbf{u}(t), t; \mathbf{p}) = \mathbf{0} \end{aligned} \tag{2.1}$$

Since the above formulation entails both static and continuous-time-dependent variables, it requires the use of numerical methods such as direct transcription (DT) to solve the problem. In DT, the infinite-dimensional problem is transcribed into a finite-dimensional nonlinear programming (NLP) formulation through time discretization [10, 12]. The transcribed version of Eqn. (2.1) can be written as:

$$\begin{aligned} &\min_{\mathbf{d}, \mathbf{X}, \mathbf{U}} && \phi(\mathbf{d}, \mathbf{X}, \mathbf{U}; \mathbf{p}) \\ &\text{subject to} \\ & && \mathbf{g}(\mathbf{d}, \mathbf{X}, \mathbf{U}; \mathbf{p}) \leq \mathbf{0} \\ & && \mathbf{h}(\mathbf{d}, \mathbf{X}, \mathbf{U}; \mathbf{p}) = \mathbf{0} \\ & && \boldsymbol{\zeta}(\mathbf{d}, \mathbf{X}, \mathbf{U}; \mathbf{p}) = \mathbf{0} \end{aligned} \tag{2.2}$$

where $\mathbf{X}$ is the matrix of discretized state trajectory decision variables, $\mathbf{U}$ is the matrix of discretized control trajectory decision variables, and $\boldsymbol{\zeta}$ is the vector of discretized dynamic constraints.

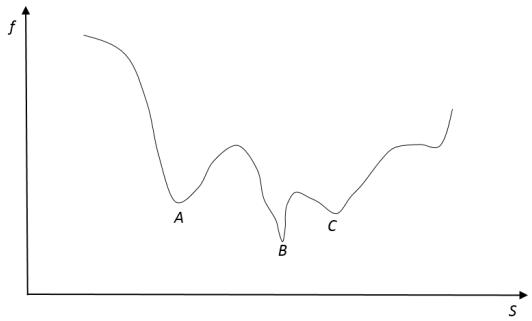

Figure 2.1: Robustness in the objective function [22]

2.2 RDO

A significant body of research has been carried out to quantify and diminish the impact of uncertainty on system's performance. Generally, these methods can be classified into robust design optimization (RDO) and reliability-based design optimization (RBDO). In RDO, we attempt to optimize the performance about the mean-value while minimizing its sensitivity to random parameters [17]. RDO enables a protective measure against uncertainty in problem parameters, without eliminating the causes of this variability. Several methods have been proposed to formulate an RDO approach in the literature [18, 19, 20, 21]. Minimizing the sensitivity of the objective function or constraints to variations in design is usually attained by including the standard deviation of the response, along with its mean in the objective function[17]. Here, we demonstrate the application of RDO principles for a simple optimization problem,

$$\begin{aligned} \min_{\mathbf{s}} \quad & f(\mathbf{s}) \\ \text{subject to} \quad & g_i(\mathbf{s}) \leq 0 \quad i = 1,...,n_g \\ & h_j(\mathbf{s}) = 0 \quad j = 1,...,n_h \end{aligned} \tag{2.3}$$

where $\mathbf{s} \in R^{n_s}$ is the vector of system design variables with n_s being the number of design variables. Inequality constraints are described by $g_i(\mathbf{s})$ and equality constraints are expressed by $h_j(\mathbf{s})$. n_g and n_h refer to the number of inequality and equality constraints, respectively.

2.2.1 Traditional RDO

Without any loss of generality, we assume that the source of uncertainty is from dependent random design variables with known variances and covariances. An RDO approach focuses on reducing the sensitivity of the objective function with respect to variations in random design parameters. Figure 2.1 illustrates the importance of robustness in problem formulation. Denoting the objective function by f, it is evident that point B is the minimum. However, if there is uncertainty introduced among the original design variables, they become random design variables, denoted by $\mathbf{S}$. From the figure, it is clear that any small variation in each design variable S at point B results in a drastic change in the value of the objective function f, and so this would not lead to a robust design solution. We can account for this variation by reformulating the objective function in terms of its expected value and standard deviation.

Figure 2.2: Reduced feasibility of the design space under RDO [23]

In RDO, inequality constraints must be satisfied within a given constraint shift index k_i, chosen by the designer. This constant reflects the probability that a fluctuation will be feasible [24]. This procedure reduces the feasible region of the design (Fig. 2.2). Using linear statistical analysis, Parkinson et al. [24] proposed an approach to maintain feasibility of the design with respect to a given constraint. When a design solution is very close to the boundaries of a constraint, we must ensure that variations in design do not cause infeasibility. This can be performed by increasing the value of the constraint by the amount of functional variation. The traditional RDO problem formulation without equality constraints can be formulated as

$$\begin{aligned} \min_{\mu_S} \quad & \mu_f + \sigma_f^2 \\ \text{subject to} \quad & \mu_{g,i} + k_i \sigma_{g,i} \leq 0 \quad i = 1, \ldots, n_g \end{aligned} \tag{2.4}$$

where μ_f is the expected value of the objective function f, $\mu_{g,i}$ is the expected value of the i^{th} inequality constraint, σ_f^2 is the variance of the objective function f and $\sigma_{g,i}$ is the standard deviation of the i^{th} inequality constraint. Using a first-order Taylor series approximation [25], we have

$$\mu_f = f(\boldsymbol{\mu}_S) \tag{2.5}$$

$$\mu_g = g(\boldsymbol{\mu}_S) \tag{2.6}$$

$$\sigma_f^2 = \sum_{i=1}^{n_s} [\frac{\partial f}{\partial S_i}\big|_{\mathbf{S}_i=\boldsymbol{\mu}_{S_i}} \sigma_{S_i}]^2 + \sum_{i=1}^{n_s}\sum_{j=1,i\neq j}^{n_s} \frac{\partial f}{\partial S_i}\big|_{\mathbf{S}_i=\boldsymbol{\mu}_{S_i}} \frac{\partial f}{\partial S_j}\big|_{\mathbf{S}_j=\boldsymbol{\mu}_{S_j}} Cov(S_i,S_j) \tag{2.7}$$

$$\sigma_g^2 = \sum_{i=1}^{n_s} [\frac{\partial g}{\partial S_i}\big|_{\mathbf{S}_i=\boldsymbol{\mu}_{S_i}} \sigma_{S_i}]^2 + \sum_{i=1}^{n_s}\sum_{j=1,i\neq j}^{n_s} \frac{\partial g}{\partial S_i}\big|_{\mathbf{S}_i=\boldsymbol{\mu}_{S_i}} \frac{\partial g}{\partial S_j}\big|_{\mathbf{S}_j=\boldsymbol{\mu}_{S_j}} Cov(S_i,S_j) \tag{2.8}$$

where $\mathbf{S}$ is the vector of random design variables. The total number of design variables are denoted by n_s. The standard deviation of f and g can simply be calculated through: $\sigma = \sqrt{\sigma^2}$. Including these terms (μ_f, σ_f) in the objective function results in a multi-objective optimization problem that requires weight coefficients and normalization, according to problem type. The issue of weighting factors and normalization is outside the scope of this study and interested readers are referred to [26, 27] for further details.

2.2.2 RDO with Equality Constraints

Equality constraints create a major challenge under uncertainty and have not been studied as extensively as inequality constraints. With the exception of a category of constraints mentioned below, strict satisfaction of equality constraints can generally not be guaranteed. Mattson and Messac classified equality constraint in RDO into two categories: (i) those that cannot be satisfied because of the inherent uncertainty in RDO problems (design-type), and (ii) those that must be satisfied regardless of the underlying uncertainty in the problem (analysis-type) [28]. Generally, the nature of the existing random variables in the equality constraints plays a significant role in determining their category and consequently, their formulation in the context of RDO. Authors in Ref.[23] and Ref.[28] presented a comprehensive guideline to distinguish and formulate each type of equality constraint. Rangavajhala et al. [23] suggests that Type (i) equality constraints should be constrained at their mean to ensure that they remain as close as possible to zero and

that their standard deviations remain minimum. An alternative approach to handling design-type constraints is to relax them into a pair of inequality constraints [23]. In this study, we assume that Type (i) equality constrains are already included in the vector of inequality constraints $\mathbf{g}(\cdot)$ and thus, all remaining equality constraints $\mathbf{h}(\cdot)$ are of analysis-type (Type(ii)).

Type (ii) equality constraints, also called analysis constraints, generally describe the physical laws of nature or dynamics of a system and must be satisfied regardless of uncertainty. Therefore, these constraints can be posed in the RDO framework as deterministic equality constraints, evaluated at the mean values of random variables. The mathematical notation of analysis constraints can be shown as:

$$\mathbf{h}(\boldsymbol{\mu}_S) = \mathbf{0} \tag{2.9}$$

2.3 RBDO

While RDO focuses on improving the quality of a product, reliability-based design optimization (RBDO) attempts to maintain the design feasibility under uncertainty [29] and meet specific probabilistic targets for the objective and constraints [17]. A performance measure approach (PMA)—which is known to be more robust and efficient compared to the reliability index approach (RIA)—is used to formulate the reliability analysis optimization problem within RBDO. A first-order reliability method (FORM) is then employed to approximate the probabilistic constraint and find the most probable point (MPP) corresponding to the target reliability level of the performance measure function. The analysis-type (physics-based) dynamic equality constraints are satisfied at the vectors of the mean-value of uncertain design variables, as well as the MPPs. We start by introducing the traditional RBDO problem using PMA formulation, along with FORM approximation..

2.3.1 Traditional RBDO using FORM & PMA

Reliability is defined as the probability that the vector of random design variables $\mathbf{S}$ is within the safe region. This definition is equivalent to the probability that the performance function $g_i(\mathbf{S})$ is less than zero, i.e. $Pr\{g_i(\mathbf{S}) \leq 0\}$ (Fig. 2.3). A general RBDO problem formulation for a simple optimization problem similar to Eqn. (2.3) but without equality constraints includes the deterministic vector of design variables

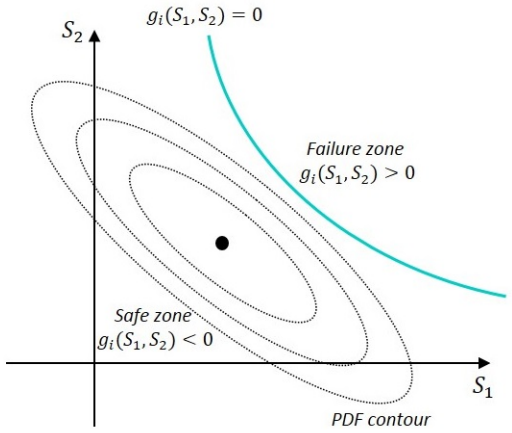

Figure 2.3: Performance measure function in the original uncertain space

$\boldsymbol{\mu}_S \in R^{n_s}$ and the random vector $\mathbf{S} \in R^{n_r}$. The probabilistic constraint is described by the performance function $g_i(\mathbf{S})$. The general RBDO problem without equality constraints can be described as [30]

$$\begin{aligned} \min_{\boldsymbol{\mu}_S} \quad & f(\boldsymbol{\mu}_S) \\ \text{subject to} \quad & Pr\{g_i(\mathbf{S}) \leq 0\} \geq \alpha_i, \quad i = 1, ..., n_g \end{aligned} \tag{2.10}$$

where f is the objective function, $Pr\{\cdot\}$ denotes the probability of success, α_i is the targeted reliability of the i^{th} probabilistic inequality constraint, and n_g is the total number of probabilistic inequality constraints. Next, we can characterize the success of the performance function $g_i(\mathbf{S})$ using the cumulative distribution function $F_{g_i}(0)$ of the i^{th} probabilistic inequality constraint as [30]:

$$Pr\{g_i(\mathbf{S}) \leq 0\} = F_{g_i}(0) \geq \alpha_i \tag{2.11}$$

where this probability can be evaluated using the joint probability density function of all the random variables

$$F_{g_i}(0) = \int_{g_i(\mathbf{S}) \leq 0} ... \int f_{\mathbf{S}}(\mathbf{S}) dS_1 ... dS_{n_r}, \quad i = 1, ..., n_g \tag{2.12}$$

A key step in RBDO methods is to ease the computational difficulties associated with the calculation of

this equation through simplification of the integrand, as well as the performance measure function. Several approaches have been proposed to evaluate this equation, including sampling techniques, local expansion, most probable point (MPP), functional expansion and numerical integration methods [31]. Despite the advantages of sampling techniques such as Monte Carlo Simulation (MCS) in easy implementation and solution accuracy, their computational time becomes a significant challenge as the number of random variables increases—making them impractical for many real-world engineering applications [25, 32]. Local expansion methods employ a first-order second moment (FOSM) approach to approximate the probabilistic constraint at the design point $\boldsymbol{\mu}_S$; however their solution can be highly inaccurate. Numerical integration methods [33] are generally based on the idea that the first few moments of a random variable adequately describe the complete probability density function of that variable. These methods, along with functional expansion methods [34] are more useful for highly nonlinear problems; however, they suffer from the 'curse of dimensionality'. The MPP method, on the other hand, can approximate the performance function $g_i(\mathbf{S})$ through a first-order or second-order Taylor series expansion at the most probable point of failure for this function. While this requires the solution of an additional optimization subproblem to find the MPP, they are often faster than sampling, numerical integration, and functional expansion methods and are more accurate than local expansion techniques. In addition, the MPP method is the only known technique in the literature that can handle probabilistic equality constraints, a fact that is quite useful given that all of the problems in our work will at least require probabilistic dynamic system equality constraints to be satisfied.. Therefore, MPP methods are used exclusively to approximate the integral of Eqn. (2.12) in this work.

The optimization subproblem in the MPP approach can be formulated using a reliability index approach (RIA) or a performance measure approach (PMA). In RIA, the probabilistic constraint is written in terms of the reliability index β [35], while in PMA, the probabilistic constraint is replaced with its deterministic counterpart $g_i(\mathbf{s}^*_{MPP,i})$ evaluated at the MPP $\mathbf{s}^*_{MPP,i}$ through inverse reliability analysis [36, 37]. It is known that the PMA is inherently more robust and efficient in evaluating inactive probabilistic constraints compared to RIA [37, 38, 35]. The PMA is further developed to address any lingering issues of instability and slow convergence, resulting in improved methods such as advanced mean value (AMV) [39, 40], conjugate mean value (CMV) [35, 36], and hybrid mean value (HMV) [36, 41].

Evaluating Eqn. (2.12) using either MPP approach generally involves two steps. First, the random variables in $\mathbf{S}$ must be transformed into the standard normal random space $\mathbf{s}_{u,i}$ so that its PDF contours are symmetric, thus improving the overall numerical approximation of Eqn. (2.12). This is accomplished

through the Rosenblatt transformation [47]

$$\mathbf{s}_{u,i} = \Phi_{cdf}^{-1}[F_{\mathbf{s}}(\mathbf{s})] \tag{2.13}$$

where Φ_{cdf}^{-1} is the inverse cumulative distribution function of the standard normal distribution. The second step is to approximate $g_i(\mathbf{S})$ through a first-order reliability method (FORM) [42, 43, 44] or a second-order reliability method (SORM)[44, 45, 46]. Generally, FORM predicts the probability of success with an accuracy that is sufficient for design applications. These local approximations are constructed around the MPP itself, which is the point on the target reliability surfaces $\mathbf{s}_{u,i}^*(\beta = \beta_{t_i})$ that maximizes $g_i(\mathbf{s}_{u,i})$ (Fig. 2.4).

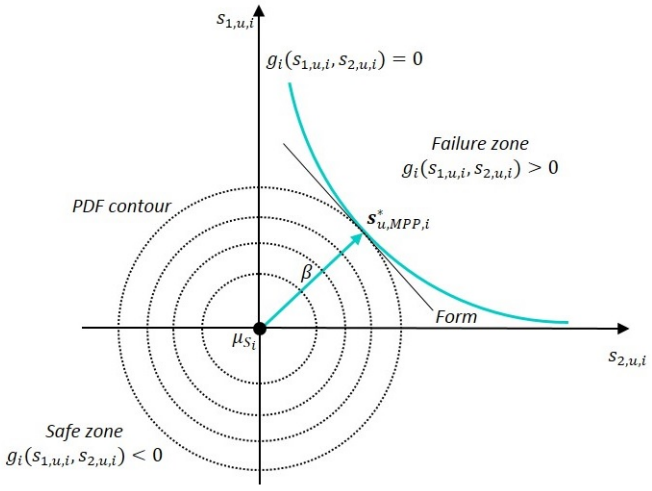

Figure 2.4: Performance measure function in the standard normal space

The traditional double-loop MPP algorithm solves an inner-loop reliability analysis problem (the MPP subproblem) in the standard normal space that is embedded within an outer-loop design optimization problem in the original random space. The outer-loop problem formulation using PMA that corresponds to the general RBDO formulation of Eqn. (2.10) is simply

$$\begin{aligned} \min_{\boldsymbol{\mu}_S} \quad & f(\boldsymbol{\mu}_S) \\ \text{s.t.} \quad & g_i(\mathbf{s}^*_{MPP,i}) \leq 0, \qquad i = 1, \ldots, n_g \end{aligned} \tag{2.14}$$

where, $\mathbf{s}^*_{MPP,i}$ denotes the MPPs associated with $\boldsymbol{\mu}_S$. The MPPs are obtained by solving the following inner-loop problem:

$$\begin{aligned} \min_{\mathbf{s_{u,i}}} \quad & -g_i(\mathbf{s}_{u,i}) \\ \text{s.t.} \quad & \left\|\mathbf{s}_{u,i}\right\| - \beta_{t_i} = 0 \\ \text{where} \quad & \beta_{t_i} = \Phi^{-1}_{cdf}(\alpha_i) \end{aligned} \tag{2.15}$$

Note that general optimization algorithms can be used to solve the MPP subproblem in Eqn. (2.15). However, more efficient methods such as AMV, CMV, and HMV are of particular interest due to the high computational costs of RBDO problems in general. Here, we briefly introduce these algorithms [36, 30]:

Advanced Mean Value AMV is a simple and efficient approach that can be used to solve the MPP optimization problem in PMA. To implement the first-order AMV method, the first iteration must generate an estimate $\mathbf{s}^*_{u_{MV,i}}$ of the MPP based on the mean-value (MV) method using $\mathbf{s}_{u_i} = 0$ as a starting point:

$$\mathbf{s}^*_{u_{MV,i}} = \beta_{t_i}\mathbf{n}(\mathbf{0}), \;\; \mathbf{n}(\mathbf{0}) = -\frac{\nabla g_i(\mathbf{0})}{\|\nabla g_i(\mathbf{0})\|} \tag{2.16}$$

In the above, $\mathbf{n}(\mathbf{0})$ is the normalized steepest descent direction at the mean value, which must be updated in the following iterations to predict the MPP based on the AMV method:

$$\begin{aligned} &\mathbf{s}^{(1)}_{u_{AMV,i}} = \mathbf{s}^*_{u_{MV,i}}, \;\; \mathbf{s}^{(k+1)}_{u_{AMV,i}} = \beta_{t_i}\mathbf{n}(\mathbf{s}^{(k)}_{u_{AMV,i}}) \\ &\mathbf{n}(\mathbf{s}^{(k)}_{u_{AMV,i}}) = -\frac{\nabla g_i(\mathbf{s}^{(k)}_{u_{AMV,i}})}{\|\nabla g_i(\mathbf{s}^{(k)}_{u_{AMV,i}})\|} \end{aligned} \tag{2.17}$$

Here, $\mathbf{n}(\mathbf{s}^{(k)}_{u_{AMV,i}})$ is the steepest descent direction at the current estimate $\mathbf{s}^{(k)}_{u_{AMV,i}}$ of the MPP using the AMV method during the k^{th} iteration. Note that this algorithm behaves well for a convex performance measure function, however, it exhibits numerical instability and inefficiency for concave functions.

Conjugate Mean Value To improve the rate of convergence and stability for concave functions, one can use the current, as well as the previous MPP information. CMV combines these information with equal weight to improve the search direction, such that it is directed towards the diagonal of the last three consec-

utive steepest descent directions:

$$\begin{aligned}
&\mathbf{s}_{u_{CMV,i}}^{(0)} = \mathbf{0},\ \mathbf{s}_{u_{CMV,i}}^{(1)} = \mathbf{s}_{u_{AMV,i}}^{(1)},\ \mathbf{s}_{u_{CMV,i}}^{(2)} = \mathbf{s}_{u_{AMV,i}}^{(2)} \\
&\mathbf{s}_{u_{CMV,i}}^{(k+1)} = \beta_{t_i} \frac{\mathbf{n}(\mathbf{s}_{u_{CMV,i}}^{(k)}) + \mathbf{n}(\mathbf{s}_{u_{CMV,i}}^{(k-1)}) + \mathbf{n}(\mathbf{s}_{u_{CMV,i}}^{(k-2)})}{\|\mathbf{n}(\mathbf{s}_{u_{CMV,i}}^{(k)}) + \mathbf{n}(\mathbf{s}_{u_{CMV,i}}^{(k-1)}) + \mathbf{n}(\mathbf{s}_{u_{CMV,i}}^{(k-2)})\|},\ \ k \geq 2 \\
&\mathbf{n}(\mathbf{s}_{u_{CMV,i}}^{(k)}) = -\frac{\nabla g_i(\mathbf{s}_{u_{CMV,i}}^{(k)})}{\|\nabla g_i(\mathbf{s}_{u_{CMV,i}}^{(k)})\|}
\end{aligned} \tag{2.18}$$

Hybrid Mean Value The HMV approach identifies the type of the performance measure function before formulating the search direction. The function-type criteria employs the steepest descent direction at three consecutive iterations:

$$\begin{aligned}
&\xi^{(k+1)} = (\mathbf{n}^{(k+1)} - \mathbf{n}^{(k)}).(\mathbf{n}^{(k)} - \mathbf{n}^{(k-1)}) \\
&sign(\xi^{(k+1)}) \begin{cases} > 0 = \text{ Convex at } \mathbf{s}_{u_{HMV,i}}^{(k+1)} \text{ w.r.t } \boldsymbol{\mu}_S \\ \leq 0 = \text{ Concave at } \mathbf{s}_{u_{HMV,i}}^{(k+1)} \text{ w.r.t } \boldsymbol{\mu}_S \end{cases}
\end{aligned} \tag{2.19}$$

In the above, $\xi^{(k+1)}$ is the performance function-type criterion and $\mathbf{n}^{(k)}$ is the steepest descent direction for a performance measure function at $\mathbf{s}_{u_{HMV,i}}^{(k)}$. Once the type of the performance measure function is is identified, AMV and CMV can be adaptively used for the MPP search. If the performance function type is convex or $k < 3$, the MPP is calculated using the AMV method. Conversely, and when the performance function type is concave, CMV is used to find the MPP.

2.3.2 RBDO with Equality Constraints

As mentioned earlier, in this work we assume that all Type (i) equality constraints are already included in the vector of inequality constraints $\mathbf{g}(\cdot)$ through constraint relaxation and all of the remaining equality constraints $\mathbf{h}(\cdot)$ are of the analysis-type (Type(ii)). To satisfy the analysis-type equality constraints within RBDO, Du and Huang developed a numerical procedure that includes the equality constraints in the RBDO model [48]. Defining the analysis-type equality constraint as a function of the random design variables $\mathbf{S} \in R^{n_r}$, we have:

$$h_j(\mathbf{S}) = 0, \qquad j = 1, ..., n_h \tag{2.20}$$

where n_r denotes the number of random design variables and n_h describes the number of analysis-type equality constraints. Assuming $n_r - n_h$ statistically independent random variables, we can partition the random design variables $\mathbf{S}$ into independent random design variables $\mathbf{S}_x$ and dependent random design variables $\mathbf{S}_y$, such that $\mathbf{S} = [\mathbf{S}_x, \mathbf{S}_y]^T$. We can rewrite Eqn. (2.20) in terms of the functional relationships between $\mathbf{S}_x$ and $\mathbf{S}_y$ [48]:

$$\mathbf{S}_y = \mathbf{a}(\mathbf{S}_x) \tag{2.21}$$

where $\mathbf{a}$ is the functional relationship between $\mathbf{S}_x$ and $\mathbf{S}_y$. Using the FORM approximation within the PMA for RBDO, and denoting the MPP of the constraint function g_i as $\mathbf{s}^*_{x_{MPP,i}}$, the algorithm initially becomes

$$\begin{aligned} \min_{\boldsymbol{\mu}_{S_x}} \quad & f(\boldsymbol{\mu}_{S_x}) \\ \text{subject to} \quad & g_i[\mathbf{s}^*_{x_{MPP,i}}, \mathbf{a}(\mathbf{s}^*_{x_{MPP,i}})] \leq 0, \qquad i = 1, ..., n_g \end{aligned} \tag{2.22}$$

where $\boldsymbol{\mu}_{S_x}$ is the mean vector of the independent random design variables. Introducing design variables at the mean values of dependent random design variables $\boldsymbol{\mu}_{S_y}$, their MPPs at $\mathbf{s}^*_{x_{MPP,i}}$ as $\mathbf{s}^*_{y_{MPP,i}}$ such that $\mathbf{s}^*_{y_{MPP,i}} = \mathbf{a}(\mathbf{s}^*_{x_{MPP,i}})$, the RBDO model can be rewritten as:

$$\begin{aligned} \min_{\boldsymbol{\mu}_{S_x}, \boldsymbol{\mu}_{S_y}, \mathbf{s}^*_{y_{MPP,i}}} \quad & f(\boldsymbol{\mu}_{S_x}, \boldsymbol{\mu}_{S_y}) \\ \text{subject to} \quad & g_i[\mathbf{s}^*_{x_{MPP,i}}, \mathbf{s}^*_{y_{MPP,i}}] \leq 0, \qquad i = 1, ..., n_g \\ & h_j(\boldsymbol{\mu}_{S_x}, \boldsymbol{\mu}_{S_y}) = 0, \qquad j = 1, ..., n_h \\ & h_k(\mathbf{s}^*_{x_{MPP,i}}, \mathbf{s}^*_{y_{MPP,i}}) = 0, \qquad k = 1, ..., n_h \times n_g, \; i = 1, ..., n_g \end{aligned} \tag{2.23}$$

In the above equation, the equality constraints are satisfied at the mean values of all random variables, as well as their MPPs. Note that since every inequality constraint has its own MPP, the total number of equality constraints at the MPP would be $n_h \times n_g$. This problem is equivalent to Eqn. (2.14) and thus it requires a MPP search algorithm. The reliability analysis step is then formulated using a FORM approximation within the PMA:

$$
\begin{aligned}
\min_{\mathbf{s}_{u,i}} \quad & -g_i(\mathbf{s}_{u,i}, \mathbf{s}^*_{y_{MPP,i}}) \\
\text{subject to} \quad & \left\|\mathbf{s}_{u,i}\right\| - \beta_{t_i} = 0 \\
\text{where} \quad & \beta_{t_i} = \Phi^{-1}_{cdf}(\alpha_i) \\
& \mathbf{s}_{u,i} = \Phi^{-1}_{cdf}[F_{\mathbf{s}_x}(\mathbf{s}_x)]
\end{aligned}
\tag{2.24}
$$

2.4 Summary

In this chapter, we introduced a dynamic system optimization formulation known as MDSDO to solve simultaneous co-design problems. This formulation enables the inclusion of physically meaningful plant design variables, such that the final co-design problem does not favor the control system design. To develop the proposed stochastic co-design formulation, we then introduced the traditional formulations for RDO and RBDO and addressed the issue of probabilistic equality constraints within each formulation. In the next chapters, we integrate the principles of RDO and RBDO with a simultaneous MDSDO problem formulation and propose three novel stochastic co-design formulations.

Chapter 3

Robust Co-Design Formulation for Stochastic Dynamic Systems

This chapter is focused on the development and implementation of the nominal, robust simultaneous co-design in MDSDO or R-MDSDO formulation. The issue of the analysis-type dynamic-system equality constraints is addressed through the systematic approach explained in the previous chapter. The effectiveness of the proposed formulation is then assessed for two case studies, with the results indicating the important role of the robust approach on the integrated system solution and its performance.

3.1 Robust MDSDO Problem Formulation

To implement a simultaneous R-MDSDO problem formulation, we assume that the source of uncertainty is from design-related decision variables and fixed problem parameters. The uncertainty is then propagated to the state trajectory decision variables, objectives and constraint functions. Therefore, we treat state decision variables as random processes. Due to the open-loop control design structure of the MDSDO problem formulation, the vector of control trajectory decision variables will remain deterministic [49]. Without any loss of generality, we assume that the design variables and parameters will be treated as random variables with known variance and covariance characteristics. Specifically, design-related decision variables are assumed to be independent random variables, and hence their covariance terms are zero. Similarly, the fixed problem parameters are assumed to be independent random variables and therefore have no covariance terms. The cross-covariance term associated with the random state trajectory decision variables is assumed to be zero [50, 51]

$$C_{XY}(t,s) = 0 \quad \forall\, t,s \tag{3.1}$$

where X and Y are distinct state decision trajectories. This assumption remains valid unless an algebraic system equality constraint defines a dependency among state variables. Moreover, we assume that the auto-covariance term of every distinct state trajectory decision variable at different time steps is zero and we only assign non-zero values for the variance term, such that [50]:

$$C_{XX}(t,s) = \begin{cases} 0 & \forall\, t \neq s \\ Var\,[X(t)] & \forall\, t = s \end{cases} \tag{3.2}$$

Here, the auto-covariance function of the state trajectory decision variable X at pairs of time instances t and s is denoted by $C_{XX}(t,s)$ and the variance of state trajectory decision variable X at time instant $t = s$ is denoted by $Var[X(t)]$. Dynamic equality constraints and algebraic equality constraints are evaluated and satisfied at the expected values of the random decision variables. A constraint shift index k_i, chosen by the designer, is used in inequality constraints to enforce k_i standard deviation satisfaction of the inequality constraint i. The nominal, robust simultaneous co-design formulation in MDSDO can be written as

$$\begin{aligned} \min_{\boldsymbol{\mu}_D, \boldsymbol{\mu}_X(t), \mathbf{u}(t)} \quad & w\phi(\boldsymbol{\mu}_D, \boldsymbol{\mu}_X(t), \mathbf{u}(t), t; \boldsymbol{\mu}_P) + (1-w)\sigma_\phi^2 \\ \text{subject to} \quad & \\ & g_i(\boldsymbol{\mu}_D, \boldsymbol{\mu}_X(t), \mathbf{u}(t), t; \boldsymbol{\mu}_P) + k_i \sigma_{g_i} \leq 0 \quad \forall\, i \\ & \mathbf{h}(\boldsymbol{\mu}_D, \boldsymbol{\mu}_X(t), \mathbf{u}(t), t; \boldsymbol{\mu}_P) = \mathbf{0} \\ & \dot{\boldsymbol{\mu}}_X(t) - \mathbf{f}(\boldsymbol{\mu}_D, \boldsymbol{\mu}_X(t), \mathbf{u}(t), t; \boldsymbol{\mu}_P) = \mathbf{0} \end{aligned} \tag{3.3}$$

where $\boldsymbol{\mu}_D$ is the vector of mean values of random design variables, $\boldsymbol{\mu}_X(t)$ is the vector of mean values of random state variables, $\mathbf{u}(t)$ is the vector of control variables and $\boldsymbol{\mu}_P$ is the vector of mean values of random parameters, which are assumed to be the same as their deterministic values $\mathbf{p}$. $\mathbf{h}(\cdot)$ denotes the vector of mean values of the algebraic equality constraints, whereas the mean dynamic equality constraints are described through $\dot{\boldsymbol{\mu}}_X(t) - \mathbf{f}(\boldsymbol{\mu}_D, \boldsymbol{\mu}_X(t), \mathbf{u}(t), t; \boldsymbol{\mu}_P) = \mathbf{0}$. The mean value of the i^{th} inequality constraint and its standard deviation are denoted by $g_i(.)$ and σ_{g_i}, respectively and w and $(1-w)$ are the weighting factors associated with the multiobjective problem formulation, which consists of the mean $\phi(\cdot)$ and variance σ_ϕ^2 of the objective function. Note that a first-order Taylor series approximation is used to calculate the

variance/standard deviation quantities in both the objective and inequality constraint functions:

$$\sigma_{f_r}^2 = \sum_{i=1}^{n_d} [\frac{\partial f_r}{\partial D_i}\big|_{\mathbf{D}=\boldsymbol{\mu}_D} \sigma_{D_i}]^2 + \sum_{i=1}^{n_p} [\frac{\partial f_r}{\partial P_i}\big|_{\mathbf{P}=\boldsymbol{\mu}_P} \sigma_{P_i}]^2 + \sum_{i=1}^{n_x} [\frac{\partial f_r}{\partial X_i}\big|_{\mathbf{X}=\boldsymbol{\mu}_X(t)}]^2 Var\,[X_i(t)] \tag{3.4}$$

In the above, n_d is the total number of design variables, σ_{D_i} is the standard deviation of the i^{th} design variable, n_p is the total number of parameters, σ_{P_i} is the standard deviation of the i^{th} parameter, and n_x is the total number of state trajectory decision variables. In addition, f_r is a random function, referring to either $\phi(\cdot)$ or $g_i(\cdot)$. Applying DT, the parameterized version of this equation takes the following form:

$$\begin{aligned}
&\min_{\boldsymbol{\mu}_D, \mathbf{M}_X, \mathbf{U}} \quad && w\phi(\boldsymbol{\mu}_D, \mathbf{M}_X, \mathbf{U}; \boldsymbol{\mu}_P) + (1-w)\sigma_\phi^2 \\
&\text{subject to} && \\
& && g_i(\boldsymbol{\mu}_D, \mathbf{M}_X, \mathbf{U}; \boldsymbol{\mu}_P) + k_i \sigma_{g_i} \leq 0 \quad \forall\, i \\
& && \mathbf{h}(\boldsymbol{\mu}_D, \mathbf{M}_X, \mathbf{U}; \boldsymbol{\mu}_P) = \mathbf{0} \\
& && \boldsymbol{\zeta}(\boldsymbol{\mu}_D, \mathbf{M}_X, \mathbf{U}; \boldsymbol{\mu}_P) = \mathbf{0}
\end{aligned} \tag{3.5}$$

Here, $\mathbf{M}_X$ is the matrix of discretized random state trajectory decision variables, $\mathbf{U}$ is the matrix of discretized control trajectory decision variables and $\boldsymbol{\zeta}(\cdot)$ is the vector of discretized dynamic equality constraints. It should be noted that in DT approaches, the interpolating polynomial cannot satisfy the dynamic equations at any time within two consecutive collocation points [52, 53, 54]. To improve the solution accuracy, a more refined discretization might be required, resulting in higher computational expense. Therefore, it is imperative to account for the trade-offs between solution accuracy and computational expense, particularly when uncertainty is introduced into the problem formulation. Algorithms that allow a more flexible mesh refinement strategy are highly suitable for this purpose. In particular, the hp-adaptive algorithm employed in GPOPS-II [55] allows the number of mesh intervals and the degree of interpolating polynomials within each interval to vary. Thus, the solution benefits from the exponential convergence at smooth regions and more collocation points at regions where the solution changes rapidly [55]. These algorithms enable a more robust solution in between the mesh intervals,thereby creating a reliable platform to investigate the impact of uncertain design variables in co-design problem formulations. Implementation of the proposed formulation is investigated next in two case studies.

3.2 Robust Co-design Case Studies using R-MDSDO

3.2.1 Mathematical Application

The first example is a simple analytical optimal control problem, modified for a co-design problem formulation. The original problem was taken from Ref. [56]. While extremely simplified, this problem offers obvious advantages in identifying implementation challenges. The deterministic problem is to find the optimal plant design $\mathbf{d} = [d_1, d_2]$, state trajectories $\mathbf{x}(t) = [x_1(t), x_2(t)]$, and control trajectory $u(t)$ to minimize the objective function ϕ:

$$\min_{\mathbf{d},\mathbf{x}(t),u(t)} \qquad \phi = \int_0^1 \tfrac{1}{2}\Big[2d_1 x_1^2(t) + d_1 x_2^2(t) + u^2(t)\Big]dt$$

subject to

$$\begin{gathered} \dot{x_1}(t) + d_2 d_1 x_2(t) = 0 \\ \dot{x_2}(t) + x_1(t) - d_1[1 - x_1^2(t)]x_2(t) + u(t) = 0 \\ \mathbf{d}_{min} \leq \mathbf{d} \leq \mathbf{d}_{max} \\ \mathbf{x}_{min} \leq \mathbf{x} \leq \mathbf{x}_{max} \end{gathered} \tag{3.6}$$

The problem is subject to the following boundary conditions: $\mathbf{x}(0) = [0,0]^T$ and $\mathbf{x}(1) = [1,10]^T$. Introducing uncertainty to the design variables requires a robust co-design formulation similar to the one introduced in the previous section. The nominal R-MDSDO problem formulation can then be shown as

$$\min_{\mu_{\mathbf{D}},\mu_{\mathbf{X}},u} \quad \phi = w\int_0^1 \tfrac{1}{2}\Big[2\mu_{D_1}\mu_{X_1}^2(t)+\mu_{D_1}\mu_{X_2}^2(t)+u^2(t)\Big]dt+(1-w)(\sigma_f)^2$$

subject to

$$\begin{gathered}\dot{\mu_{X_1}}(t)+\mu_{D_2}\mu_{D_1}\mu_{X_2}(t)=0\\ \dot{\mu_{X_2}}(t)+\mu_{X_1}(t)-\mu_{X_1}[1-\mu_{X_1}^2(t)]\mu_{X_2}(t)+u(t)=0\\ \boldsymbol{\mu}_{D_{min}}+3\sigma_D\leq\boldsymbol{\mu}_D\leq\boldsymbol{\mu}_{D_{max}}-3\sigma_D\\ \boldsymbol{\mu}_{X_{min}}+3\sqrt{C_{XX}(t,t)}\leq\boldsymbol{\mu}_X\leq\boldsymbol{\mu}_{X_{max}}-3\sqrt{C_{XX}(t,t)}\end{gathered} \tag{3.7}$$

where $w=0.5$ is the weight coefficient associated with the multiobjective problem formulation. The standard deviation of the random plant decision variables is equal to $\sigma_{D_1}=0.2$, $\sigma_{D_2}=0.5$ and the variance of the random process for X_1 and X_2 is denoted by $C_{X_1X_1}(t,t)=0.09$ and $C_{X_2X_2}(t,t)=0.09$, respectively. The constraint shift index $k=3$ is chosen throughout the whole study. The problem was implemented in the commercially available MATLAB-based software, GPOPS-II [55], which approximates the continuous-time optimal control problems using a new class of variable-order Gaussian quadrature methods. GPOPS-II employs a DT-based approach to transcribe the infinite dimensional problem into a problem formulation similar to that of Eqn. (2.2). The transcribed problem is then solved with an appropriate NLP solver such as IPOPT [57]. The problem was solved on a 32 GB of RAM and an Intel(R) Xenon(R) CPU E5-2637 v3 @ 3.50 GHz processor system, with the key GPOPS-II settings listed in Table. 3.1.

Table 3.1: GPOPS-II settings

Field	Setting
Mesh method	hp-LiuRao-Legendre
Mesh tolerance	10^{-4}
NLP solver	IPOPT
IPOPT tolerance	10^{-5}
IPOPT max iterations	5000

Table 3.2 compares the solution of deterministic MDSDO and R-MDSDO problem formulations. The results indicate the critical impact of uncertainty on the optimal solution of a robust co-design problem formulation. The vector of plant design variables has changed significantly compared to the deterministic case (50.03%). Although the value of the objective function has increased by 2.29% in R-MDSDO approach, the risk associated with this design is much less. In other words, the results are robust against uncertainties in design.

Table 3.2: Co-design results for mathematical application

	d_1	d_2	Objective	t(s)
MDSDO [a]	-0.07	3	54.6	0.31
R-MDSDO [b]	-0.13	1.5	55.85	0.32
Diff [c]	50.03%		2.29%	

[a] Deterministic MDSDO solution, [b] R-MDSDO solution, [c] Percent difference

Optimal state and control trajectories are illustrated in Fig. 3.1 and Fig. 3.2. This result also indicates the impact of including robust measures in co-design problem formulations. Although the optimal state trajectories are very similar, the optimal control strategy has undergone obvious change. We note that, despite the slight variations in optimal state and control trajectories, the co-design solution of the problem has significantly changed.

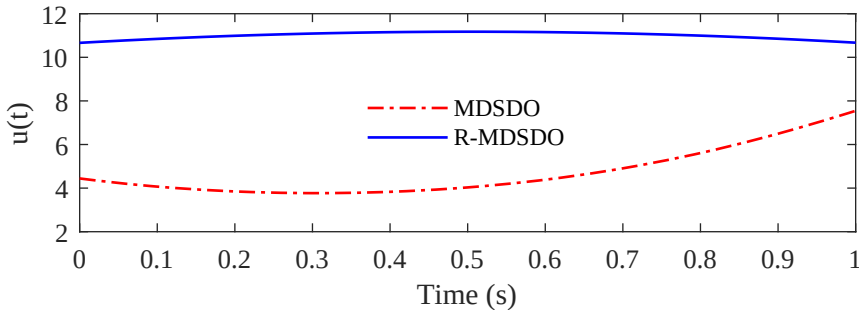

Figure 3.1: Optimal control trajectory $u(t)$ for MDSDO and R-MDSDO of mathematical application

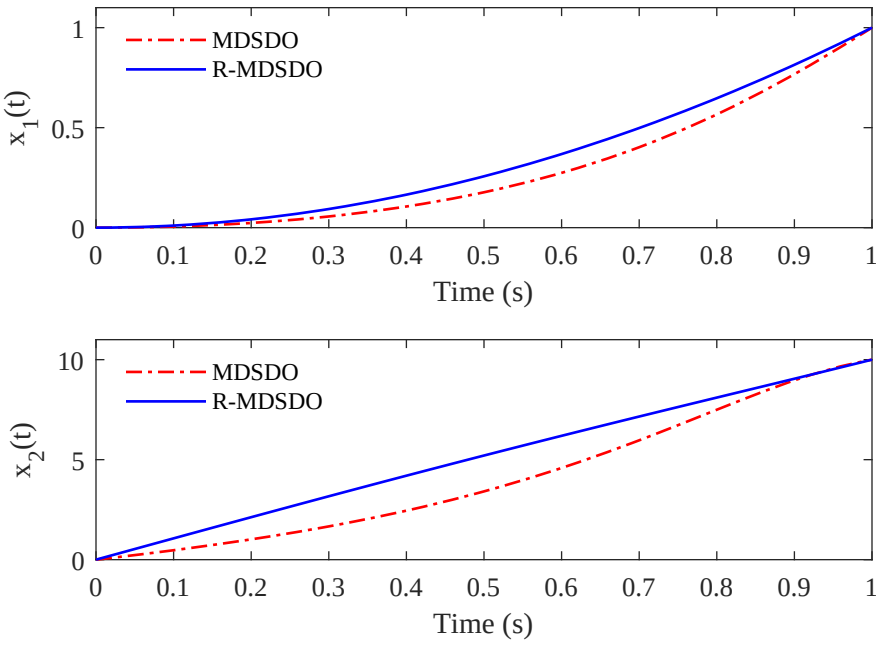

Figure 3.2: Optimal state trajectories for MDSDO and R-MDSDO of mathematical application

3.2.2 Engineering Application: Hang Glider Co-Design

A more complex co-design problem is chosen for the engineering application. This problem is a modified version of the range maximization flight of a hang glider. Originally taken from [58], the problem is modified to include design variables. Here, the hang glider is approximately described as a point mass subject to its weight W, a lift force L and drag force D_r. The motion of the glider is described by four state equations. A distribution for the thermal updraft with respect to the horizontal distance x_1 is given by the upward wind velocity [59]

$$v_a(x_1) = v_{a_{max}} \exp(-(\frac{x_1}{R} - 2.5)^2)(1 - (\frac{x_1}{R} - 2.5)^2) \tag{3.8}$$

where, $R = 100$ m and $v_{a_{max}} = 2.5$ m/s. The difference between initial and final altitude is used to maximize the horizontal range. The problem is modified to include the calculation of a trapezoidal wing surface area, such that a_1 and a_2 are the bases and b is the height of the wing. The problem is constructed with a plant design $\mathbf{d} = [a_1, a_2, b]^T$, state trajectories $\mathbf{x} = [x_1(t), x_2(t), x_3(t), x_4(t)]^T$ and $u = c_l(t)$. The state trajectories $x_1(t)$ and $x_2(t)$ are horizontal and vertical positions, respectively, and $x_3(t)$ and $x_4(t)$ denote horizontal and

vertical absolute velocity components of the glider. The glider is controlled through the lift coefficient $c_l(t)$. We note that $x_1(t_f)$ and t_f are decision variables. The deterministic co-design problem using MDSDO can be formulated as:

$$\min_{\mathbf{d},\mathbf{x}(t),\mathbf{u}(t),x_1(t_f),t_f} \quad -x_1(t_f) \tag{3.9a}$$

subject to

$$\dot{x_1}(t) - x_3(t) = 0 \tag{3.9b}$$

$$\dot{x_2}(t) - x_4(t) = 0 \tag{3.9c}$$

$$\dot{x_3}(t) - \frac{1}{m}(-L\sin(\eta) - D_r\cos(\eta)) = 0 \tag{3.9d}$$

$$\dot{x_4}(t) - \frac{1}{m}(L\cos(\eta) - D_r\sin(\eta) - W) = 0 \tag{3.9e}$$

$$L/D_r - 7.6 \leq 0 \tag{3.9f}$$

$$\frac{(2b+f_l)^2}{S} - 11 \leq 0 \tag{3.9g}$$

$$S_{min} \leq S \leq S_{max} \tag{3.9h}$$

$$x_{min} \leq \mathbf{x}(t) \leq x_{max} \tag{3.9i}$$

$$a_{1min} \leq a_1 \leq a_{1max} \tag{3.9j}$$

$$a_{2min} \leq a_2 \leq a_{2max} \tag{3.9k}$$

$$b_{min} \leq b \leq b_{max} \tag{3.9l}$$

Total mass of the pilot and glider is $m = 100$ kg and $W = mg$ is the corresponding weight with g being the gravitational constant. f_l is the fuselage length and assumed to be constant. Equation (3.9b) to (3.9e) are dynamic equations and Eqns. (3.9f) to (3.9h) represent the bounds on glide ratio, aspect ratio and the wing surface area, and are included in the design to keep the problem realistic [60]. The relative velocity v_r is at angle η to the horizontal plane, and the two are calculated by:

$$
\begin{aligned}
v_r &= \sqrt{x_3^2 + (x_4 - v_a(x_1))^2} \\
\eta &= \arctan\left(\tfrac{x_4 - v_a(x_1)}{x_3}\right)
\end{aligned}
\tag{3.10}
$$

Lift L and drag D_r forces are calculated through:

$$
\begin{aligned}
L &= \tfrac{1}{2} c_l \rho S {v_r}^2 \\
D_r &= \tfrac{1}{2} c_d \rho S {v_r}^2 \\
c_d &= 0.034 + 0.069662 {c_l}^2
\end{aligned}
\tag{3.11}
$$

where c_l and c_d are lift and drag coefficients and S describes the area of trapezoidal wings, calculated through $S = 2[\frac{1}{2}(a_1 + a_2)b]$. Air density corresponding to standard pressure and temperature at an altitude of 1000 m is equal to $\rho = 1.3$ kg/m^3. The glider is controlled through lift coefficient and is restricted by:

$$
c_l \leq c_{lmax} = 1.4 \tag{3.12}
$$

The problem is solved with the following boundary conditions:

$$
\begin{aligned}
x_1(0) &= 0 && \text{m} \\
x_2(0) &= 1000 && \text{m} \\
x_2(t_f) &= 900 && \text{m} \\
x_3(0) = x_3(t_f) &= 13.23 && \text{m/s} \\
x_4(0) = x_4(t_f) &= -1.288 && \text{m/s}
\end{aligned}
\tag{3.13}
$$

Before we introduce uncertainty to the system, we remind the reader that there are two terms in every robust objective function: One evaluated at the expected value of the design and one that corresponds to the standard deviation. In order to formulate the robust objective function in this problem, the standard deviation of the final condition on $x_1(x_1(t_f))$ is treated as a decision variable and is included in the objective function of the robust co-design problem formulation. The constraint shift index of $k = 3$ is chosen to guarantee

constraint satisfaction within k standard deviations of the mean. The robust co-design problem formulation can be written as

$$
\begin{aligned}
&\min_{\mu_{\mathbf{D}},\mu_{\mathbf{X}},\mathbf{u},\mu_{x_1}(t_f),\sigma_{x_i}(t_f),t_f} -w\mu_{X_1}(t_f)+(1-w)(\sigma_{X_1(t_f)})^2 \\
&\dot{\mu_{X_1}}(t)-\mu_{X_3}(t)=0 \\
&\dot{\mu_{X_2}}(t)-\mu_{X_4}(t)=0 \\
&\dot{\mu_{X_3}}(t)-\tfrac{1}{m}(-\mu_L\sin(\mu_\eta)-\mu_{D_r}\cos(\mu_\eta))=0 \\
&\dot{\mu_{X_4}}(t)-\tfrac{1}{m}(\mu_L\cos(\mu_\eta)-\mu_{D_r}\sin(\mu_\eta)-W)=0 \\
&(\mu_L/\mu_{D_r})\leq 7.6 \\
&\tfrac{(2\mu_b+0.5)^2}{\mu_S}+3\sigma_{g\_3.9g}\leq 11 \\
&\mu_{S_{min}}+3\sigma_{g\_3.9h}\leq\mu_S\leq\mu_{S_{max}}-3\sigma_{g\_3.9g} \\
&\mu_{X_{min}}+3\Sigma_{\mathbf{X}}\leq\mu_{\mathbf{X}}\leq\mu_{X_{max}}-3\Sigma_{\mathbf{X}} \\
&\mu_{a_{1min}}+3\sigma_{a_1}\leq\mu_{a_1}\leq\mu_{a_{1max}}-3\sigma_{a_1} \\
&\mu_{a_{2min}}+3\sigma_{a_2}\leq\mu_{a_2}\leq\mu_{a_{2max}}-3\sigma_{a_2} \\
&\mu_{b_{min}}+3\sigma_b\leq\mu_b\leq\mu_{b_{max}}-3\sigma_b
\end{aligned}
\tag{3.14}
$$

where $w=0.5$ is the weight coefficient associated with the multiobjective nature of robust design optimization problems. The problem was solved with the assumption that the standard deviations for random plant decision variables are: $\sigma_{a_1}=0.04$, $\sigma_{a_2}=0.04$, $\sigma_b=0.04$. The covariance matrix of the random process for the vector of state decision trajectories is denoted by $\mathbf{\Sigma}_X$, in which $C_{x_2x_2}(t,t)=0.0625$, $C_{x_3x_3}(t,t)=0.1225$, and $C_{x_4x_4}(t,t)=0.09$, respectively. The problem was implemented in the commercially available software, GPOPS-II [55], with the same basic settings introduced in Table 3.1 and was solved on a 32 GB of RAM and an Intel(R) Xenon(R) CPU E5-2637 v3 @ 3.50 GHz processor system.

Table 3.3: Co-design results for hang glider co-design

	$a_1(m)$	$a_2(m)$	$b(m)$	σ_{x_1}	$x_{tf}(m)$	t (s)
MDSDO	1.7	2.54	4.01	-	1274.6	27.3
R-MDSDO	1.51	2.41	4.12	0.2	1267.5	96.04
Diff		5.06%			0.56%	

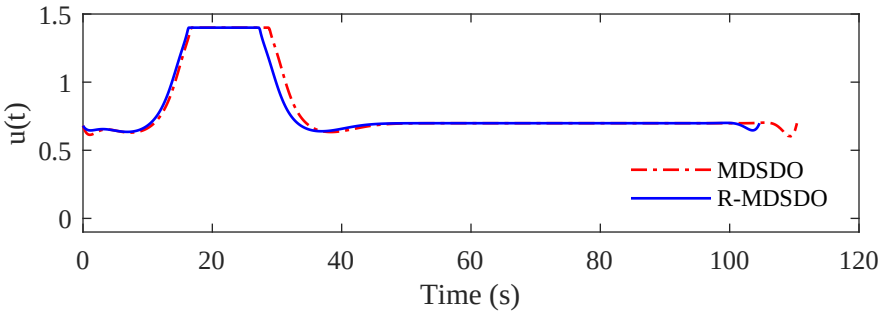

Figure 3.3: Optimal control trajectory $u(t)$ for MDSDO and R-MDSDO of hang glider

The results from both the deterministic MDSDO and R-MDSDO formulations are compared in Table 3.3. The vector of plant design has changed by 5.06% compared to the deterministic case. Also, the maximum range is reduced by 0.56% in the RDO approach. Although less favorable, the associated risk with this design is much less. The trajectories of the optimal control and state decision variables are illustrated in Fig. 3.3 and Fig. 3.4, respectively. It can be observed that under uncertainty, optimal control and state trajectories of the system tend to deviate from the solution of the deterministic problem. While the robust problem takes longer time to solve, its solution is much less sensitive to variations in design.

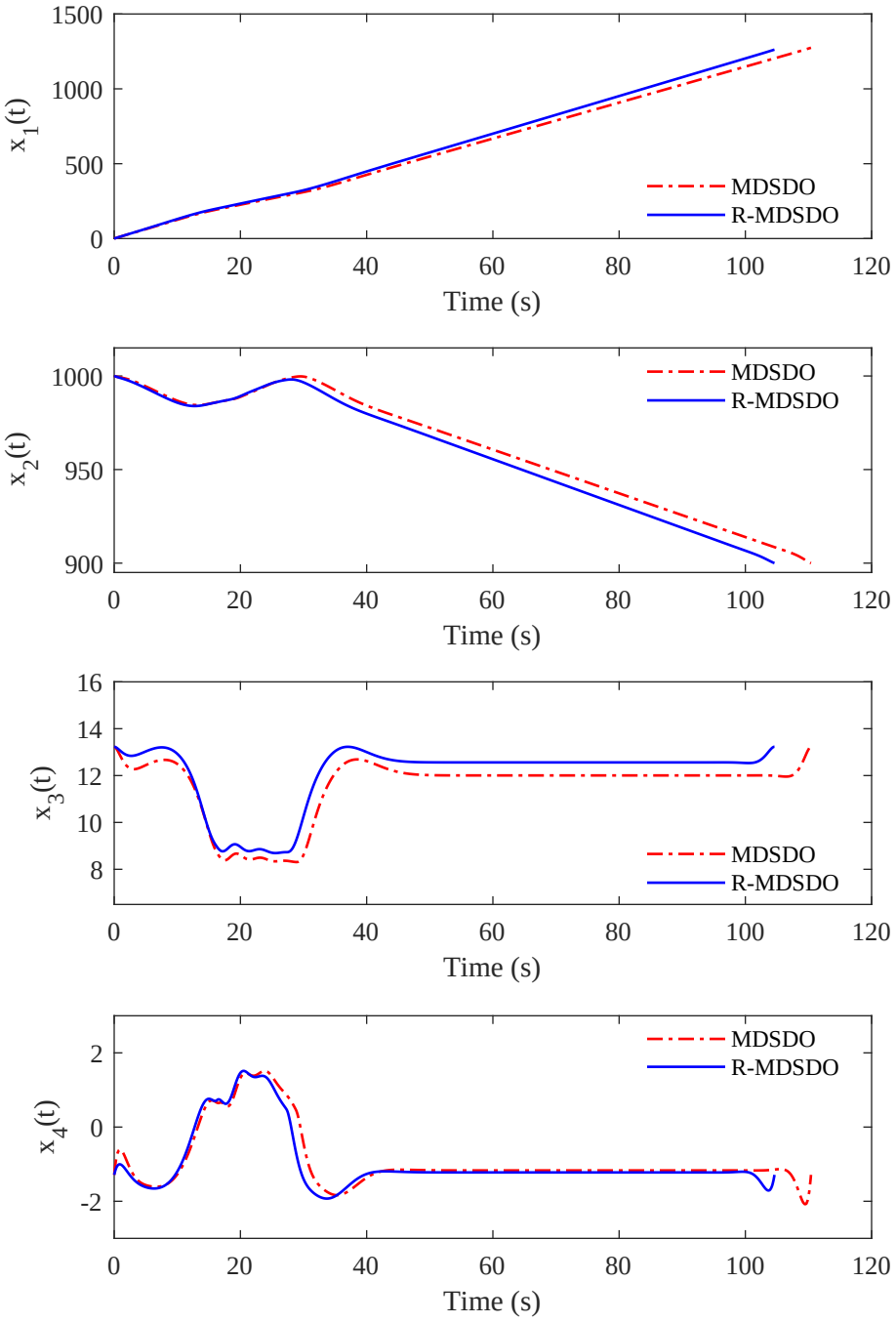

Figure 3.4: Optimal state trajectories for MDSDO and R-MDSDO of hang glider

3.3 Summary

In this chapter, we developed a nominal R-MDSDO formulation for the co-design of stochastic dynamic systems. The proposed formulation was applied to a mathematical co-design test problem and an engineering application (hang glider co-design problem), where the results indicated the significant impact of the robust approach on the integrated system-level solution of these dynamic systems. Specifically, by accounting for uncertainties through R-MDSDO, a more conservative solution was obtained that was less sensitive to design variations.

Chapter 4

Reliability-based Co-Design Formulation for Stochastic Dynamic Systems

To ensure that the design feasibility is maintained in a reliable manner within the co-design formulation, a more rigorous evaluation of probabilistic constraints is needed. Thus, in this chapter, we use RBDO principles to develop a novel reliability-based MDSDO formulation for stochastic dynamic systems. In particular, in this chapter we develop a double-loop MPP formulation for the RB-MDSDO approach. The proposed formulation addresses the issue of the analysis-type dynamic and algebraic equality constraints for direct transcription (DT) variants of the simultaneous MDSDO [61]. The application of the proposed double-loop RB-MDSDO approach is investigated for the complex co-design problem of an automotive active-suspension.

4.1 Reliability-based MDSDO Problem Formulation

The double-loop RB-MDSDO with MPP approach includes the vector of mean values of uncertain plant design decision variables $\boldsymbol{\mu}_D$, the vector of mean values of state trajectory decision variables $\boldsymbol{\mu}_X(t)$, the MPPs of design decision variables $\mathbf{d}^*_{MPP,i}$, the MPPs of state decision variables $\mathbf{x}^*_{MPP,i}(t)$, and the vector of deterministic control variables $\mathbf{u}(t)$. The objective function ϕ is optimized over the set of decision variables $[\boldsymbol{\mu}_D, \boldsymbol{\mu}_X(t), \mathbf{x}^*_{MPP,i}(t), \mathbf{u}(t)]$ and subject to the probabilistic inequality constraints $\mathbf{g}(\cdot)$, algebraic equality constraints $\mathbf{h}(\cdot)$, and dynamic system equality constraints. Both the algebraic equality constraints and dynamic system equality constraints must be satisfied at the mean value vector of design decision variables and state trajectory decision variables, as well as their MPPs:

$$
\begin{aligned}
\min_{\boldsymbol{\mu}_D,\boldsymbol{\mu}_X(t),\mathbf{x}^*_{MPP,i}(t),\mathbf{u}(t)} \quad & \phi(\boldsymbol{\mu}_D,\boldsymbol{\mu}_X(t),\mathbf{u}(t)) \\
\text{subject to} \quad & g_i(\mathbf{d}^*_{MPP,i},\mathbf{x}^*_{MPP,i}(t),\mathbf{u}(t)) \leq 0, \qquad i=1,...,n_g \\
& \mathbf{h}(\boldsymbol{\mu}_D,\boldsymbol{\mu}_X(t),\mathbf{u}(t)) = \mathbf{0} \\
& \mathbf{h}_i(\mathbf{d}^*_{MPP,i},\mathbf{x}^*_{MPP,i}(t),\mathbf{u}(t)) = \mathbf{0}, \qquad i=1,...,n_g \\
& \dot{\boldsymbol{\mu}}_X(t) - f(\boldsymbol{\mu}_D,\boldsymbol{\mu}_X(t),\mathbf{u}(t)) = \mathbf{0} \\
& \dot{\boldsymbol{\mu}}_X(t) - f_i(\mathbf{d}^*_{MPP,i},\mathbf{x}^*_{MPP,i}(t),\mathbf{u}(t)) = \mathbf{0}, \qquad i=1,...,n_g
\end{aligned}
\tag{4.1}
$$

The MPP problem in the standard normal space can then be formulated as:

$$
\begin{aligned}
\min_{\mathbf{d}_{u,i}} \quad & -g_i(\mathbf{d}_{u,i},\mathbf{x}^*_{MPP,i}(t),\mathbf{u}(t)) \\
\text{s.t.} \quad & \left\|\mathbf{d}_{u,i}\right\| - \beta_{t_i} = 0
\end{aligned}
\tag{4.2}
$$

where

$$
\mathbf{d}_{u,i} = \Phi^{-1}_{cdf}[F_{g_i}(\mathbf{d})] \tag{4.3}
$$

Note that in the above formulation, the time-dependent performance measure function requires careful attention. This is because in reliability-based co-design problem formulations, probabilistic path constraints must be treated as performance measure functions. As a result, in the proposed formulations, one can employ a worst-case approach that identifies the least reliable point of the trajectory. Another approach is to identify the least reliable design point by maximizing the integral of the probabilistic path constraint. The general MPP optimization problem pertaining to this point is then implemented as usual. Applying DT, we can write the transcribed version of Eqn. (4.1) as

$$
\begin{aligned}
\min_{\boldsymbol{\mu}_D, \mathbf{M}_X, \mathbf{x}^*_{MPP,i}, \mathbf{U}} \quad & J(\boldsymbol{\mu}_D, \mathbf{M}_X, \mathbf{U}) \\
\text{subject to} \quad & g_i(\mathbf{d}^*_{MPP,i}, \mathbf{x}^*_{MPP,i}, \mathbf{U}) \leq 0, \quad i = 1, ..., n_g \\
& \mathbf{h}(\boldsymbol{\mu}_D, \mathbf{M}_X, \mathbf{U}) = \mathbf{0} \\
& \mathbf{h}_i(\mathbf{d}^*_{MPP,i}, \mathbf{x}^*_{MPP,i}, \mathbf{U}) = \mathbf{0}, \quad i = 1, ..., n_g \\
& \boldsymbol{\zeta}(\boldsymbol{\mu}_D, \mathbf{M}_X, \mathbf{U}) = \mathbf{0} \\
& \boldsymbol{\zeta}_i(\mathbf{d}^*_{MPP,i}, \mathbf{x}^*_{MPP,i}, \mathbf{U}) = \mathbf{0}, \quad i = 1, ..., n_g
\end{aligned}
\tag{4.4}
$$

where $\mathbf{d}^*_{MPP,i}$ denotes the vector of design-related MPPs of the i^{th} constraint and $\mathbf{x}^*_{MPP,i}$ denotes the matrix of discretized state trajectory decision variables at $\mathbf{d}^*_{MPP,i}$. The MPP optimization problem can be formulated as:

$$
\begin{aligned}
\min_{\mathbf{d}_{u,i}} \quad & -g_i(\mathbf{d}_{u,i}, \mathbf{x}^*_{MPP,i}, \mathbf{U}) \\
\text{s.t.} \quad & \left\| \mathbf{d}_{u,i} \right\| - \beta_{t_i} = 0
\end{aligned}
\tag{4.5}
$$

4.2 Reliability-based Co-design Case Study Using RB-MDSDO

Implementation of the proposed formulation is investigated in a complex co-design problem of an automotive active-suspension, developed in Ref. [1]. Here, we only employ the model to solve the co-design problem of the automotive active-suspension when it is excited through a rough surface. In the following, we briefly introduce the development of the models. Further details can be found in Ref. [1].

4.2.1 Co-design of an Automotive Active-suspension system

The vehicle active-suspension model developed here is a linear quarter-car model. This linearity implies that the force acting on the spring is directly proportional to the vertical extension or compression of the spring. The model entails the sprung mass and its vertical position as m_s and z_s, respectively, and the unsprung mass and its vertical position as m_{us} and z_{us}, respectively (see Fig. (4.1)). As the vehicle travels

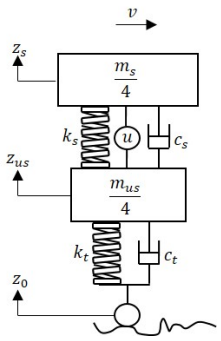

Figure 4.1: Quarter car active suspension model with active control

with the speed $v = 20$ m/s, it is excited by road variations, denoted by z_0. Th road input profile was generated from Ref. [1] using a Gaussian random number generator and a series of filtering steps [62, 63], with the international roughness index (IRI) of 7.37. This value corresponds to an unpaved road or a damaged paved road and demonstrates the amount of suspension travel in meters per a kilometer of longitudinal distance. The active suspension model of the system can be described using linear state-space differential equations that entail the realization of control trajectory decision $u(t)$ via an actuator and five state trajectory decision variables $\mathbf{x}(t)$, where $x_1(t)$ is the tire deflection, $x_2(t)$ is the unsprung mass velocity, $x_3(t)$ is the suspension stroke, and $x_4(t)$ is the sprung mass velocity. Note that the fifth state decision variable $x_5(t)$, is the damper fluid temperature, described later in the damper model development section. The dynamic system equality constraints for the first four state decision variables are described below:

$$\dot{\mathbf{x}}(t) = \mathbf{A}\mathbf{x}(t) + \mathbf{B}u(t) + \mathbf{C}\dot{z_0} \tag{4.6}$$

where $\mathbf{x}(t)$, $\mathbf{A}$, $\mathbf{B}$ and $\mathbf{C}$ can be described as:

$$\mathbf{x}(t) = \begin{bmatrix} z_{us} - z_0 \\ \dot{z}_{us} \\ z_s - z_{us} \\ \dot{z}_s \end{bmatrix}, \mathbf{A} = \begin{bmatrix} 0 & 1 & 0 & 0 \\ -\frac{4k_t}{m_{us}} & -\frac{4(c_s+c_t)}{m_{us}} & \frac{4k_s}{m_{us}} & \frac{4c_s}{m_{us}} \\ 0 & -1 & 0 & 1 \\ 0 & \frac{4c_s}{m_s} & -\frac{4k_s}{m_s} & -\frac{4c_s}{m_s} \end{bmatrix}, \mathbf{B} = \begin{bmatrix} 0 \\ -\frac{1}{m_{us}} \\ 0 \\ \frac{1}{m_s} \end{bmatrix}, \mathbf{C} = \begin{bmatrix} -1 \\ \frac{4c_t}{m_{us}} \\ 0 \\ 0 \end{bmatrix}$$

In this formulation, k_t is the tire stiffness, k_s is the spring stiffness for the sprung mass, c_t is the damping ratio of the tire and c_s is the damping ratio of the sprung mass.

4.2.1.1 Spring Model

A helical compression spring with round wire and squared ground ends is developed in a coil-over configuration that allows the coil spring and the damper to be integrated coaxially into a single assembly [64]. The vector of plant design decision variables for the spring model includes the helix diameter D_h, wire diameter d_w, spring pitch p and the number of active coils N_a. Note that N_a is treated as a continuous variable in this study. Then the spring constant can be formulated as:

$$k_s = \frac{d_w^4 G}{8 D_h^3 N_a (1 + \frac{1}{2C^2})} \tag{4.7}$$

where G is the shear modulus of elasticity associated with alloy steel wire, made of Chromium-Silicon ASTM A401, and C is the spring index, defined as $C = D_h/d_w$. The free length of the spring L_0 and its solid length L_s can be calculated as:

$$\begin{aligned} L_0 &= pN_a + 2d_w \\ L_s &= d(N_a + Q - 1) \end{aligned} \tag{4.8}$$

where $Q = 1.75$ is a correction factor for squared, ground ends. The static suspension deflection can be calculated as $\delta_g = \frac{m_s g}{4k_s}$, where $g = 9.81\ m/s^2$. The spring shear stress τ at maximum deflection is modeled in the following. Note that since helical springs are never used as both compression and extension springs, the application of helical springs fall under the condition of fluctuating load, resulting in the midrange shear stress τ_m and the amplitude shear stress τ_a. These values are estimated using the Bergsträsser factor, K_B, to account for the shear, as well as the curvature effect:

$$\tau = K_B \frac{8 F D_h}{\pi d_w^3} \tag{4.9}$$

$$\tau_m = K_B \frac{8 F_m D_h}{\pi d_w^3} \tag{4.10}$$

$$\tau_a = K_B \frac{8F_a D_h}{\pi d_w^3} \tag{4.11}$$

where $K_B = \dfrac{4C+2}{4C-3}$ and the axial force F, its mean F_m and its amplitude F_a can be calculated as:

$$F = k_s(L_0 - L_s) \tag{4.12}$$

$$F_m = \frac{F_{min} + F_{max}}{2} \tag{4.13}$$

$$F_a = \frac{F_{min} - F_{max}}{2} \tag{4.14}$$

where $F_{min} = k_s(\delta_g - x_3(t))$ and $F_{max} = k_s(x_3(t) + \delta_g)$. In these equations, $x_3(t)$ describe the maximum spring deflection on a rough surface. The shear yield strength S_{sy} is assumed to be proportional to the ultimate tensile strength of the spring S_{ut} where $S_{sy} = 0.65 S_{ut}$. The ultimate tensile strength is obtained through an empirical equation $S_{ut} = \dfrac{A}{d_w^m}$ with A as the intercept and m as the slope. Note that d_w is measured in mm. All the spring model parameters are included in Table 4.1.

4.2.1.2 Damper Model

A single-tube telescopic damper is modeled with three plant design decision variables, where D_0 is the valve diameter, D_p is the piston diameter, and D_s is the damper stroke chosen as an independent design variable. Similar to the spring design, damper model assumes linear damping, implying that the force exerted on the damper is proportional to the damper piston velocity. In developing this model, we further assume that the effects of the foot valve is neglected and the piston valves are assumed to be spring-biased spool valves. The spool valve frontal area is described as $A_0 = \dfrac{\pi D_0^2}{4}$ and the maximum valve lift at maximum allowed damper pressure $P_{allow} = 4.75 \times 10^6$ Pa is denoted by:

$$x_m = \frac{A_0 P_{allow}}{k_v} \tag{4.15}$$

Table 4.1: Spring model parameters

Parameter	Value	Unit
Sprung mass ($m_s/4$)	325	kg
Unsprung mass($m_{us}/4$)	65	kg
Tire stiffness (k_t)	232.5×10^3	N/m
Tire damping ratio(c_t)	0	Ns/m
Correction factor (Q)	1.75	-
Shear modulus (G)	77.2	GPa
Maximum spring length ($L_{0,max}$)	0.4	m
Maximum outer spring diameter ($D_{0,max}$)	0.25	m
Spring damper clearance (δ_s)	0.009	m
Damper piston diameter (t_d)	0.002	m
Bumpstop thickness (L_B)	0.02	m
Design factor (n_d)	1.2	-
Effective stress (A)	1974×10^6	Pamm$^{\text{m}}$
Exponent (m)	0.108	m
Vehicle speed (v)	20	m/s

where $k_v = 7500$ N/m is the spool valve spring constant. The damper valve coefficient is calculated as:

$$C_2 = \eta A_f \sqrt{x_m} \tag{4.16}$$

where $A_f = 0.1$ is an area factor. The suspension damping coefficient can then be calculated as:

$$c_s = \frac{D_p^4}{8 C_d C_2 D_0^2} \sqrt{\frac{\pi k_v \rho}{2}} \tag{4.17}$$

where $\rho = 850$kg/m^3 is the damper fluid density and $C_d = 0.7$ is the discharge coefficient for for spool valves. The energy dissipation in the damper results in fluid temperature increase, which is an integral part of the damper design. Heat generation in the damper is calculated as $q_{gen} = c_s \dot{x}_3^2$, where $\dot{x}_3$ is the damper piston velocity. The fluid volume can be calculated as $v_f = \pi D_p^2 \frac{D_s + l_{d1} + l_{d3}}{4}$, where l_{d1} and l_{d3} represent the

space required for damper valving and casting extensions, respectively. The shell height can be calculated as $L_2 = D_s + l_{d1} + l_{d3}$ and the external surface area of the shell can be calculated as $A_4 = 2\pi r_2 L_2$, where r_2 is the outer shell radius. The heat flow from the damper fluid through the shell can be modeled as a DAE, which can be converted to a single ordinary differential equation:

$$\dot{T}_1 = -\frac{b_2 b_3}{b_1 b_2 + b_1 b_3} T_1 + \frac{b_2 b_3}{b_1 b_2 + b_1 b_3} T_4 + \frac{q_{gen}}{b_1} \tag{4.18}$$

where T_1 and T_4 are the damper fluid temperature and the constant atmospheric temperature, respectively. b_1, b_2, and b_3 are calculated as:

$$b_1 = \rho v_f c_{pl} \tag{4.19}$$

$$b_2 = \frac{2\pi L_2 k_2}{\ln(\frac{r_2}{r_1})} \tag{4.20}$$

$$b_3 = hA_4 \tag{4.21}$$

where c_{pl} is the heat capacity of the damper fluid, k_2 is the conduction coefficient of the steel damper tube, r_1 is the inner shell radius,

$$P_{max} = \frac{4c_s(x_4 - x_2)}{\pi D_p^2} \tag{4.22}$$

$$x_{v,max} = \frac{A_0 P_{max}}{k_v} \tag{4.23}$$

where x_2 and x_4 are the second and forth state decision trajectories. All the values for parameters in the damper design can found in Table 4.2.

Table 4.2: Spring model parameters

Parameter	Value	Unit
Function coefficient (η)	0.9	-
Seal max pressure (P_{allow})	4.75×10^6	Pa
Spool vale spring constant (k_v)	7500	N/m
Area factor (A_f)	0.1	–
Damper fluid density (ρ)	850	kg/m^3
Discharge coefficient (C_d)	0.7	–
Damper fluid heat capacity (c_{pl})	2500	J/kgK
Damper tube conduction factor (k_2)	60.5	W/mK
Atmospheric temperature (T_4)	300	K
Convection coefficient (h)	50	W/m^{2}K
Damper valving space (l_{d1})	0.02	m
Damper component space (l_{d2})	0.04	m
Casting extension space (l_{d3})	0.02	m
Maximum damper temperature (T_{1allow})	390	K
Maximum damper stroke velocity ($\dot{x}_{3allow}$)	5	m/s
Maximum spool valve lift ($x_{v,allow}$)	0.03	m

4.2.2 Active suspension co-design formulation

The co-design problem within MDSDO can now be formulated using the spring and damper models. The objective function is defined as the weighted sum of the tire deflection $z_{us} - z_0$, sprung mass acceleration $\ddot{z}_s$, and active control u:

$$\min_{\mathbf{d},\mathbf{x}(t),u(t)} \quad \phi = \int_0^{t_f} \left[w_1 (z_{us} - z_0)^2 + w_2 \ddot{z}_s^2 + w_3 u^2 \right] dt \tag{4.24a}$$

subject to

$$4 \leq C \leq 12 \tag{4.24b}$$

$$L_0 - 5.26 D_h \leq 0 \tag{4.24c}$$

$$\frac{L_0}{L_{0,max}} - 1 \leq 0 \tag{4.24d}$$

$$\frac{d_w + D_h}{D_{0,max}} - 1 \leq 0 \tag{4.24e}$$

$$d_w + D_h + D_p + 2(\delta_s + t_d) \leq 0 \tag{4.24f}$$

$$x_3 - L_0 + L_s + L_B + \delta_g \leq 0 \tag{4.24g}$$

$$\frac{n_d \tau}{S_{sy}} - 1 \leq 0 \tag{4.24h}$$

$$0.15 + 1 - \frac{L_0 - L_s}{\delta_g + 1.1 x_3} \leq 0 \tag{4.24i}$$

$$\frac{\tau_a}{S_{e2}} + \frac{\tau_m}{S_{sy}} - 1 \leq 0 \text{ where } S_{e2} = \frac{0.24 S_{ut}}{n_d} \tag{4.24j}$$

$$\frac{n_d \tau_a}{241 \times 10^6} - 1 \leq 0 \tag{4.24k}$$

$$L_0 - L_s - D_s \leq 0 \tag{4.24l}$$

$$\frac{2D_s + l_{d1} + l_{d2}}{L_{0,max}} - 1 \leq 0 \tag{4.24m}$$

$$\frac{T_1}{T_{1allow}} - 1 \leq 0 \tag{4.24n}$$

$$\frac{P_{max}}{P_{allow}} - 1 \leq 0 \tag{4.24o}$$

$$\frac{x_4 - x_2}{x_{3allow}} \leq 1 \tag{4.24p}$$

$$\frac{x_{v,max}}{x_{v,allow}} \leq 1 \tag{4.24q}$$

$$\dot{\mathbf{x}}(t) - \mathbf{f}(\mathbf{d}, \mathbf{x}(t), u(t), t) = \mathbf{0} \tag{4.24r}$$

The problem is solved for $t_f = 2$ s, which is treated as a fixed parameter. The objective weights $w_1 = 10^4$, $w_2 = 0.5$, and $w_3 = 10^{-5}$ are to ensure the same order of magnitude for every term in the objective function. Similarly, a normalization scheme is employed to keep the constraints within the same order of magnitude.

Equation (4.24b) ensures that the spring index is within a reasonable range to avoid entanglement and to be realistic. To prevent buckling, Eqn. (4.24c) must be satisfied. The uncompressed length of the spring must fit within the specified pocket length. This constraints is described in Eqn. (4.24d). To prevent interface with vehicle components, Eqn. (4.24e) ensures that the outer spring diameter does not exceed $D_{0,max}$. The spring must fit around the damper with a certain clearance, as described in Eqn. (4.24f). Suspension case space constraint is described in Eqn. (4.24g). Spring shear stress τ at maximum deflection must not exceed shear yield stress. This constraint is described in Eqn. (4.24h). To ensure the linearity of Eqn. (4.6) and the validity of the model, Eqn. (4.24i) must be satisfied. Soderberg fatigue criterion with Zimmerli data are described in Eqn. (4.24j) and Eqn. (4.24k). Eqn. (4.24l) ensures adequate damper range of motion and Eqn. (4.24m) makes sure that the damper fits within the pocket length. Maximum damper fluid temperature must not exceed the maximum allowable temperature and the maximum damper pressure must not exceed the seal maximum pressure. These two requirements are described in Eqn. (4.24n) and Eqn. (4.24o). To protect the suspension system from excessive velocities, Eqn. (4.24p) is imposed. The clearance requirement for the maximum amount of spool valve lift is included in Eqn. (4.24q). Finally, dynamic-system equality constraints from Eqn. (4.6) and Eqn. (4.18) are included in Eqn. (4.24r).

The proposed double-loop RB-MDSDO problem formulation is then used to solve the co-design problem of the automotive active-suspension. Due to the complexity of the model, and to reduce the number of probabilistic inequality constraints, the vector of uncertain design variables only include the damper valve diameter D_0, the damper piston diameter D_p, and the damper stroke D_s. These uncertain design variables result in the total of five performance measure functions:

$$G_1 : \ Pr\{Eqn.\ (4.24f)\} \geq \Phi_{cdf}(5)$$

$$G_2 : \ Pr\{Eqn.\ (4.24l)\} \geq \Phi_{cdf}(5)$$

$$G_3 : \ Pr\{Eqn.\ (4.24m)\} \geq \Phi_{cdf}(5)$$

$$G_4 : \ Pr\{Eqn.\ (4.24o)\} \geq \Phi_{cdf}(5)$$

$$G_5 : \ Pr\{Eqn.\ (4.24p)\} \geq \Phi_{cdf}(5)$$

where the reliability target of $\beta_t = 5$ is assumed for all performance measure functions. We assume Gaussian distribution for uncertain design variables where, $\sigma_{D_0} = 0.001$, $\sigma_{D_p} = 0.001$, and $\sigma_{D_s} = 0.003$. Note that the design space of random design decision variables is reduced using a constraint shift index of $k = 3$. By employing the proposed formulations, we can formulate the double-loop RB-MDSDO problems.

4.2.3 Results and Discussion

The double-loop RB-MDSDO problem was implemented in the commercially available software, GPOPS-II [55] on a 32 GB of RAM and an Intel(R) Xenon(R) CPU E5-2637 v3 @ 3.50 GHz processor system, with the setting shown in Table 4.3.

Table 4.3: GPOPS-II settings.

Field	Setting
Mesh method	hp-LiuRao-Legendre
Mesh tolerance	10^{-4}
NLP solver	IPOPT
IPOPT tolerance	10^{-5}
IPOPT max iterations	1000

In this study, we exploit the potential computational benefit that can be gained for the double-loop RB-MDSDO problem formulation by using methods such as AMV, CMV, HMV. The gradient information, which are required for the implementation of such algorithms, are expected to incur a computational burden on the optimizer—thereby increasing the computational time. Therefore, the gradient information for $G1$, $G2$, and $G3$ was calculated manually, while the gradient information for $G4$, and $G5$ was calculated through forward differentiation in ADIMAT toolbox [65]. The solution of these methods are compared to the solution of a general optimizer such as MATLAB's fmincon function, using an interior-point algorithm.

The results are described in Table. 4.4 and indicate that accounting for uncertainties in the co-design of automotive active suspension has a significant impact on its system-level solution. Specifically, all of the

Table 4.4: Automotive suspension co-design solution using double-loop RB-MDSDO approaches

Field	DET[a]	AMV [b]	CMV[c]	HMV[d]	GO[e]	Unit
d_w	0.016	0.017	0.017	0.017	0.017	m
D_h	0.156	0.157	0.157	0.157	0.157	m
p	0.037	0.035	0.035	0.035	0.035	m
Na	7.055	6.66	6.66	6.66	6.61	-
μ_{D_0}	0.007	0.008	0.008	0.008	0.008	m
μ_{D_p}	0.03	0.033	0.033	0.033	0.033	m
μ_{D_s}	0.17	0.155	0.155	0.155	0.155	m
ϕ	1.3975	1.4634	1.4634	1.4634	1.4634	-
t	93	2611	3580	3665	100,246	s
k_s	23760	29457	29457	29457	29457	Nm^{-1}
c_s	724.54	750.07	750.07	750.07	750.07	Nsm^{-1}

[a] Deterministic [b] Advanced mean value [c] Conjugate mean value [d] Hybrid mean value [e] General optimization using fmincon

plant design decision variables have changed compared to the deterministic case. In total, the vector of plant design decision variables has undergone a 5.6% change. These variations have a direct impact on critical intermediate variables such as k_s and c_s, which have changed dramatically, by 23.98% and 3.52%, respectively. Therefore, these variations significantly impact the performance of the vehicle under rough surface input. Finally, the value of the objective function has increased by 4.72% compared with the deterministic case.

According to Table. 4.4, solving the MPP optimization problem through AMV approach offers computational efficiency for this problem; however, this is a problem-dependent outcome. Nevertheless, reliability methods such as AMV, CMV, and HMV are expected to surpass generic optimization algorithms in computational efficiency. Due to the numerical stability of the HMV approach, it is recommended for a larger class of co-design problems. The control decision trajectory, and sprung mass response to the rough surface are illustrated in Fig. (4.2) and Fig. (4.3), respectively. As we can see from these figures, the control input and the sprung mass response for the deterministic solution is slightly different from the solution of stochastic approaches.

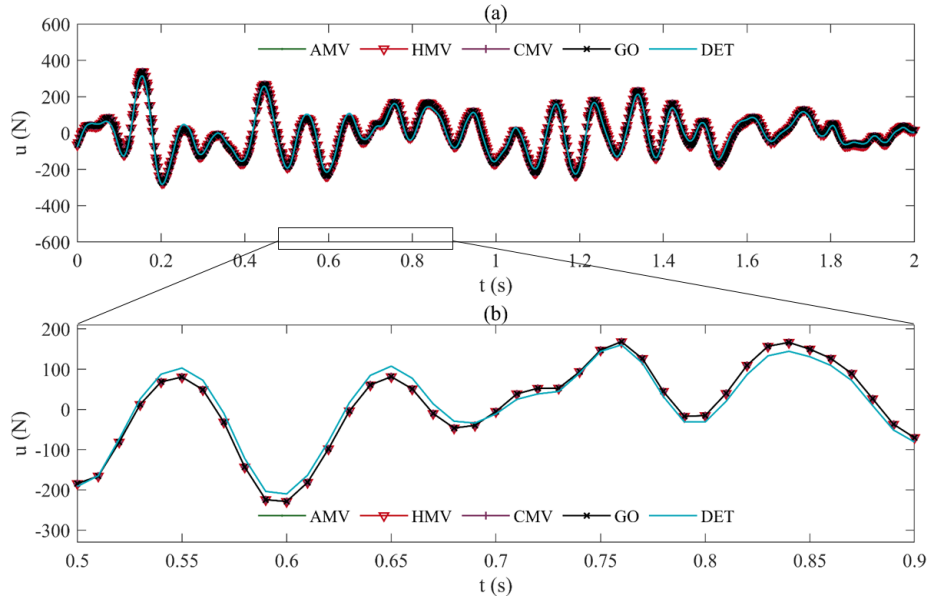

Figure 4.2: Control force for active automotive suspension: (a) complete time-history (b) magnified trajectory for $t \in [0.5\ 0.9]$.

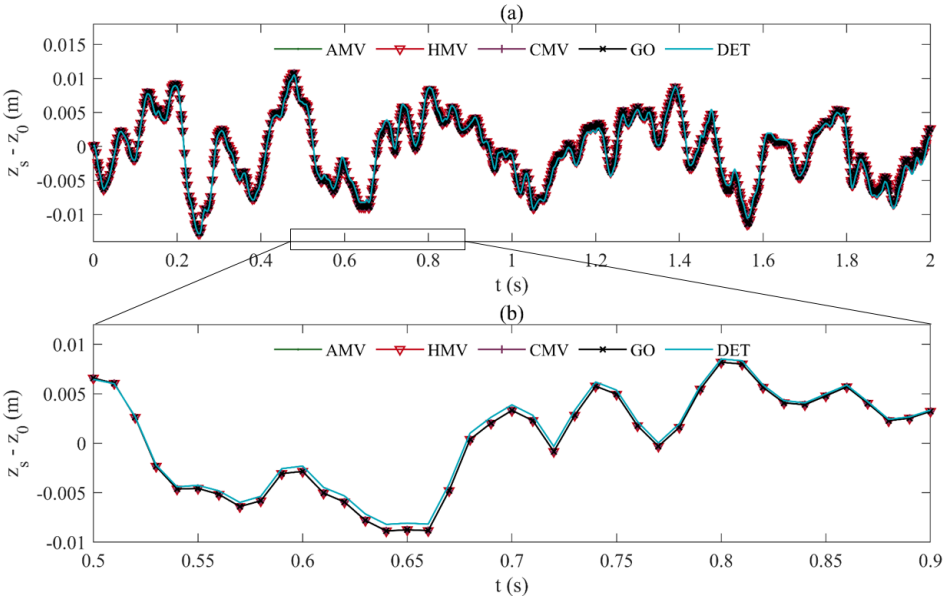

Figure 4.3: Sprung mass response to rough surface input: (a) complete time-history (b) magnified trajectory for $t \in [0.5\ 0.9]$.

4.3 Summary

The integration of balanced co-design optimization methods such MDSDO with stochastic optimization techniques is necessary for the real-world application and implementation of many complex dynamic systems. In this chapter, we developed a novel RB-MDSDO formulation for co-design of stochastic dynamic systems. Using efficient reliability methods such as AMV, CMV, HMV for the solution of the inner-loop MPP optimization problem, we implemented and solved multiple double-loop RB-MDSDO approaches for the co-design of an automotive active-suspension system and demonstrated the significance of these advanced formulation on a complex co-design problem. In addition, the results indicated the computational advantage of these efficient methods compared to general optimization algorithms.

Chapter 5

Assessment of Single-Loop MPP Reliability Analysis for RB-MDSDO

This chapter develops a single-loop RB-MDSDO formulation to improve the computational efficiency of RB-MDSDO for co-design problems. Developing a more efficient approach for RB-MDSDO is necessary because the number of decision variables in the problem formulation grows exponentially as the number of analysis-type equality constraints and/or probabilistic inequality constraints are increased. Using the sequential optimization and reliability assessment (SORA) algorithm, we decouple the previously proposed problem formulation, such that the optimization problem is solved within the deterministic step, while the reliability analysis is performed in the standard normal random space. This single-loop approach is expected to improve the efficiency of the double-loop RB-MDSDO approach and offer a practical methodology for the widespread application of the RB-MDSDO approaches. In order to identify the implementation challenges, we first solve the proposed formulation for two small-scale co-design problems. In the next step, the complex, co-design problem of an automotive active-suspension, which was introduced in Chapter 4, is solved and the results are compared to the solution of the double-loop MPP approach.

5.1 Traditional SORA

The idea behind SORA is to develop a single-loop MPP strategy where the deterministic optimization and the reliability assessment are decoupled from each other and are executed sequentially, until some convergence criteria are achieved. Du and Chen [66, 67] employed a series of sequential cycles of optimization and reliability assessment using an efficient MPP search algorithm. In SORA, the deterministic optimization is performed first to achieve an optimal solution, then the reliability analysis is executed to verify the satisfaction of reliability constraints and to provide improvement directions for the next cycle of the SORA algorithm [48]. Here, for the sake of brevity, we only describe the problem formulations in each major step

of this algorithm. Further details about the convergence criteria and the flowchart of the algorithm can be found in [66, 67].

The SORA algorithm starts with a deterministic problem that includes the mean value vector of the random design variables $\boldsymbol{\mu}_S$. After the first cycle, the deterministic optimization problem uses the information from the reliability assessment step of the previous cycle. In other words, after the first cycle of SORA, the constraints within the deterministic optimization are modified to shift the MPPs into the feasible region of the deterministic bounds. Therefore, we employ shifting vectors, similar to the ones introduced by Du and Chen [68] to establish the equivalent deterministic optimization problem in each cycle of SORA. These shifting vectors are described by $\mathbf{v}$:

$$\mathbf{v}_i^{(m)} = \boldsymbol{\mu}_S^{(m-1)} - \mathbf{s}_{MPP,i}^{*,(m-1)} \tag{5.1}$$

where $\mathbf{s}_{MPP,i}^{*,(m-1)}$ is the MPP of the vector of uncertain design variables from the $(m-1)^{th}$ SORA cycle and $\boldsymbol{\mu}_S^{(m-1)}$ is the vector of mean values from the $(m-1)^{th}$ cycle. The deterministic optimization problem for the m^{th} cycle of SORA can then be formulated as:

$$\begin{aligned} &\min_{\boldsymbol{\mu}_S^{(m)}} && f(\boldsymbol{\mu}_S^{(m)}) \\ &\text{subject to} && g_i(\boldsymbol{\mu}_S^{(m)} - \mathbf{v}_i^{(m)}) \leq 0, \quad i = 1, ..., n_g \end{aligned} \tag{5.2}$$

The output of Eqn. (5.2), denoted by $\boldsymbol{\mu}_S^{(m)}$, will be the input to the reliability assessment step, where a transformation into the random normal space will be performed. The MPP of the random design variables associated with the i^{th} performance measure is found through the following formulation

$$\begin{aligned} &\min_{\mathbf{s}_{u,i}^{(m)}} && -g_i(\mathbf{s}_{u,i}^{(m)}) \\ &\text{subject to} && \left\| \mathbf{s}_{u,i}^{(m)} \right\| - \beta_{t_i} = 0 \\ &\text{where} && \mathbf{s}_{u,i}^{(m)} = \Phi_{cdf}^{-1}[F_{g_i}(\mathbf{s}^{(m)})] \end{aligned} \tag{5.3}$$

This sequential algorithm has been implemented for multiple applications within the RBDO literature. For

more details, interested readers are referred to [69, 70, 48].

5.2 SORA with Equality Constraints

Here, we employ the approach developed by Du and Huang to address the issue of analysis-type equality constraints [48]. Using the FORM approximation within the PMA for RBDO, and denoting the MPP of the constraint function g_i in $(m-1)^{th}$ cycle of SORA for independent random variables as $\mathbf{s}_{x_{MPP,i}}^{*,(m-1)}$, and for dependent random variables as $\mathbf{s}_{y_{MPP,i}}^{*,(m-1)}$, Du and Huang formulated the deterministic step of the SORA algorithm as:

$$
\begin{aligned}
\min_{\boldsymbol{\mu}_{S_x}^{(m)},\boldsymbol{\mu}_{S_y}^{(m)},\mathbf{s}_{y_{MPP,i}}^{*,(m)}} \quad & f(\boldsymbol{\mu}_{S_x}^{(m)},\boldsymbol{\mu}_{S_y}^{(m)}) \\
\text{subject to} \quad & g_i(\boldsymbol{\mu}_S^{(m)}-\mathbf{v}_i^{(m)},\mathbf{s}_{y_{MPP,i}}^{*,(m)}) \le 0, \qquad i=1,...,n_g \\
& h_j(\boldsymbol{\mu}_{S_x}^{(m)},\boldsymbol{\mu}_{S_y}^{(m)}) = 0, \qquad j=1,...,n_h \\
& h_k(\boldsymbol{\mu}_S^{(m)}-\mathbf{v}_i^{(m)},\mathbf{s}_{y_{MPP,i}}^{*,(m)}) = 0, \qquad k=1,...,n_h\times n_g,\ i=1,...,n_g
\end{aligned}
\tag{5.4}
$$

where $\mathbf{v}_i^{(m)}$ denotes the shifting vector associated with the i^{th} inequality constraint, resulted from the previous cycle of SORA. The equality constraints are satisfied at the mean values of all random variables, as well as their MPPs. Note that since every inequality constraint has its own MPP, the total number of equality constraints at the MPP will be $n_h \times n_g$. Moreover, note that $\mathbf{s}_{x_{MPP,i}}^{*,(m-1)}$ come from the previous cycle of SORA and are included in the deterministic optimization through the shifting vector $\mathbf{v}_i^{(m)}$. The MPPs of the dependent random variables $\mathbf{s}_{y_{MPP,i}}^{*,(m)}$ are obtained during the $(m)^{th}$ cycle of SORA. This problem is equivalent to Eqn. (5.2) and thus it requires a MPP search algorithm. The reliability assessment is then formulated using a FORM approximation within the PMA. Note that the MPP subproblem must satisfy the analysis-type equality constraints, as well as the usual reliability constraint during optimization.

$$
\begin{aligned}
\min_{\mathbf{s}_{u,i}^{(m)},\mathbf{s}_y^{(m)}} \quad & -g_i(\mathbf{s}_{u,i}^{(m)},\mathbf{s}_y^{(m)}) \\
\text{subject to} \quad & \left\|\mathbf{s}_{u,i}^{(m)}\right\| - \beta_{t_i} = 0 \\
& h_j(\mathbf{s}_{u,i}^{(m)},\mathbf{s}_y^{(m)}) = 0, \qquad j = 1,...,n_h \\
\text{where} \quad & \mathbf{s}_{u,i}^{(m)} = \Phi_{cdf}^{-1}[F_{g_i}(\mathbf{s}_x^{(m)})]
\end{aligned}
\tag{5.5}
$$

5.3 RB-MDSDO Problem Formulation Using SORA

The integrated nature of co-design formulations results in the propagation of uncertainties from random plant design decision variables to the analysis-type equality constraints, thereby affecting the open-loop optimal control trajectories. To quantify the impact of these uncertainties on the system-level co-design solution, we propose the novel single-loop RB-MDSDO formulation using SORA.

The single-loop MPP formulation in RB-MDSDO executes the deterministic optimization problem first, followed by the reliability assessment. The deterministic optimization problem, which is the first major block in SORA algorithm, doesn't explicitly account for the random variations or processes in the design decision variables or state trajectory decision variables; rather it employs shifting vectors $\mathbf{v}_i^{(m)}$ to shift the MPPs of the design decision variables into the feasible region of the deterministic bounds, while making sure that the state dynamics are satisfied at the mean values, as well as the MPPs. It is still assumed that the overall MPP strategy will consist of the PMA in conjunction with the FORM to solve the problem robustly and efficiently. This problem formulation includes the vector of mean values of the plant design decision variables $\boldsymbol{\mu}_D^{(m)}$, the mean values of state decision decision variable $\boldsymbol{\mu}_X^{(m)}(t)$, the MPPs of design decision variables $\mathbf{d}_{MPP,i}^{*,(m)}$, the MPPs of state decision variables $\mathbf{x}_{MPP,i}^{*,(m)}(t)$, the shifting vectors $\mathbf{v}_i^{(m)}$ and the vector of deterministic control variables $\mathbf{u}^{(m)}(t)$ at the $(m)^{th}$ cycle of SORA. The objective function ϕ is optimized over the set of decision variables $[\boldsymbol{\mu}_D^{(m)}, \boldsymbol{\mu}_X^{(m)}(t), \mathbf{x}_{MPP,i}^{*,(m)}(t), \mathbf{u}^{(m)}(t)]$ and subject to the probabilistic inequality constraints $\mathbf{g}(\cdot)$, algebraic equality constraints $\mathbf{h}(\cdot)$, and dynamic system equality constraints. Note that both algebraic equality constraints and dynamic system equality constraints must be satisfied both at the the mean values and the MPPs of design and state decision variables. This formulation can be described as

$$
\begin{aligned}
&\min_{\boldsymbol{\mu}_D^{(m)},\boldsymbol{\mu}_X^{(m)}(t),\mathbf{x}_{MPP,i}^{*,(m)}(t),\mathbf{u}^{(m)}(t)} && \phi(\boldsymbol{\mu}_D^{(m)},\boldsymbol{\mu}_X^{(m)}(t),\mathbf{u}^{(m)}(t)) \\
&\text{subject to} && g_i(\boldsymbol{\mu}_D^{(m)}-\mathbf{v}_i^{(m)},\mathbf{x}_{MPP,i}^{*,(m)}(t),\mathbf{u}^{(m)}(t))\leq 0, && i=1,...,n_g \\
& && \mathbf{h}(\boldsymbol{\mu}_D^{(m)},\boldsymbol{\mu}_X^{(m)}(t),\mathbf{u}^{(m)}(t))=\mathbf{0} && \\
& && \mathbf{h}_i(\boldsymbol{\mu}_D^{(m)}-\mathbf{v}_i^{(m)},\mathbf{x}_{MPP,i}^{*,(m)}(t),\mathbf{u}^{(m)}(t))=\mathbf{0}, && i=1,...,n_g \\
& && \dot{\boldsymbol{\mu}}_X(t)-\mathbf{f}(\boldsymbol{\mu}_D^{(m)},\boldsymbol{\mu}_X^{(m)}(t),\mathbf{u}^{(m)}(t))=\mathbf{0} && \\
& && \dot{\mathbf{x}}_{MPP,i}^{*,(m)}(t)-\mathbf{f}_i(\boldsymbol{\mu}_D^{(m)}-\mathbf{v}_i^{(m)},\mathbf{x}_{MPP,i}^{*,(m)}(t),\mathbf{u}^{(m)}(t))=\mathbf{0}, && i=1,...,n_g
\end{aligned}
\tag{5.6}
$$

where the shifting vector for the $(m)^{th}$ cycle of SORA can be found using $\mathbf{v}_i^{(m)}=\boldsymbol{\mu}_D^{(m-1)}-\mathbf{d}_{MPP,i}^{*,(m-1)}$. The MPP subproblem in the reliability assessment step can then be formulated as:

$$
\begin{aligned}
&\min_{\mathbf{d}_{u,i}^{(m)}(t),\mathbf{x}_i^{(m)}(t)} && -g_i(\mathbf{d}_{u,i}^{(m)},\mathbf{x}_i^{(m)}(t),\mathbf{u}^{*,(m)}(t)) \\
&\text{subject to} && \left\|\mathbf{d}_{u,i}^{(m)}\right\|-\beta_{t_i}=0 \\
& && \mathbf{h}(\mathbf{d}_{u,i}^{(m)},\mathbf{x}_i^{(m)}(t),\mathbf{u}^{*,(m)}(t))=\mathbf{0} \\
& && \dot{\mathbf{x}}(t)-\mathbf{f}(\mathbf{d}_{u,i}^{(m)},\mathbf{x}_i^{(m)}(t),\mathbf{u}^{*,(m)}(t))=\mathbf{0} \\
&\text{where} && \mathbf{d}_{u,i}^{(m)}=\Phi_{cdf}^{-1}[F_{g_i}(\mathbf{d}^{(m)})]
\end{aligned}
\tag{5.7}
$$

This formulation requires the use of numerical methods such as DT. The transcribed version of Eqn. (5.6) can be described as

$$
\begin{aligned}
\min_{\boldsymbol{\mu}_D^{(m)},\mathbf{M}_X^{(m)},\mathbf{x}_{MPP,i}^{*,(m)},\mathbf{U}^{(m)}} \quad & \phi(\boldsymbol{\mu}_D^{(m)},\mathbf{M}_X^{(m)},\mathbf{U}^{(m)}) \\
\text{subject to} \quad & g_i(\boldsymbol{\mu}_D^{(m)}-\mathbf{v}_i^{(m)},\mathbf{x}_{MPP,i}^{*,(m)},\mathbf{U}^{(m)}) \leq 0, \quad i=1,...,n_g \\
& \mathbf{h}(\boldsymbol{\mu}_D^{(m)},\mathbf{M}_X^{(m)},\mathbf{U}^{(m)}) = \mathbf{0} \\
& \mathbf{h}_i(\boldsymbol{\mu}_D^{(m)}-\mathbf{v}_i^{(m)},\mathbf{x}_{MPP,i}^{*,(m)},\mathbf{U}^{(m)}) = \mathbf{0}, \quad i=1,...,n_g \\
& \boldsymbol{\zeta}(\boldsymbol{\mu}_D^{(m)},\mathbf{M}_X^{(m)},\mathbf{U}^{(m)}) = \mathbf{0} \\
& \boldsymbol{\zeta}_i(\boldsymbol{\mu}_D^{(m)}-\mathbf{v}_i^{(m)},\mathbf{x}_{MPP,i}^{*,(m)},\mathbf{U}^{(m)}) = \mathbf{0}, \quad i=1,...,n_g
\end{aligned}
\tag{5.8}
$$

where $\mathbf{M}_X^{(m)}$ is the matrix of discretized, state trajectory mean-value decision variables in $(m)^{th}$ SORA cycle. This problem is equivalent to the general RBDO problem and thus, requires a reliability assessment algorithm within the standard normal space to find the MPPs. The MPP subproblem can then formulated as:

$$
\begin{aligned}
\min_{\mathbf{d}_{u,i}^{(m)},\mathbf{X}_i^{(m)}} \quad & -g_i(\mathbf{d}_{u,i}^{(m)},\mathbf{X}_i^{(m)},\mathbf{U}^{*,(m)}) \\
\text{subject to} \quad & \left\|\mathbf{d}_{u,i}\right\|^{(m)} - \beta_{t_i} = 0 \\
& \mathbf{h}(\mathbf{d}_{u,i}^{(m)},\mathbf{X}_i^{(m)}(t),\mathbf{u}^{*,(m)}(t)) = \mathbf{0} \\
& \boldsymbol{\zeta}(\mathbf{d}_{u,i}^{(m)},\mathbf{X}_i^{(m)},\mathbf{U}^{*,(m)}) = \mathbf{0} \\
\text{where} \quad & \mathbf{d}_{u,i}^{(m)} = \Phi_{cdf}^{-1}[F_{g_i}(\mathbf{d}^{(m)})]
\end{aligned}
\tag{5.9}
$$

Note that the deterministic optimal control solution from the deterministic optimization block of SORA is a fixed input trajectory into the reliability assessment step. The SORA flowchart of the RB-MDSDO formulation is described in Fig. 5.1. We note that the output of the deterministic step at the $(m)^{th}$ cycle of SORA to the reliability assessment block is the optimal mean value of independent design variables, $\boldsymbol{\mu}_D^{(m)}$, and optimal control decision trajectory $\mathbf{U}^{*,(m)}$. For the first SORA cycle, since there's no information available from the reliability assessment step, the the MPP of the independent random design variables $\mathbf{d}_{MPP,i}^{*,(0)}$ is prescribed as the mean of the independent random design variables $\boldsymbol{\mu}_D^{(0)}$, such that $v_i^{(0)} = \mathbf{0}$. After the initial cycle of SORA, the reliability analysis step inputs the MPP of the independent random design

variables of the previous cycle $\mathbf{d}_{MPP,i}^{*,(m-1)}$ to the deterministic step, through the shifting vector. Note that the inclusion of the analysis-type equality constraints in the reliability analysis step is to ensure their feasibility.

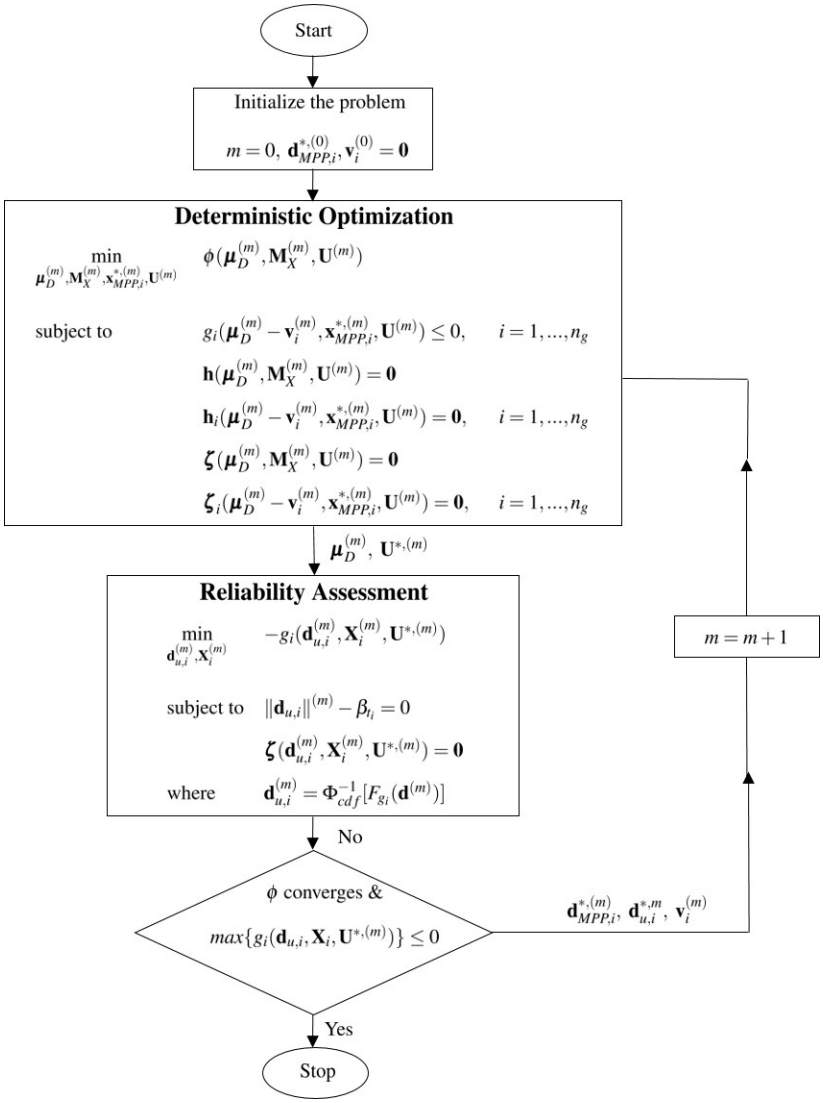

Figure 5.1: SORA within RB-MDSDO

A major challenge in the implementation of the proposed RB-MDSDO algorithm arises when state trajectory decision variables are bounded through inequality path constraints. As opposed to the conventional static inequality constraints, the dynamic nature of these trajectories necessitates a different approach when the associated performance measure function is formulated. This makes the implementation of the RB-

MDSDO problem formulation a challenging task. One could treat each discretized path constraint at every single collocation point as an inequality constraint—employed within RB-MDSDO problem formulation as a performance measure function. This, however, is not practical as the number of performance measure functions will be directly influenced by the total number of collocation points in the discretized problem. To address this issue, we identify the least reliable design point for each probabilistic path constraint by maximizing the integral of the probabilistic path constraint at every reliability assessment step. This approach enables the determination of plant designs and state trajectories that would cause the highest constraint violation over the whole trajectory under uncertainty. The stopping criteria is then set as the convergence of the optimization subproblems, as well as the satisfaction of the performance measure function at the MPP. It is noteworthy to mention that while this approach is limiting in the sense that it does not provide insights into the characteristics of this random process, it does address the reliability requirements of the RB-MDSDO formulation when the uncertainty is propagated into the system only from plant design decision variables or problem parameters.

5.4 Reliability-based Co-design Case Studies Using Single-loop RB-MDSDO Implementations

Implementation challenges and the efficiency of the proposed formulation is investigated in three case studies. The first example is a simple analytical constrained Van der Pol oscillator optimal control problem, modified for a co-design problem formulation. The original problem was taken from Ref.[71, 72]. While extremely simplified, this problem offers obvious advantages in identifying implementation challenges. The second example is the range maximization co-design problem of a hang glider, introduced in Chapter 3.2.2. Finally, the last case study solves the co-design problem of an automotive active-suspension system and compares the results with those obtained from Chapter 4.2. This comparison allows us to interpret the effectiveness and efficiency of the proposed RB-MDSDO approaches for complex co-design problems.

5.4.1 Van der Pol oscillator

The deterministic problem is to find the optimal plant design $\mathbf{d} = [d_1, d_2]$, state trajectories $\mathbf{x}(t) = [x_1(t), x_2(t)]$, and control trajectory $u(t)$ to minimize the objective function ϕ:

$$\min_{\mathbf{d},\mathbf{x}(t),\mathbf{x}(t_f),u(t)} \quad \phi = \int_0^5 \Big[x_1^2(t) + x_2^2(t) + u^2(t)\Big]dt$$

subject to

$$\begin{aligned}
&\dot{x_1}(t) - x_1(t)(1 - x_2^2(t)) + D_2 D_1 x_2(t) - u(t) = 0 \\
&\dot{x_2}(t) - x_1(t) = 0 \\
&\mathbf{d}_{min} \leq \mathbf{d} \leq \mathbf{d}_{max} \\
&\mathbf{x}_{min} \leq \mathbf{x} \leq \mathbf{x}_{max} \\
&u_{min} \leq u(t) \leq u_{max} \\
&g = -0.4 - x_1(t) \leq 0
\end{aligned} \tag{5.10}$$

The problem is subject to the following boundary conditions: $\mathbf{x}(0) = [0,1]^T$. We note that $\mathbf{x}(t_f)$ is a decision variable and is already included in the vector of state decision variables. Assuming that both design variables D_1 and D_2 are uncertain normal variables with $\sigma_{D1} = 0.02$ and $\sigma_{D2} = 0.03$, and the reliability target of $\beta_t = 3$ for the performance measure function $g: \ -0.4 - x_1(t) \leq 0$, the RB-MDSDO problem can be formulated such that in the deterministic step of the SORA algorithm, the following optimization problem is solved:

$$\min_{\boldsymbol{\mu}_D^{(m)},\boldsymbol{\mu}_X^{(m)}(t),\mathbf{x}_{MPP}^{*,(m)}(t),u^{(m)}(t)} \quad J = \int_0^5 \Big[\mu_{X_1}^{2,(m)}(t) + \mu_{X_2}^{2,(m)}(t) + u^{2,(m)}(t)\Big]dt \tag{5.11}$$

The objective function is subject to the following constraints.

$$\dot{\mu}_{X_1}^{(m)}(t) - \mu_{X_1}^{(m)}(t)(1 - \mu_{X_2}^{2,(m)}(t)) + \mu_{D_2}^{(m)}\mu_{D_1}^{(m)}\mu_{X_2}^{(m)}(t) - u^{(m)}(t) = 0 \tag{5.12}$$

$$\dot{\mu}_{X_2}^{(m)}(t) - \mu_{X_1}^{(m)}(t) = 0 \tag{5.13}$$

$$\dot{x}_{1,MPP}^{*,(m)}(t) - x_{1,MPP}^{*,(m)}(t)(1 - x_{2,MPP}^{2,*,(m)}(t)) + d_{2,MPP}^{*,(m-1)} d_{1,MPP}^{*,(m-1)} x_{2,MPP}^{*,(m)}(t) - u^{(m)}(t) = 0 \tag{5.14}$$

$$\dot{x}_{2,MPP}^{*,(m)}(t) - x_{1,MPP}^{*,(m)}(t) = 0 \tag{5.15}$$

$$\boldsymbol{\mu}_{D_{min}} + 3\boldsymbol{\sigma}_d \leq \boldsymbol{\mu}_D \leq \boldsymbol{\mu}_{D_{max}} - 3\boldsymbol{\sigma}_d \tag{5.16}$$

$$\boldsymbol{\mu}_{X_{min}} \leq \boldsymbol{\mu}_X(t) \leq \boldsymbol{\mu}_{X_{max}} \tag{5.17}$$

$$u_{min} \leq u(t) \leq u_{max} \tag{5.18}$$

$$G = -0.4 - X_1^*(t) \leq 0 \tag{5.19}$$

Note that the design space of the plant decision variables is reduced under uncertainty. The reliability assessment step then pertains to finding the MPP associated with the maximum violation of the performance measure trajectory within the standard normal space $\mathbf{d}_{u,i}$. Due to the assumption of normality for the uncertain plant design variables, the Rosenblatt transformation [47] would be linear:

$$\mathbf{d}_{u,i} = \frac{\mathbf{D} - \boldsymbol{\mu}_D}{\boldsymbol{\sigma}_D} \tag{5.20}$$

Then the reliability assessment step can be formulated as:

$$\min_{\mathbf{d}_u^{(m)}, \mathbf{x}^{(m)}(t)} \quad -\int_0^5 \Big[-0.4 - x_1^{(m)}(t) \Big] dt$$

subject to

$$\begin{aligned}
&\left\| \mathbf{d}_u^{(m)} \right\| - \beta_{t_i} = 0 \\
&\dot{x}_1^{(m)}(t) - x_1^{(m)}(t)(1 - x_2^{2,(m)}(t)) + (\mu_{D_2}^{(m)} + d_{2,u}\sigma_2)(\mu_{D_1}^{(m)} + d_{1,u}\sigma_1) x_2{}^{(m)}(t) - u^{*,(m)}(t) = 0 \\
&\dot{x}_2^{(m)}(t) - x_1{}^{(m)}(t) = 0
\end{aligned} \tag{5.21}$$

The problem was solved using the commercially available MATLAB©-based software, GPOPS-II [55]. We solved both the deterministic and the reliability assessment steps of the RB-MDSDO SORA algorithm on a 32 GB of RAM and an Intel(R) Xenon(R) CPU E5-2637 v3 @ 3.50 GHz processor system, with the key GPOPS-II settings introduced in Table 5.1.

Table 5.1: GPOPS-II settings.

Field	Setting
Mesh method	hp-LiuRao-Legendre
Mesh tolerance	10^{-6}
NLP solver	IPOPT
IPOPT tolerance	10^{-7}
IPOPT max iterations	5000

Table 5.2 compares the solution of the deterministic and the proposed RB-MDSDO problem formulations. The results indicate the critical impact of uncertainty on the optimal solution of co-design formulations within MDSDO and the necessity to account for this uncertainty through stochastic approaches such as the proposed RB-MDSDO formulation.

Table 5.2: Co-design results for Van der Pol oscillator

	d_1	d_2	$d^*_{1,MPP}$	$d^*_{2,MPP}$	J	Time (s)
MDSDO [a]	0.324	0.21	-	-	1.969	0.82
RB-MDSDO [b]	0.008	0.014	-0.035	-0.051	1.978	8.02
Diff [c]	96.31%				0.46%	

[a] Deterministic MDSDO solution, [b] Single-loop RB-MDSDO solution, [c] Percent difference

The solution converged in $m = 7$ SORA cycles, and the vector of plant design variables has changed significantly compared to the deterministic case (96.31%). Although the value of the objective function has increased by 0.46% in RB-MDSDO approach, the associated solution is more reliable compared to the deterministic case. The probability of failure for the probabilistic path constraint, G, was benchmarked through MCS, where $n = 100,000$ points were sampled about the MDSDO and RB-MDSDO solutions, respectively.

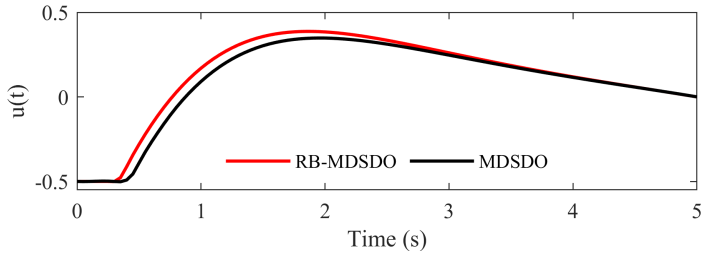

Figure 5.2: Comparison of deterministic and stochastic optimal control trajectory $u(t)$ for Test Problem 1

The simulation results show that the probability of failure has dropped from $Pr_{f,MDSDO}\{G\} = 0.294$ in MDSDO to $Pr_{f,RB-MDSDO}\{G\} = 0.03097$ in RB-MDSDO—indicating the effectiveness of the proposed approach. The probability of failure can be further improved by increasing the reliability target or using SORM. Figures 5.3 and 5.4 show the results of the MCS for the state decision trajectories about the solution of the MDSDO and RB-MDSDO approach, respectively. A sample size of $n = 1,000$ is used to create the MCS plots. From this figure, it is evident that the resultant trajectories violate G more often than the RB-MDSDO solution shown in Fig. 5.4.

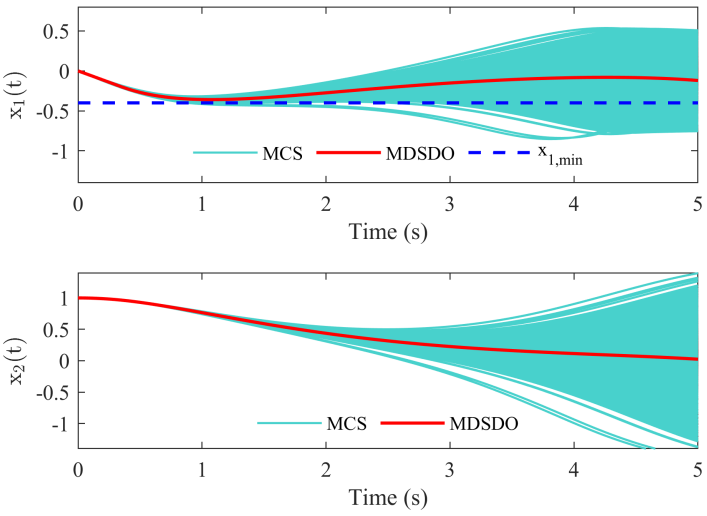

Figure 5.3: Van der Pol oscillator: MCS about the solution of MDSDO, $P_f = 0.294$

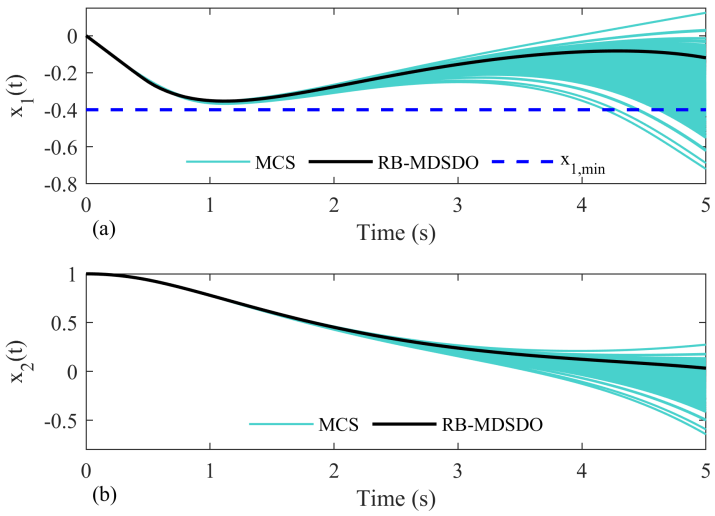

Figure 5.4: Van der Pol oscillator: MCS about the solution of RB-MDSDO for state trajectories: (a) $x_1(t)$ (b) $x_2(t)$

5.4.2 Hang glider

The problem statement and formulation for the hang glider problem was introduced in Chapter 3.2.2. To avoid repetition, this section only discusses the details pertaining to RB-MDSDO formulation. Interested readers are referred to Section 3.2.2 for more details on the hang glider problem. In order to formulate the single-loop RB-MDSDO problem, we assume a reliability target of $\beta = 3$. The standard deviation of the independent plant design variables is assumed to be $\sigma_{a_1} = 0.1$, $\sigma_{a_2} = 0.1$, $\sigma_b = 0.1$. We note that since the Eqn. (3.9f) is completely deterministic, we are left with two performance measure functions, namely Eqn. (3.9g) and Eqn. (3.9h). These performance measure functions are distinguished by index $i = 1$ and $i = 2$, respectively. Using a single-loop MPP formulation in RB-MDSDO, along with FORM and PMA, the objective for the deterministic step of SORA for hang glider co-design can be formulated as

$$\min_{\boldsymbol{\mu}_d^{(m)},\boldsymbol{\mu}_x^{(m)}(t),\mathbf{x}_{MPP,i}^{*,(m)}(t),\mathbf{u}^{(m)}(t),\boldsymbol{\mu}_{x_1}^{(m)}(t_f),t_f} \quad -\mu_{x_1}^{(m)}(t_f) \tag{5.22}$$

where (m) denotes the m^{th} cycle of SORA. This is subject to the following constraints:

$$\dot{\mu}_{x_1}^{(m)}(t) - \dot{\mu}_{x_3}^{(m)}(t) = 0 \tag{5.23}$$

$$\dot{\mu}_{x_2}^{(m)}(t) - \dot{\mu}_{x_4}^{(m)}(t) = 0 \tag{5.24}$$

$$\dot{\mu}_{x_3}^{(m)}(t) - \frac{1}{m}(-\mu_L \sin(\mu_\eta) - \mu_{D_r} \cos(\mu_\eta)) = 0 \tag{5.25}$$

$$\dot{\mu}_{x_4}^{(m)}(t) - \frac{1}{m}(\mu_L \cos(\mu_\eta) - \mu_{D_r} \sin(\mu_\eta) - W) = 0 \tag{5.26}$$

$$\dot{x}_{1_{MPP,i}}^{(m)}(t) - \dot{x}_{3_{MPP,i}}^{(m)}(t) = 0 \qquad i = 1,2 \tag{5.27}$$

$$\dot{x}_{2_{MPP,i}}^{(m)}(t) - \dot{x}_{4_{MPP,i}}^{(m)}(t) = 0 \qquad i = 1,2 \tag{5.28}$$

$$\dot{x}_{3_{MPP,i}}^{(m)}(t) - \frac{1}{m}(-L_{MPP,i} \sin(\eta_{MPP,i}) - D_{r_{MPP,i}} \cos(\eta_{MPP,i})) = 0 \qquad i = 1,2 \tag{5.29}$$

$$\dot{x}_{4_{MPP,i}}^{(m)}(t) - \frac{1}{m}(L_{MPP,i} \cos(\eta_{MPP,i}) - D_{r_{MPP,i}} \sin(\eta_{MPP,i}) - W) = 0 \qquad i = 1,2 \tag{5.30}$$

$$\frac{L}{D_r} - 11 \leq 0 \tag{5.31}$$

$$\frac{(2b_{MPP,1} + f_l)^2}{S_{MPP,1}} - g_{1,max} \leq 0 \tag{5.32}$$

$$S_{MPP,2} - S_{max} \leq 0 \tag{5.33}$$

$$\boldsymbol{\mu}_{x_{min}} \leq \boldsymbol{\mu}_x(t) \leq \boldsymbol{\mu}_{x_{max}} \tag{5.34}$$

$$\mu_{a_{1_{min}}} + 3\sigma_{a_1} \leq \mu_{a_1} \leq \mu_{a_{1_{max}}} - 3\sigma_{a_1} \tag{5.35}$$

$$\mu_{a_{2_{max}}} + 3\sigma_{a_2} \leq \mu_{a_2} \leq \mu_{a_{2_{max}}} - 3\sigma_{a_2} \tag{5.36}$$

$$\mu_{b_{min}} + 3\sigma_b \leq \mu_b \leq \mu_{b_{max}} - 3\sigma_b \tag{5.37}$$

Note that in this formulation, the dynamic system equality constraints are satisfied at both the vector of mean values, as well as the MPPs. All the deterministic decision variables including the vector of mean values of plant design variables $\boldsymbol{\mu}_d^{(m)}$, optimal control trajectory $\mathbf{u}^{(m)}(t)$, and $t_f^{(m)}$ will be inputs to the re-

liability assessment step. Moreover, under uncertainty, it is customary to push the design space inward so as to avoid the boundaries of the design space under uncertainty. This would be a trivial case of making the box constraints reliable when they have a Gaussian distribution. Solving the MPP subproblem in the reliability assessment step requires relaxation of the final boundary conditions on the system. This makes sense because it is reasonable to assume that the initial conditions of the systems could still be prescribed by the designer under uncertainty, however, this uncertainty will be propagated into the system and thus, we cannot guarantee that the final conditions will always be met under uncertainty. Thus, the MPP subproblem must be solved with the following condition:

$$\begin{aligned} x_1^{(m)}(t_0) &= 0 && m \\ x_2^{(m)}(t_0) &= 1000 && m \\ x_3^{(m)}(t_0) &= 13.23 && m/s \\ x_4^{(m)}(t_0) &= -1.288 && m/s \end{aligned} \tag{5.38}$$

$$\min_{\mathbf{d}_{u,i},\mathbf{x}_i(t)} \quad -g_i$$

subject to

$$\begin{aligned} &\dot{x}_{1,i}(t) - x_3(t) = 0 \\ &\dot{x}_{2,i}(t) - x_4(t) = 0 \\ &\dot{x}_{3,i}(t) - \tfrac{1}{m}(-L_i \sin(\eta_i) - D_{ri}\cos(\eta_i)) = 0 \\ &\dot{x}_{4,i}(t) - \tfrac{1}{m}(L_i \cos(\eta_i) - D_{ri}\sin(\eta_i) - W) = 0 \\ &\left\|\mathbf{d}_{u,i}\right\| - \beta_{t_i} = 0 \end{aligned} \tag{5.39}$$

where

$$\begin{aligned}
\mathbf{d}_{u,i} &= \Phi_{cdf}^{-1}[F_{g_i}(\mathbf{d})] \\
g_1 &= \frac{(2b+f_l)^2}{S} - g_{1,max} \leq 0 \\
g_2 &= S - S_{max}
\end{aligned} \tag{5.40}$$

The problem was solved using the commercially available software, GPOPS-II [55] on a 32 GB of RAM and an Intel(R) Xenon(R) CPU E5-2637 v3 @ 3.50 GHz processor system, with the setting shown in Table 3.1.

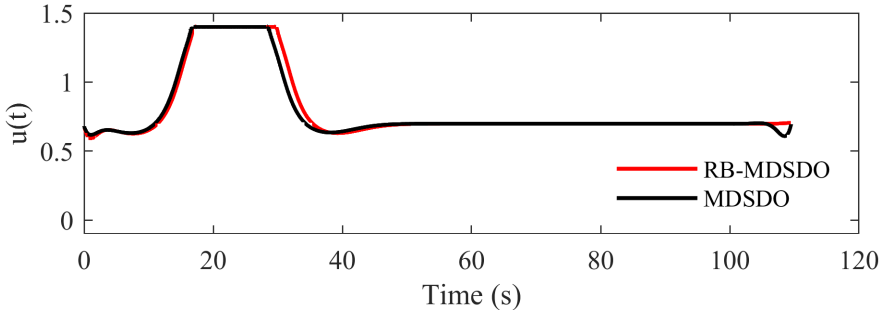

Figure 5.5: Hang glider: Optimal control trajectory

Table 5.3: Co-design results for hang glider

	a_1	a_2	b	$x_1(t_f)$	t (s)
MDSDO [a]	1.62	2.48	4.63	1,290.4	13.58
RB-MDSDO [b]	1.44	2.46	4.3	1,272.7	289.8
Diff [c]	6.85%			1.37%	

[a] Deterministic MDSDO solution, [b] RB-MDSDO solution, [c] Percent difference

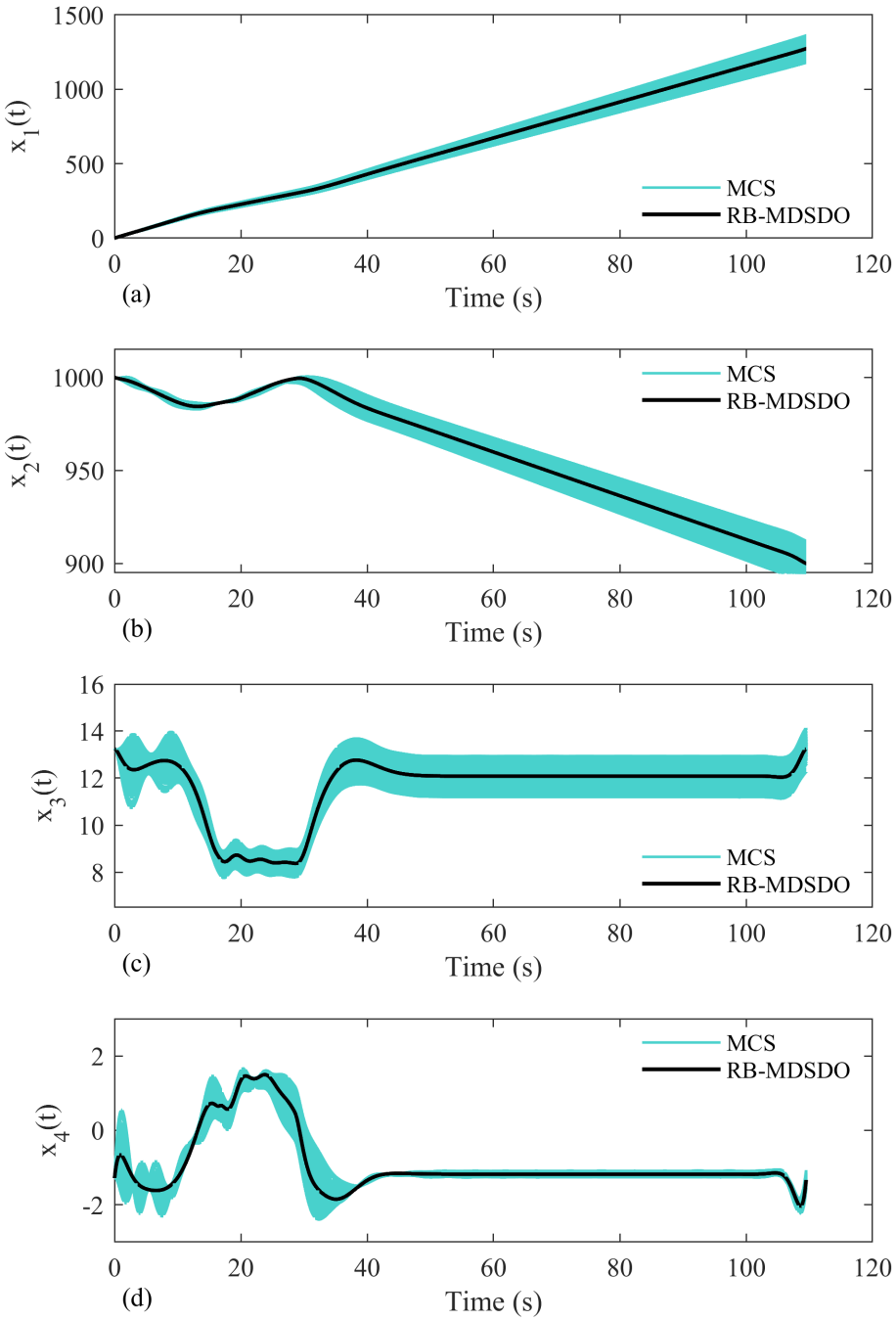

Figure 5.6: Hang glider: MCS about the solution of RB-MDSDO for state trajectories

The problem was solved in $m = 4$ SORA cycles and the results from both deterministic MDSDO and single-loop RB-MDSDO formulations are compared in Tab. 5.3. The vector of plant design has changed by 6.85% compared to the deterministic case. Also, the maximum range is reduced by 1.37% in the RB-MDSDO approach. Although less favorable, the associated risk with this design is much less. The MPPs associated with plant design variables at $m = 4$ SORA cycle for $i = 1$ and $i = 2$ are found to be $a^{*,(4)}_{1,MPP,i} = 1.62$, $a^{*,(4)}_{2,MPP,i} = 2.63$, and $b^{*,(4)}_{MPP,i} = 4.47$. and $a^{*,(4)}_{1,MPP,i} = 1.25$, $a^{*,(4)}_{2,MPP,i} = 2.27$, and $b^{*,(4)}_{MPP,i} = 4.44$, respectively. The probabilities of failure for both of the performance measure functions are then benchmarked MCS with $n = 100,000$ samples as indicated in Table 5.4:

Table 5.4: Probabilities of failure using Monte Carlo Simulation with $n = 100,000$ samples

	MDSDO	RB-MDSDO
$Pr_f\{G_1\}$	0	0
$Pr_f\{G_2\}$	0.4986	0.0468

The optimal control and state trajectories are illustrated in Fig. 5.5 and Fig. 5.6, respectively. The state trajectories are plotted against state trajectories that are obtained by performing MCS about the solution of RB-MDSDO. A sample size of $n = 1000$ is used to create these figures. It can be observed that under uncertainty, optimal control trajectories and states of system tend to deviate from the solution of the deterministic problem.

5.4.3 Active suspension co-design problem

This case study solves the co-design problem of an automotive active-suspension system under uncertainty. By solving and implementing the proposed single-loop RB-MDSDO for this complex problem, and comparing the results to the double-loop RB-MDSDO solution from Chapter 4, we discuss the scalability and efficiency of RB-MDSDO problem formulations for complex co-design problems under uncertainty.

The problem statement and its formulation was introduced in Chapter 4.2. Here, to avoid repetition, we only present the results from the single-loop RB-MDSDO approach and compare them with the solutions

Table 5.5: Automotive suspension co-design solution using double-loop and single-loop RB-MDSDO approaches

Field	DET[a]	AMV [b]	CMV[c]	HMV[d]	GO[e]	SORA[f]	Unit
d_w	0.016	0.017	0.017	0.017	0.017	0.017	m
D_h	0.156	0.157	0.157	0.157	0.157	0.157	m
p	0.037	0.035	0.035	0.035	0.035	0.035	m
Na	7.055	6.66	6.66	6.66	6.61	6.66	-
μ_{D_0}	0.007	0.008	0.008	0.008	0.008	0.008	m
μ_{D_p}	0.03	0.033	0.033	0.033	0.033	0.033	m
μ_{D_s}	0.17	0.155	0.155	0.155	0.155	0.155	m
ϕ	1.3975	1.4634	1.4634	1.4634	1.4634	1.4634	-
t	93	2611	3580	3665	100,246	2125	s
k_s	23760	29457	29457	29457	29457	29457	Nm^{-1}
c_s	724.54	750.07	750.07	750.07	750.07	750.07	Nsm^{-1}

[a] Deterministic [b] Advanced mean value [c] Conjugate mean value [d] Hybrid mean value [e] General optimization using fmincon
[f] Sequential optimization and reliability assessment

obtained from Section 4. These results are described in Table. 5.5 and indicate that the single-loop RB-MDSDO approach is more efficient compared with the double-loop RB-MDSDO approaches. Even though efficient double-loop reliability methods such as AMV, CMV, and HMV offer a significant computational advantage for the double-loop MPP-based algorithms, the single-loop nature of SORA enables a more time-efficient framework for co-design of stochastic dynamic systems. The control decision trajectory, and sprung mass response to the rough surface are illustrated in Fig. (5.7) and Fig. (5.8), respectively. As we can see from these figures, the control input and the sprung mass response for the deterministic solution is slightly different from the solution of stochastic approaches.

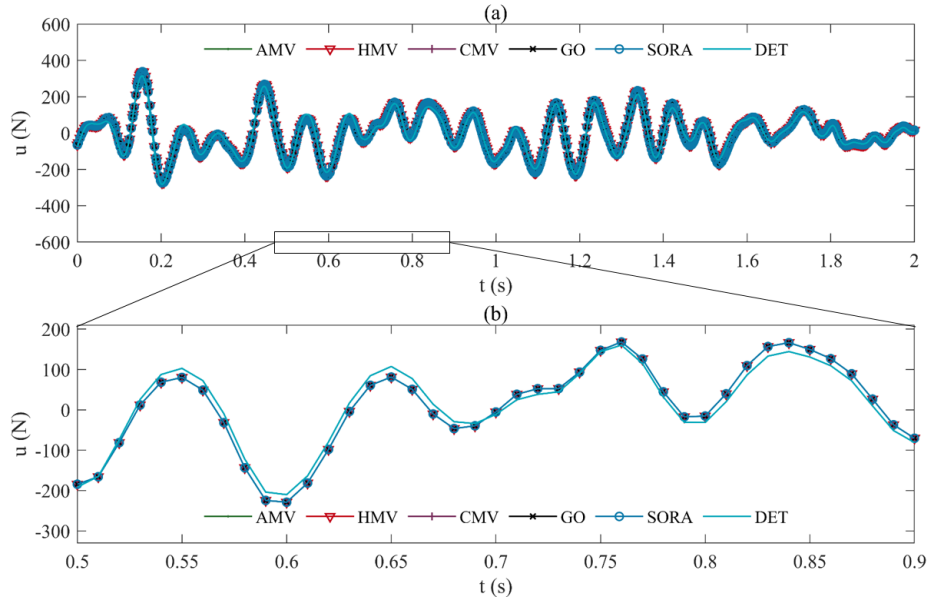

Figure 5.7: Control force for active automotive suspension: (a) complete time-history (b) magnified trajectory for $t \in [0.5\ 0.9]$.

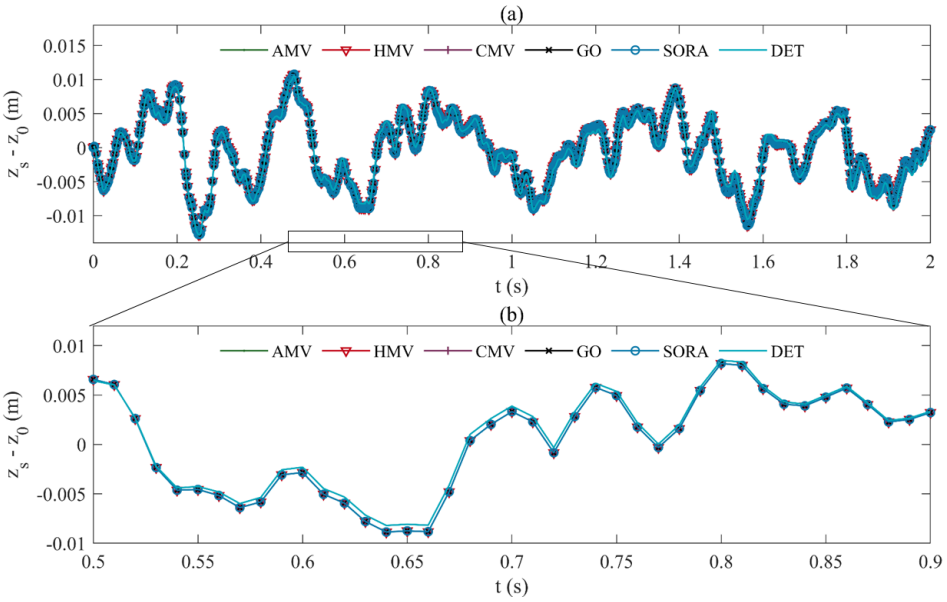

Figure 5.8: Sprung mass response to rough surface input: (a) complete time-history (b) magnified trajectory for $t \in [0.5\ 0.9]$.

5.5 Summary

This chapter introduced a single-loop MPP-based reliability analysis for RB-MDSDO problem formulation. The analysis-type dynamic equality constraints, and the algebraic equality constraints were satisfied at the vector of mean values, as well as the MPPs. The proposed formulation was then solved for three case studies to identify the implementation challenges. By solving the complex co-design problem of an automotive active suspension system and comparing the results with the double-loop RB-MDSDO, we concluded that the single-loop RB-MDSDO offers computational efficiency and is more suitable for complex dynamic systems.

Chapter 6

Application to Co-design of Hybrid-Electric Vehicle Powertrain

In the past few decades, environmental concerns have motivated more fuel-efficient vehicle alternatives in the transportation sector. Electrification of road transport through HEVs presents a viable solution to this challenge by reducing tailpipe emissions through efficient, yet more complex energy management strategies. These strategies are inherently coupled with powertrain design and thus, their identification requires methods such as co-design, resulting in a system-level optimal solution and improved performance of the vehicle.

The application of co-design approaches to HEVs has been widely investigated in the literature. The tradeoffs between fuel consumption and emissions in a simultaneous co-design problem formulation for a parallel HEV was investigated using fuzzy set theory [73]. Patil calculated a unidirectional coupling term to account for the dependence of the optimal control problem on plant design for a plug-in hybrid electric vehicle (PHEV) [74]. By calculating this term, he optimally sized the battery in a co-design formulation. Bayrak et al. introduced a heuristic approach to enumerate feasible HEV modes and find an optimal hybrid-electric powertrain architecture with the optimal control strategy determined for each mode in a nested algorithm [75]. The authors extended their study to account for a variety of loading scenarios in Ref. [76]. A convex programming approach has also been used for the simultaneous energy management and component sizing of HEVs [77, 13]. Houshmand implemented a simultaneous co-design problem formulation using multidisciplinary dynamic system design optimization for component sizing and supervisory energy management of a PHEV in Ref. [78]. A decomposition-based design optimization framework has also been used to find the powertrain design, component sizing and optimal energy management in a nested combined physical and control system design problem formulation in Ref. [79]. By simultaneously exploiting design and control spaces, these studies successfully implemented various co-design methodologies to achieve system-level optimal plant design and energy management strategies. A comprehensive review of the application of these

system-level optimization methods to HEVs can be found in Ref. [80].

Despite the successful implementation of deterministic co-design formulations for HEVs, not much research has been performed to account for the uncertainties that prevail in the design and control of these systems. These uncertainties may stem from a variety of sources including imperfect manufacturing processes, measurement errors and/or uncertain operational conditions and could potentially have a significant impact on HEV component sizing and control strategies. Consequently, this could also impact key vehicle performance measures such as energy efficiency and cost. Therefore, it is important to quantify and minimize the impact of these uncertainties on the integrated system solution of HEVs.

In this chapter, we address some of the limitations of the literature on stochastic co-design of HEVs by formulating and solving two co-design problems for a power-split HEV powertrain that account for uncertainties in both design decision variables and fixed problem parameters. Specifically, we implement and solve the complex co-design problem of a power-split hybrid-electric vehicle (HEV) powertrain using (i) an R-MDSDO, and (ii) an RB-MDSDO formulation. Moderate-fidelity mathematical models of the major components of a power-split HEV powertrain including the engine, electric motor, generator and battery pack are used to identify the optimal plant design variables, state trajectory decision variables, and control trajectory decision variables, such that the vehicle powertrain cost is minimized. This Chapter clearly demonstrates the utility of the previously proposed formulations by solving a real-world complex co-design problem under uncertainties.

6.1 Model development

A single-mode, power-split HEV powertrain model of the MY2004 Toyota Prius, along with its major components including the engine, electric machines, and battery was developed based on [78] and is illustrated in Fig. (6.1). The power-split HEV configuration combines the benefits of series and parallel hybrid configuration by employing a planetary gear set that enables a mechanical as well as an electrical path for the power output of the engine. To model the cost of the vehicle powertrain, cost models associated with each component are also presented in this section.

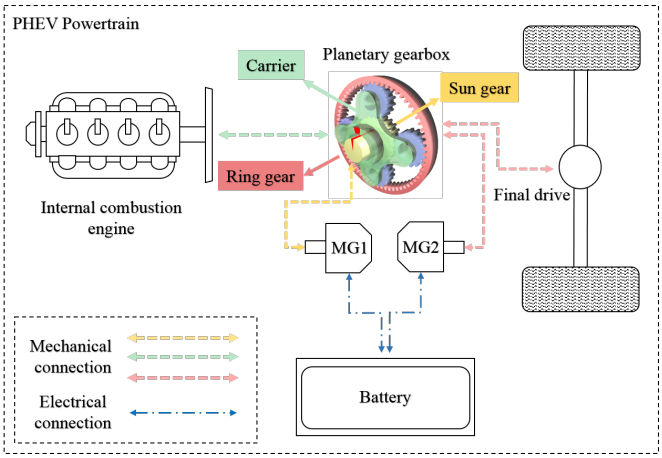

Figure 6.1: Power-split HEV powertrain configuration and components [81].

6.1.1 Powertrain model

The HEV powertrain model is characterized by one plant design variable: final drive of the transmission, FDR; two distinct state trajectory decision variables: engine speed, ω_e, and electric motor speed, ω_{mg2}; and three control trajectory decision variables: engine torque, τ_e, electric motor torque, τ_{mg2}, and generator torque τ_{mg1}. Dynamic equations for this model are based on longitudinal vehicle dynamics with the assumption of zero pinion gear inertia [82].

$$\begin{bmatrix} J_e & 0 & 0 & R+S \\ 0 & J_{mg1} & 0 & -S \\ 0 & 0 & J'_{mg2} & -R \\ -(R+S) & S & R & 0 \end{bmatrix} \begin{bmatrix} \dot{\omega}_e \\ \dot{\omega}_{mg1} \\ \dot{\omega}_{mg2} \\ F \end{bmatrix} = \begin{bmatrix} \tau_e \\ \tau_{mg1} \\ \tau'_{mg2} \\ 0 \end{bmatrix} \tag{6.1}$$

$$\omega_{mg1} = (1+\frac{R}{S})\omega_e - \frac{R}{S}\omega_{mg2} \tag{6.2}$$

$$J'_{mg2} = J_{mg2} + (J_w + m_{veh}r_{tire}^2)/FDR^2 \tag{6.3}$$

$$\tau'_{mg2} = \tau_{mg2} - F_{road}r_{tire}/FDR \tag{6.4}$$

The interaction force between the sun and planet gears is denoted by F. The number of teeth on the ring and sun gear are described by R and S, respectively. The rotational inertias of the engine, generator, electric motor, and wheels are described by J_e, J_{mg1}, J_{mg2}, and J_w, respectively. Tire radius is described by r_{tire}, and J'_{mg2} and τ'_{mg2} are the effective rotational inertia and torque of the electric motor, respectively. The vehicle's mass m_{veh}, is calculated through:

$$m_{veh} = m_e + m_{mg1} + m_{mg2} + m_{batt} + m_{chassis} + m_{ft} + m_{driver} \tag{6.5}$$

where m_e, m_{mg1}, m_{mg2}, m_{batt}, $m_{chassis}$, m_{ft} and m_{driver} are the engine, generator, motor, battery pack, chassis, full fuel tank and the driver masses, respectively. Road load on the vehicle F_{road} is estimated by calculating the rolling force F_{roll} and F_{drag}

$$F_{road} = F_{roll} + F_{drag} = \mu m_{veh} g + \frac{1}{2}\rho A_{fr} C_d (\frac{\omega_{mg2} r_{tire}}{FDR})^2 \tag{6.6}$$

where the rolling friction coefficient and the gravitational constant are denoted by μ, and g, respectively. ρ is the air density, A_{fr} is the vehicle frontal area, and C_d is the drag coefficient of the vehicle. The rotational acceleration of the engine $\dot{\omega}_e$, and electric motor $\dot{\omega}_{mg2}$ can be obtained by rearranging Eqn. (6.1) into its state-space form

$$\dot{\omega}_{mg2} = \frac{\tau_{mg2} - \frac{r_{tire}}{FDR}(F_{road}) + C\tau_e + \frac{C(R+S)-R}{S}\tau_{mg1}}{J'_{mg2} + J_{mg1}(\frac{R}{S})^2 - CJ_{mg1}\frac{R(R+S)}{S^2}} \tag{6.7}$$

$$C = \frac{J_{mg1} R(R+S)}{S^2 (J_e + J_{mg1}(\frac{R+S}{S})^2)} \tag{6.8}$$

$$\dot{\omega}_e = \frac{\tau_e + (\frac{R+S}{S})\tau_{mg1} + J_{mg1}\frac{R}{S^2}(R+S)\dot{\omega}_{mg2}}{J_e + J_{mg1}(\frac{R+S}{S})^2} \tag{6.9}$$

Table 6.1 describes the fixed parameters and constants for the powertrain model.

Table 6.1: Constants and fixed parameters for Toyota Prius 2004 powertrain.

Parameter	Notation	Value	Unit
Air density	ρ	1.225	kg/m^3
Gravitational constant	g	9.81	m/s^2
Ring gear teeth number	R	78	-
Rolling friction	μ	0.007	-
Rotational inertia of the wheels	J_w	0.74	kg.m^2
Sun gear teeth number	S	30	-
Tire radius	r_{tire}	0.282	m
Vehicle chassis mass	$m_{chassis}$	900	kg
Full fuel tank mass	m_{ft}	33.74	kg
Driver mass	m_{driver}	82.65	kg
Vehicle frontal area	A_{fr}	1.746	m^2

6.1.1.1 Engine model

A four-stroke internal combustion engine model was developed that consists of three plant design variables: engine stroke length L_{st}, engine bore diameter D_b, and compression ratio CR; one state trajectory decision variable: ω_e; and one control trajectory decision variable: τ_e. This model estimates the maximum allowable engine torque, fuel consumption rate, engine mass and rotational inertia. Maximum torque of the engine can be obtained by:

$$\tau_{e,max}(\omega_e) = \frac{bmep_{max}(\omega_e)V_{dis}}{4\pi} \tag{6.10}$$

where the maximum brake mean effective pressure $bmep_{max}$, is estimated empirically though interpolation [83] and engine displacement V_{dis} is calculated as a function of the number of cylinders n_{cyl}, D_b, and L_{st} as:

$$V_{dis} = n_{cyl}\frac{\pi}{4}D_b^2 L_{st} \tag{6.11}$$

Fuel consumption rate is then calculated as a function of indicated mean effective pressure $imep$, indicated thermal efficiency η_{IT}, and lower heating value of the fuel $LHV = 43.448$ kJ/g [84]:

$$\dot{m}_{fuel} = \frac{imepV_{dis}\frac{\omega_e}{2\pi}}{2000\eta_{IT}LHV} \tag{6.12}$$

Indicated mean effective pressure can be obtained as:

$$imep = bmep + fmep \tag{6.13}$$

where the engine brake mean effective pressure $bmep$ and its friction mean effective pressure $fmep$, can be estimated for engine displacements of 845 cc up to 2000 cc:

$$bmep = \frac{4\pi\tau_e}{V_{dis}} \tag{6.14}$$

$$fmep = 97 + 15(\frac{\omega_e}{1000}(\frac{60}{2\pi})) + 5(\frac{\omega_e}{1000}(\frac{60}{2\pi}))^2 \tag{6.15}$$

The indicated thermal efficiency can be obtained in terms of CR and heat capacity ratio $\kappa = 1.5$

$$\eta_{IT} = 1 - \frac{1}{CR^{\kappa-1}} \tag{6.16}$$

For the sake of simplicity, engine mass and its inertia are estimated based on constant peak power-to-weight/inertia ratios:

$$m_e = \frac{\tau_{e,max}(\omega_e = 5000\ rpm * \frac{2\pi}{60})}{0.6869} \tag{6.17}$$

$$J_e = \frac{m_e}{839} \tag{6.18}$$

6.1.1.2 Electric machine models

The generator and electric motor models were developed based on the mathematical formulations for the interior permanent magnet synchronous machines (IPMSM) from Ref. [85]. These models assume a symmetric performance curve with respect to the axes, and positive and negative values of torque and speed as appropriate. The variables for the electric machines are distinguished by mgi, where $i = 1$ and $i = 2$, such that $mg1$ is associated with the generator and $mg2$ is associated with the electric motor. These moderate-fidelity models predict the maximum electric machine torque at a given speed, the maximum electric machine speed, the electrical power generation/consumption at a given torque and speed, and the electric machine mass and rotational inertia. These models consist of three design-related decision variables: the stack length L_{mgi}, the stator inner diameter D_{mgi}, and the maximum stator current $I_{mgi,max}$; one state trajectory decision variable: ω_{mgi}; and one control decision trajectory: τ_{mgi}. The maximum torque of the machines is calculated by

$$\tau_{mgi,max} = \begin{cases} m_p p_i(\psi_{m,i} I_{mgi,o} cos\gamma_{i,max} + \frac{1}{2}(\xi_i - 1) L_{d_i} I_{mgi,o}^2 sin2\gamma_{i,max}), & 0 \leq \omega_{mgi} p_i \leq \omega_{mgi,b} p_i \\ m_p p_i(\psi_{m,i} I_{mgi,o} cos\gamma_i(\omega_{mgi} p_i) + \frac{1}{2}(\xi_i - 1) L_{d_i} I_{mgi,o}^2 sin2\gamma_i(\omega_{mgi} p_i)), & \omega_{mgi,b} p_i \leq \omega_{mgi} p_i \leq \omega_{mgi,max} p_i \end{cases} \tag{6.19}$$

where the number of phases in the electric machines is m_p, the number of pole pairs is p_i, the magnetic flux linkage is denoted by $\psi_{m,i}$, and $\xi_i = \frac{L_{q_i}}{L_{d_i}}$ is the saliency ratio calculated through d-q axis phase inductance L_{d_i} and L_{q_i}. Note that the rated current per phase $I_{mgi,o}$ is computed as $I_{mgi,o} = \frac{I_{mgi,max}}{\sqrt{2}}$. With the exception of p_i and m_p, which are fixed parameters, the other variables are intermediate terms that are functions of the design variables. Interested readers can refer to Ref. [78] for details. Equation (6.19) divides the calculation

of torque per ampere current angle γ_i into speeds before and after the electric machine base or rated speed $\omega_{mgi,b}$. At $\omega_{mgi} \leq \omega_{mgi,b}$, the torque per ampere current angle is a maximizer $\gamma_{i,max}$ for the torque and is calculated by differentiating Eqn. (6.19) with respect to γ_i:

$$sin\gamma_{i,max} = \begin{cases} \dfrac{-\psi_{m,i} + \sqrt{\psi_{m,i}^2 + 8(\xi_i - 1)^2 L_{d_i}^2 I_{mgi,o}^2}}{4(\xi_i - 1) L_{d_i} I_{mgi,o}} & \text{if } \xi_i > 1 \\ 0 & \text{if} \xi_i = 1 \end{cases} \tag{6.20}$$

The torque per ampere current angle $\gamma_i(\omega_{mgi} p_i)$ at any speed $\omega_{mgi} \geq \omega_{mgi,b}$ is obtained by a curve-fitting model which is a function of the electric machine design variables. The rated speed itself is given by

$$\omega_{mgi,b} = \frac{1}{p_i}\left(\frac{-C_B \pm \sqrt{(C_B^2 - 4C_A C_C)}}{2C_A}\right) \tag{6.21}$$

where C_A, C_B and C_C are related to the stator phase resistance R_{s_i} and maximum rated voltage $V_{mgi,max}$ of each electric machine as prescribed in the following equations:

$$C_A = \frac{1}{p_i(L_{q_i} I_{mgi,o} cos\gamma_{i,max})^2 + (-L_{q_i} I_{mgi,o} sin\gamma_{i,max} + \psi_{m,i})^2} \tag{6.22}$$

$$C_B = 2R_{s_i}(L_{q_i} I_{mgi,o}^2 cos\gamma_{i,max} sin\gamma_{i,max} - L_{d_i} I_{mgi,o}^2 sin\gamma_{i,max} cos\gamma_{i,max} + \psi_{m,i} I_{mgi,o} cos\gamma_{i,max}) \tag{6.23}$$

$$C_C = (R_{s_i} I_{mgi,o})^2 - V_{mgi,max}^2 \tag{6.24}$$

Note that $V_{mgi,max}$ can be obtained based on the maximum rated DC voltage $V_{DC,max}$ as $V_{mgi,max} = \frac{V_{DC,max}}{\sqrt{2}} \frac{2}{\pi}$. Also, note that R_{s_i} is a function of the electric machine design variables, the details of which can be found in [85]. The maximum electric machine speed $\omega_{mgi,max}$ occurs when the maximum torque of the electric machine reaches zero ($\tau_{mgi,max}(\omega_{mgi} * p_i) = 0$). The electrical power generation/consumption P_{mgi} is calculated

as a function of d-q axis stator voltages V_{d_i} and V_{q_i}:

$$P_{mgi} = m_p(-V_{d_i} I_{mgi} sin\gamma_i(\omega_{mgi} p_i) + V_{q_i} I_{mgi} cos\gamma_i(\omega_{mgi} p_i)) \tag{6.25}$$

$$V_{d_i} = -R_{s_i} I_{mgi} sin\gamma_i(\omega_{mgi} p_i) - \omega_{mgi} p_i L_{q_i} I_{mgi} cos\gamma_i(\omega_{mgi} p_i) \tag{6.26}$$

$$V_{q_i} = R_{s_i} I_{mgi} cos\gamma_i(\omega_{mgi} p_i) - \omega_{mgi} p_i L_{d_i} I_{mgi} sin\gamma_i(\omega_{mgi} p_i) + \omega_{mgi} p_i \psi_{m,i} \tag{6.27}$$

Here, I_{mgi} is obtained by solving the following equation for a given τ_{mgi}:

$$\tau_{mgi} = m_p p_i(\psi_{m,i} I_{mgi} cos\gamma_i(\omega_{mgi} p_i) + \frac{1}{2}(\xi_i - 1) L_{d_i} I_{mgi}^2 sin2\gamma_i(\omega_{mgi} p_i)) \quad \forall\ \omega_{mgi} p_i\ \in [0, \omega_{mgi,max} p_i] \tag{6.28}$$

Electric machine mass is calculated by accounting for the mass of stator core m_{sc_i}, stator teeth m_{st_i}, stator winding m_{sw_i}, rotor core m_{rc_i} and the permanent magnet m_{pm_i}:

$$m_{mgi} = m_{sc_i} + m_{st_i} + m_{sw_i} + m_{rc_i} + m_{pm_i} \tag{6.29}$$

$$m_{sc_i} = \frac{\pi}{4} \rho_s (D_{so_i}^2 - (D_{mgi} + 2h_{sl_i})^2) L_{mgi} \tag{6.30}$$

$$m_{st_i} = N_{slot_i} \rho_s h_{sl_i} w_{tb_i} L_{mgi} \tag{6.31}$$

$$m_{rc_i} = \rho_s L_{mgi} (\pi((\frac{D_{mgi}}{2} - g_{mech_i})^2 - D_{ri_i}^2) - N_{pm_i} w_{m_i} h_{m_i}) \tag{6.32}$$

$$m_{pm_i} = N_{pm_i} \rho_{pm} l_{pm_i} h_{pm_i} w_{pm_i} \tag{6.33}$$

$$m_{sw_i} = m_p \rho_{cu} A_{cu_i} l_{con_i} \tag{6.34}$$

Here, ρ_{cu} is the density of copper, g_{mech_i} is the mechanical air gap, N_{pm_i} is the number of permanent magnets, N_{slot_i} is the number of stator slots, ρ_{pm} is the density of the permanent magnet material, and ρ_s is the density of steel. All of the latter quantities are fixed problem parameters, described in Table 6.2. The remaining quantities are intermediate variables that are functions of the electric machine design variables and are

Table 6.2: 2004 Toyota Prius electric machines parameters.

Parameter	$mg1$	$mg2$	Unit
ρ_{cu}	8690		kg/m^3
g_{mech_i}	0.64	0.73	mm
N_{pm_i}	16	16	-
m_p	3	3	-
p_i	4	8	-
N_{slot_i}	48	48	-
ρ_{pm}	7550		kg/m^3
ρ_s	7800		kg/m^3
$V_{DC,max}$	500	500	V

explained in Refs. [86, 87, 88]. D_{so_i} is the outer stator diameter, h_{sl_i} is the stator slot depth, w_{tb_i} is the width of a stator tooth at its base, D_{ri_i} is the rotor inner diameter, l_{con_i} is the total length of the copper winding, and A_{cu_i} is the cross-sectional area of copper. Also, l_{pm_i}, w_{pm_i}, and h_{pm_i} denote the permanent magnet length, width, and height, respectively. Finally, the rotational inertia of the machines are obtained by:

$$J_{mgi_i} = \frac{1}{8}(m_{rc_i} + m_{pm_i})(D_{ri_i}^2 + (D_{mgi} - 2g_{mech_i})^2) + \frac{1}{2}\rho_s(\frac{\pi}{4}D_{ri_i}^2 L_{mgi})\frac{D_{ri_i}^2}{4}$$

6.1.1.3 Battery pack model

A lithium-ion battery model based on the work of [89] is used to predict the rate change of the battery pack state of charge, battery pack charging and discharging power limits, and battery pack mass. The number of battery cells in series N_s and parallel N_p constitute design-related decision variables, and the battery state of charge SOC is a state trajectory decision variable. The SOC rate of change is calculated as

$$\dot{SOC} = \frac{V_{oc}(SOC) - \sqrt{V_{oc}^2(SOC) - 4P_{batt}R_i(SOC)}}{2QR_i(SOC)} \tag{6.35}$$

where P_{batt} is the battery power calculated as $P_{batt} = P_{mg1} + P_{mg2}$. Battery internal resistance is denoted by $R_i(SOC)$, and its capacity is Q. The open circuit voltage $V_{oc}(SOC)$ is defined as the voltage of the battery when it is disconnected from any circuit. These terms can be calculated as:

$$V_{oc}(SOC) = N_s V_{oc,cell}(SOC) \tag{6.36}$$

$$R_i(SOC) = \frac{N_s}{N_p} R_{i,cell}(SOC) \tag{6.37}$$

$$Q = N_p Q_{cell} \tag{6.38}$$

The specifications of an A123 Systems ANR26650M1A battery cell used in Toyota Prius 2004 are used to develop this model. The map for the open circuit voltage of the battery cell $V_{oc,cell}(SOC)$, and its internal resistance $R_{i,cell}(SOC)$ are is obtained from [90]. Battery cell capacity Q_{cell} is equal to 2.3 Ah. The mass of the battery pack m_{batt} is based on the mass of each individual cell $m_{cell} = 0.0727$ kg and is calculated as:

$$m_{batt} = N_s N_p m_{cell} \tag{6.39}$$

Finally, for the proper operation and safety of battery cells, their charging and discharging current is limited based on the allowable current $I_{lim_{cell}}(SOC)$ and allowable voltage $V_{lim}(SOC)$:

$$I_{lim_{cell}}(SOC) = \frac{V_{oc,cell}(SOC) - V_{lim}(SOC)}{R_{i,cell}(SOC)} \tag{6.40}$$

In the above, $V_{lim}(SOC)$ is calculated at minimum and maximum allowable battery SOC, equivalent to 2.08 V and 3.7 V for discharging and charging, respectively. Accordingly, the battery pack power limit $P_{lim}(SOC)$ can be calculated as:

$$P_{lim}(SOC) = V_{oc}(SOC)N_p I_{lim_{cell}}(SOC) - R_i(SOC)[N_p I_{lim}(SOC)]^2 \tag{6.41}$$

For more details on the battery model, interested readers are referred to [89] and [91].

6.1.2 Component cost model

6.1.2.1 Engine cost model

A capital cost model for an in-line four cylinder engine was developed in this section [92]. This model outputs the engine cost in USD ($) as a function of its maximum brake power $P_{e,max}$ in kW at 5000 rpm. Note that the engine capital cost C_e is independent of the manufacturing year and is valid up to 2030.

$$C_e = 14.5P_{e,max} + 531 \tag{6.42}$$

6.1.2.2 Electric machine cost models

A capital cost model for the electric machines was developed as a function of the manufacturing year Y between 2015 and 2030 [93, 94, 95]. This model outputs the capital cost of the motor/generator, C_{mgi} in USD ($) as a function of the motor/generator power rating $P_{mgi,max}$ in kW.

$$C_{mgi} = (-0.6193Y + 1268.4)P_{mgi,max} + 425 \tag{6.43}$$

6.1.2.3 Battery pack cost model

The cost of the battery pack for hybrid and plug-in hybrid applications has been widely investigated in the literature [96]. This model is based on a linear regression approach to the data from [97, 95, 98, 99, 96, 94]. The model represents the battery cost C_{batt} in USD ($) as a function of the manufacturing year Y, rated battery energy $E_{batt,max}$, and rated battery power $P_{batt,max}$

$$C_{batt}(\$) = (-17.056Y + 34947)E_{batt,max} + 22P_{batt,max} + 680 \tag{6.44}$$

Note that the coefficient of $P_{batt,max}$ is a specific constant cost factor in \$/kW and the manufacturing cost is \$ 680 [94]. The battery usable energy curve, along with the power-to-energy ratio curve were used to estimated the maximum battery power.

6.2 HEV powertrain co-design formulations

In this section, we develop the deterministic HEV powertrain co-design problem formulations. The objective is to minimize the total vehicle powertrain cost over a standard US06 duty cycle, which represents aggressive driving behavior with intermittent fluctuations in speed and acceleration over 8.01 miles and 596 seconds. An acceleration performance criteria is also included as a dynamic phase in both the deterministic and robust formulations. Therefore, each co-design formulation is posed as a two-phase dynamic optimization problem, where Phase (1) constrains the $0-100$ kph acceleration performance time and Phase (2) minimizes the HEV powertrain cost over the standard duty cycle. This formulation results in obtaining the optimal powertrain component designs, the optimal state and control trajectories during each phase of the problem, and the optimal $0-100$ kph acceleration time.

6.2.1 Deterministic MDSDO formulation

The deterministic HEV powertrain co-design problem formulation shown is based on the nominal MDSDO formulation described in Eqn. (2.1). The decision variables include

$$\begin{aligned}
\mathbf{d} &= [N_s, N_p, L_{mgi}, D_{mgi}, I_{mgi,max}, L_{st}, D_b, CR, FDR] \\
\mathbf{x}(t) &= [\omega_e, \omega_{mg2}, SOC] \\
\mathbf{u}(t) &= [\tau_e, \tau_{mg1}, \tau_{mg2}]
\end{aligned}$$

and $0-100$ kph acceleration time $t_{100} = t_{f1}$, where t_{f1} is the final time of Phase (1) of the co-design problem. Because the number of fixed parameters in $\mathbf{p}$ are quite numerous, they are not explicitly shown here but are generally assumed to be present in the objective function and constraints as appropriate. With these definitions, the objective function is given by

$$\min_{\mathbf{d},\mathbf{x}(t),\mathbf{u}(t),t_{f1}} \quad \int_{t_{f1}}^{t_{f2}} \left[C_{fuel}\dot{m}_{fuel}(\mathbf{d},\mathbf{x}(t),\mathbf{u}(t),t;\mathbf{p})\right]dt + C_{cap}(\mathbf{d};\mathbf{p}) \tag{6.45}$$

where $C_{fuel} =$ \$ 2.76/gallon is the gasoline price, assumed to be constant throughout vehicle's lifetime, and t_{f2} is the final time of Phase (2) of the co-design problem. The capital cost $C_{cap}(\mathbf{d};\mathbf{p})$ consists of the cost of the major powertrain components including the engine $C_e(\mathbf{d};\mathbf{p})$, generator $C_{mg1}(\mathbf{d};\mathbf{p})$, motor $C_{mg2}(\mathbf{d};\mathbf{p})$, and battery $C_{batt}(\mathbf{d};\mathbf{p})$. Using a linear depreciation cost model, we can distribute the capital costs over the driving distance [100]:

$$C_{cap}(\mathbf{d};\mathbf{p}) = \frac{d_{cyc}}{d_{yr}y_v}(C_e(\mathbf{d};\mathbf{p}) + C_{mg1}(\mathbf{d};\mathbf{p}) + C_{mg2}(\mathbf{d};\mathbf{p}) + C_{batt}(\mathbf{d};\mathbf{p})) \tag{6.46}$$

In this equation, $d_{cyc} = 8.01$ mi is the distance of the US06 driving cycle. $d_{yr} = 10,650$ mi is the average annual mileage, estimated based on the maximum and minimum average annual miles for vehicles by vehicle age [101]. Accordingly, the average vehicle lifetime, $y_v = 9$ yr, is estimated from the same data, and based on the fact that automotive companies warrant the battery in HEVs for 8 to 10 years. The objective function in Eqn. (6.45) is subject to multiple constraints:

$$0 \leq \tau_e \leq \tau_{e,max}(\mathbf{d},\mathbf{x}(t),t;\mathbf{p}) \tag{6.47}$$

$$0 \leq \omega_e \leq \omega_{e,max} \tag{6.48}$$

$$\dot{\omega}_{e,min} \leq \dot{\omega}_e \leq \dot{\omega}_{e,max} \tag{6.49}$$

$$-\tau_{mg1,max}(\mathbf{d},\mathbf{x}(t),t;\mathbf{p}) \leq \tau_{mg1} \leq \tau_{mg1,max}(\mathbf{d},\mathbf{x}(t),t;\mathbf{p}) \tag{6.50}$$

$$-\omega_{mg1,max}(\mathbf{d};\mathbf{p}) \leq \omega_{mg1} \leq \omega_{mg1,max}(\mathbf{d};\mathbf{p}) \tag{6.51}$$

$$\tau_{mg1}\omega_{mg1} \leq 0 \tag{6.52}$$

$$-\tau_{mg1}\omega_{mg1} - \tau_e\omega_e \leq 0 \tag{6.53}$$

$$-\tau_{mg2,max}(\mathbf{d},\mathbf{x}(t),t;\mathbf{p}) \leq \tau_{mg2} \leq \tau_{mg2,max}(\mathbf{d},\mathbf{x}(t),t;\mathbf{p}) \tag{6.54}$$

$$0 \leq \omega_{mg2} \leq \omega_{mg2,max}(\mathbf{d};\mathbf{p}) \tag{6.55}$$

$$SOC_{min} \leq SOC \leq SOC_{max} \tag{6.56}$$

$$SOC_{t_{f1}} = SOC_{t_{f2}} = 0.8 \tag{6.57}$$

$$P_{lim,min}(\mathbf{d},\mathbf{x}(t),t) \leq P_{batt}(\mathbf{d},\mathbf{x}(t),\mathbf{u}(t),t;\mathbf{p}) \leq P_{lim,max}(\mathbf{d},\mathbf{x}(t),t) \tag{6.58}$$

$$E_{batt,min} \leq E_{batt}(\mathbf{d}) \leq E_{batt,max} \tag{6.59}$$

$$V_{veh,min}(t) \leq \frac{\omega_{mg2} r_{tire}}{FDR} \leq V_{veh,max}(t) \tag{6.60}$$

$$V_{veh,min}(t_{f1}) \leq \frac{\omega_{mg2}(t_{f1}) r_{tire}}{FDR} \leq V_{veh,max}(t_{f1}) \tag{6.61}$$

$$t_{f1} \leq t_{f1,max} \tag{6.62}$$

$$\mathbf{d}_{min} \leq \mathbf{d} \leq \mathbf{d}_{max} \tag{6.63}$$

$$\dot{\mathbf{x}}(t) - \mathbf{f}(\mathbf{d},\mathbf{x}(t),\mathbf{u}(t),t;\mathbf{p}) = \mathbf{0} \tag{6.64}$$

Engine performance maps and the rate of change in engine speed are described in Eqns. (6.47)-(6.49). Performance map constraints for the generator are shown in Eqns. (6.50) and (6.51), and its proper operation is given by Eqns. (6.52) and (6.53). Equations (6.54) and (6.55) describe the performance map constraints for the electric motor. Battery operation and safety is ensured by limiting the battery pack's state of charge as in Eqn. (6.56). Equation (6.57) ensures that the battery pack has the same *SOC* at the end of the trip. The power of the battery pack is maintained within the allowable range through Eqn. (6.58) and its energy is

maintained within the feasible range for HEVs through Eqn. (6.59). Constraint (6.60) is included to ensure that the vehicle follows the US06 driving cycle with a tolerance of ± 5 km/hr. The vehicle's acceleration performance corresponding to $0-100$ kph is included in Eqns. (6.61) and (6.62), where t_{f1} is the final time of Phase (1). We note that the bounds on $V(t_{f1})$ are tight enough to ensure $0-100$ kph constraint satisfaction in no more than $t_{f1,max} = 10$ seconds. Finally, design variables are bounded in Eqn. (6.63) and dynamic constraints are described in Eqn. (6.64).

6.2.2 Integer value constraint heuristics

Battery design variables N_s and N_p are discrete in nature and thus, require methods from mixed-integer nonlinear programming to be solved. Here, we treat N_s and N_p as continuous variables and relax all of the integer-related constraints [102, 103]. Then, we augment the objective function with penalty terms for integer constraint violation. We employed a continuously differentiable penalty function with constant penalty terms $\hat{P}_1$ and $\hat{P}_2$

$$P(N_s, N_p) = \hat{P}_1 \sin(N_s \pi)^2 + \hat{P}_2 \sin(N_p \pi)^2 \tag{6.65}$$

where the penalty terms $\hat{P}_1 = 10$ and $\hat{P}_2 = 10$ are weighting factors, emphasizing the significance of each term in the objective function. This penalty function is augmented to the objective functions introduced in Eqn. (6.45).

6.3 Robust MDSDO of HEV powertrain

The co-design problem of HEV powertrain under uncertainty can be addressed through the proposed R-MDSDO problem formulation. Therefore, in this section, we formulate and solve a robust co-design problem for a power-split HEV powertrain that accounts for uncertainties in both design decision variables and fixed problem parameters. The impact of these uncertainties within the HEV powertrain model and problem formulation is demonstrated by comparing the results from R-MDSDO to those from the associated deterministic co-design problem.

6.4 R-MDSDO formulation

The robust HEV powertrain co-design problem formulation is based on the nominal R-MDSDO problem formulation shown in Eqn. (3.3). In this study, we assume that the sources of uncertainty are from random plant design variables D_b, L_{st}, L_{mgi}, and D_{mgi} as well as random problem parameters C_{fuel}, d_{yr}, y_v, m_{driver}, copper resistivity coefficient R_{cu}, copper wire diameter D_{cu}. For simplicity, all random variables are assumed to be Gaussian. Because the random design variables are all geometric, they are assumed to have uncertainty due to machining variations, and their standard deviations were obtained or estimated from the literature as appropriate [104]. It is well-known that C_{fuel} is highly-variable due to volatile market conditions, and so its standard deviation was estimated using the maximum of the weekly price data from January 1990 to March 2012 [105]. Similarly, m_{driver} is known to be highly-uncertain due to the wide array of potential drivers, and so its standard deviation was extracted from Ref. [106] for men and women between the ages of 20-39. The randomness in R_{cu} is driven by the fluctuating temperature conditions that the vehicle must operate in; therefore, its standard deviation was estimated over a 20 deg temperature difference. A 1 *mm* measurement tolerance is used as the basis for the uncertainty in D_{cu}. The uncertainty in d_{yr} is estimated based on the minimum and the maximum miles per vehicle by vehicle age according to Ref. [101]. Finally, since automotive companies warrant the battery pack in HEVs for 8 to 10 years, the range of variations for this parameter is estimated to be two years. The standard deviation for the latter three parameters is estimated with the assumption of Gaussian distribution for the range of $\pm 3\sigma$ variations for the associated uncertain parameters. Note that the standard deviation values for all random variables can be found in Table 6.3.

The uncertainties propagated onto the state trajectory decision variables are accounted for by considering measurement errors and tolerances for each quantity as appropriate. For example, a percentage uncertainty of 0.51 is used from Ref. [107] to estimate the variance in the engine and electric motor speed measurements. The SOC variance was chosen to keep the estimation error less than 5%. Note that the variance value for each state trajectory decision variable can be found in Table III. With all the uncertainties now defined, the objective function for the R-MDSDO problem formulation of the HEV powertrain co-design problem can be shown as

Table 6.3: Standard Deviations/Variances of Random Design Variables, Parameters, and State Trajectories.

$\boldsymbol{D}$	$\boldsymbol{P}$	$\boldsymbol{X}$
$\sigma_{L_{mg1}} = 0.01$	$\sigma_{C_{fuel}} = 0.95$	$Var[\omega_e(t)] = 0.89$
$\sigma_{D_{mg1}} = 0.01$	$\sigma_{m_{driver}} = 32.86$	
$\sigma_{L_{mg2}} = 0.01$	$\sigma_{d_{yr}} = 950$	$Var[\omega_{mg2}(t)] = 1.60$
$\sigma_{D_{mg2}} = 0.01$	$\sigma_{y_v} = 0.333$	
$\sigma_{D_b} = 0.01$	$\sigma_{R_{cu}} = 5.5 \times 10^{-9}$	$Var[SOC(t)] = 0.0083$
$\sigma_{L_{st}} = 0.01$	$\sigma_{D_{cu_1}} = 1.67 \times 10^{-4}$	

$$\min_{\mathbf{d},\boldsymbol{\mu}_D,\boldsymbol{\mu}_X(t),\mathbf{u}(t),t_{f1}} \quad \phi = w\left[\int_{t_{f1}}^{t_{f2}} \Big[\mu_{C_{fuel}}\dot{m}_{fuel}(\boldsymbol{\mu}_D,\boldsymbol{\mu}_X(t),\mathbf{u}(t),t;\boldsymbol{\mu}_P)\Big]dt + C_{cap}(\mathbf{d},\boldsymbol{\mu}_D;\boldsymbol{\mu}_P)\right] + (1-w)\sigma_\phi^2 \tag{6.66}$$

Here, $\mathbf{d} = [N_s, N_p, I_{mgi,max}, CR, FDR]$, $\boldsymbol{\mu}_D = [\mu_{L_{mgi}}, \mu_{D_{mgi}}, \mu_{L_{st}}, \mu_{D_b}]$, $\boldsymbol{\mu}_P = [\mu_{C_{fuel}}, \mu_{m_{driver}}, \mu_{R_{cu}}, \mu_{D_{cu}}, \mu_{d_{yr}}, \mu_{y_v}]$, and σ_ϕ is the standard deviation of the objective function. Also, $w = 0.85$ is the weighting factor associated with the multiobjective problem formulation. Defining $\mathbf{S} = (\mathbf{d}, \boldsymbol{\mu}_D, \boldsymbol{\mu}_X(t), \mathbf{u}(t), t; \boldsymbol{\mu}_P)$, the constraints are:

$$0 \leq \tau_e \leq \tau_{e,max}(\mathbf{S}) - k_{6.47}\sigma_{6.47} \tag{6.67}$$

$$0 \leq \mu_{\omega_e} \leq \omega_{e,max} - k_{\omega_e}\sqrt{Var[\omega_e(t)]} \tag{6.68}$$

$$\dot{\omega}_{e,min} + k_{6.49}\sigma_{6.49} \leq \dot{\mu}_{\omega_e} \leq \dot{\omega}_{e,max} - k_{6.49}\sigma_{6.49} \tag{6.69}$$

$$-\tau_{mg1,max}(\mathbf{S}) + k_{6.50}\sigma_{6.50} \leq \tau_{mg1} \leq \tau_{mg1,max}(\mathbf{S}) - k_{6.50}\sigma_{6.50} \tag{6.70}$$

$$-\omega_{mg1,max}(\mathbf{d},\boldsymbol{\mu}_D;\boldsymbol{\mu}_P) + k_{6.51}\sqrt{Var[\omega_{mg1}(t)]} \leq \mu_{\omega_{mg1}} \leq \omega_{mg1,max}(\mathbf{d},\boldsymbol{\mu}_D;\boldsymbol{\mu}_P) - k_{6.51}\sqrt{Var[\omega_{mg1}(t)]} \tag{6.71}$$

$$\tau_{mg1}\mu_{\omega_{mg1}} \leq 0 \tag{6.72}$$

$$-\tau_{mg1}\mu_{\omega_{mg1}} - \tau_e\mu_{\omega_e} \leq 0 \tag{6.73}$$

$$-\tau_{mg2,max}(\mathbf{S}) + k_{6.54}\sigma_{6.54} \leq \tau_{mg2} \tag{6.74}$$

$$\leq \tau_{mg2,max}(\mathbf{S}) - k_{6.54}\sigma_{6.54} \tag{6.75}$$

$$0 \leq \mu_{\omega_{mg2}} \leq \omega_{mg2,max}(\mathbf{d}, \boldsymbol{\mu}_D; \boldsymbol{\mu}_P) - k_{\omega_{mg2}}\sqrt{Var[\omega_{mg2}(t)]} \tag{6.76}$$

$$SOC_{min} + k_{SOC}\sqrt{Var[SOC(t)]} \leq \mu_{SOC} \tag{6.77}$$

$$\leq SOC_{max} - k_{SOC}\sqrt{Var[SOC(t)]} \tag{6.78}$$

$$\mu_{SOC}(t_{f_1}) = \mu_{SOC}(t_{f_2}) = 0.8 \tag{6.79}$$

$$P_{lim,min}(\mathbf{d}, \boldsymbol{\mu}_X, t) + k_{6.58}\sigma_{6.58} \leq P_{batt}(\mathbf{S}) \leq P_{lim,max}(\mathbf{d}, \boldsymbol{\mu}_X, t) - k_{6.58}\sigma_{6.58} \tag{6.80}$$

$$E_{batt,min} \leq E_{batt}(\mathbf{d}) \leq E_{batt,max} \tag{6.81}$$

$$V_{veh,min}(t) + k_{6.60}\sigma_{6.60} \leq \frac{\mu_{\omega_{mg2}} r_{tire}}{FDR} \leq V_{veh,max}(t) - k_{6.60}\sigma_{6.60} \tag{6.82}$$

$$V_{veh,min}(t_{f1}) + k_{6.61}\sigma_{6.61} \leq \frac{\mu_{\omega_{mg2}}(t_{f1}) r_{tire}}{FDR} \tag{6.83}$$

$$\leq V_{veh,max}(t_{f1}) - k_{6.61}\sigma_{6.61} \tag{6.84}$$

$$t_{f1} \leq t_{f1,max} \tag{6.85}$$

$$\mathbf{d}_{min} \leq \mathbf{d} \leq \mathbf{d}_{max} \tag{6.86}$$

$$\boldsymbol{\mu}_{D_{min}} + k_D\sigma_D \leq \boldsymbol{\mu}_D \leq \boldsymbol{\mu}_{D_{max}} - k_D\sigma_D \tag{6.87}$$

$$\dot{\boldsymbol{\mu}}_x(t) - \mathbf{f}(\mathbf{S}) = \mathbf{0} \tag{6.88}$$

In all of the above equations, $k_{(.)} = 3$ and all $\sigma_{(.)}$ with numerical subscripts represent the standard deviation of the corresponding equation from the deterministic formulation. Note that since Eqns. (6.72) and (6.73) are functionality constraints of the generator, they are treated deterministically to allow for real-world operation of these machines. Also, note that boundary conditions are assumed to be of Type (i) equality constraints [50], and thus are only satisfied at their expected value.

6.4.1 Results and Discussion

The co-design problems were solved using the commercially-available MATLAB®-based software, GPOPS−II [55]. The required Jacobian information for the robust co-design problem was obtained by

forward differentiation in ADIMAT toolbox [65]. The problems were solved on two Intel Xeon E5-2637 v3 processors containing 32GB RAM and using the key GPOPS-II settings introduced in Table 6.4.

Table 6.4: GPOPS-II settings.

Field	Setting
Mesh method	hp-LiuRao-Legendre
Mesh tolerance	10^{-3}
NLP solver	IPOPT
IPOPT tolerance	10^{-4}
IPOPT max iterations	1000

The optimal design variables from the R-MDSDO problem formulation are compared with the deterministic case in Table 6.5. As expected, uncertainties in **d** and **p** significantly affect several component designs of the HEV powertrain. In particular, N_s has dropped, resulting in 4.11% and 3.92% reductions in m_{batt} and rated battery capacity, respectively. Although the rated generator capacity remains relatively flat, D_{mg1} has decreased dramatically, resulting in a 25.43% reduction in m_{mg1}. For the electric motor, $I_{mg2,max}$ has increased by 8.07%, which in turn boosts the rated power by 7.3%. The only component designs that remain relatively unaffected by uncertainties in **d** and **p** in this study are the engine and transmission final drive.

Table 6.5: Numerical Results for Deterministic and Robust HEV Powertrain Co-Design Problem Formulations.

Component	Quantity	MDSDO	R-MDSDO	Unit
Battry Pack	N_s	76	73	-
	N_p	27	27	-
	m_{batt}	149.18	143.29	kg
	Rated Capacity	15.57	14.96	kWh
Generator	D_{mg1}	156.86	129.82	mm
	L_{mg1}	27.90	27.93	mm
	$I_{mg1,max}$	67.50	67.55	A
	m_{mg1}	12.76	9.5188	kg
	Rated Power	31.92	31.98	kW
Electric Motor	D_{mg2}	145.71	146.31	mm
	L_{mg2}	92.4	91.81	mm
	$I_{mg2,max}$	118.58	128.15	A
	m_{mg2}	29.5	29.5	kg
	Rated Power	55.38	59.74	kW
Engine	D_b	67.97	68.01	mm
	L_{st}	76.23	76.29	mm
	CR	13	12.99	-
	m_e	39.59	39.67	kW
	Rated Power	110.08	110.31	kg
Transmission	FDR	2.7	2.7	-
Operational Cost		0.154	0.178	$
Capital Cost		1.113	1.092	$
Total Cost		1.267	1.270	$
Run Time		13,827	20,521	s

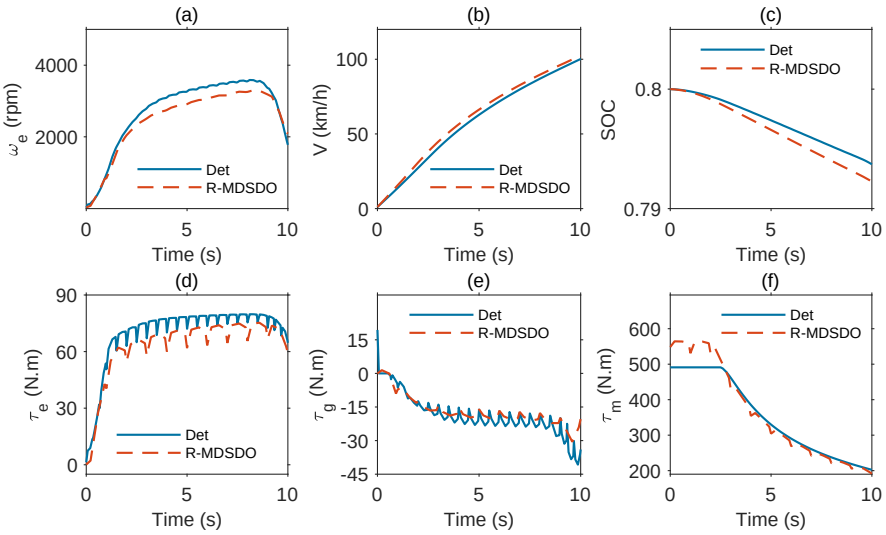

Figure 6.2: State and control trajectories for Phase (1): acceleration performance.

Optimal state and control decision trajectories from the deterministic and R-MDSDO formulations are compared in Figs. 6.2-6.4. The results illustrate how HEV powertrain energy management strategies are significantly impacted when we account for uncertainties in co-design problem formulations. Figure 6.2 describes these trajectories during the $0-100$ kph acceleration time, or Phase (1). Note that the $0-100$ kph requirement is satisfied more aggressively in the R-MDSDO formulation because its associated powertrain design solution results in a more conservative estimate of total optimal powertrain cost, the latter of which often competes with vehicle acceleration performance. According to Fig. 6.2 (f) and due to the higher efficiency and instant torque that electric machines can deliver—especially at low speeds—the electric motor operates at a higher torque to ensure the satisfaction of the $0-100$ kph acceleration requirement in a robust manner. Consequently, due to the larger power demand from the motor, the battery power demand is larger and *SOC* drops more aggressively for the R-MDSDO solution (Fig. 6.2 (c)). This in turn leads to the engine operating at a slightly lower power under robust considerations.

The trajectories associated with the US06 driving cycle, or Phase (2) are described in Fig. 6.3 and Fig. 6.4. According to Fig. 6.3 (c) Fig. 6.4 (a), in the robust case, the engine runs at a more consistent power level and the SOC drops more significantly during the highway drive portion. Specifically, the fluctuations in engine torque and speed in the robust case are not nearly as much as in the deterministic case (in fact, the powertrain never even enters into an EV operation mode), and the motor pulls more electrical power

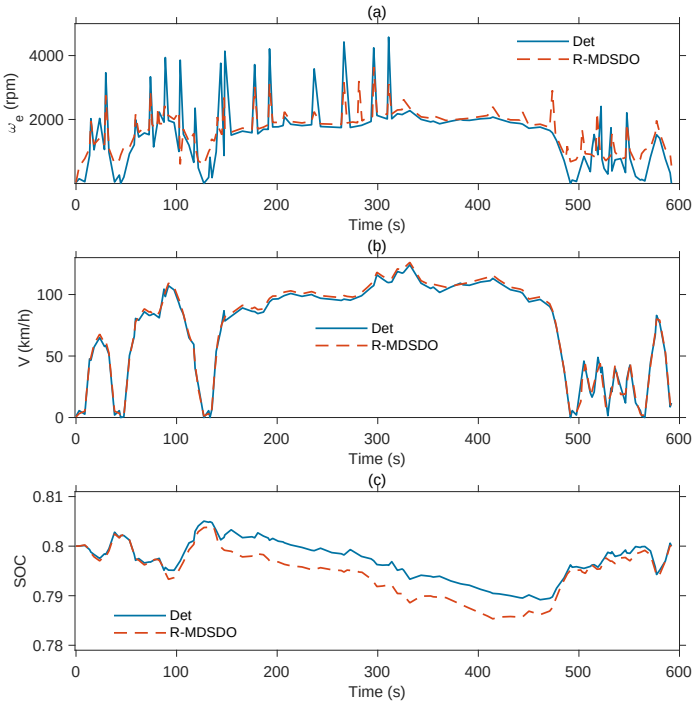

Figure 6.3: State trajectories for Phase (2): US06 drive cycle.

from the battery during the highway drive portion of the drive cycle. This behavior can be justified because given the large uncertainty in C_{fuel}, it is preferable to avoid operating the engine over-aggressively. Instead, more electrical power could be used from the battery rather than the engine-generator set during high-power operation such as highway driving. The detailed breakdown of cost in each case is also displayed in Table 6.5. As expected, the total cost of the objective function has increased by 0.24% compared to the deterministic case. While this percent difference appears almost negligible, there was still a significant impact of uncertainty on the component designs and energy management strategy. In fact, in the R-MDSDO solution, the operational cost has increased by 13.48%, while the capital cost has dropped by 1.89%. The reduced sensitivity of the R-MDSDO solution to uncertainties is characterized in Fig. 6.5. Finally, the proposed R-MDSDO approach incurs a high computational cost that is mainly associated with computing the derivative information to estimate the variance quantities of both the objective and inequality constraint functions. The computational efficiency of R-MDSDO could be significant reduced using alternative techniques such as automatic differentiation.

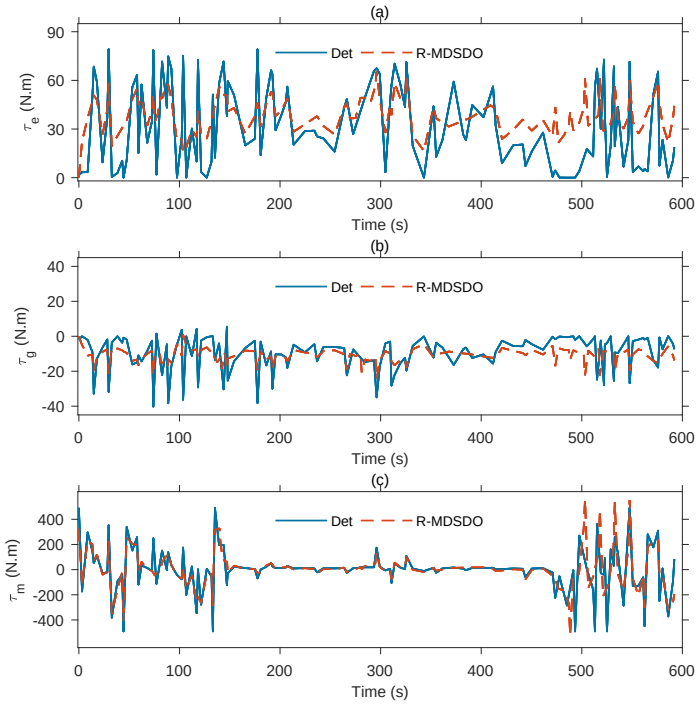

Figure 6.4: Control trajectories for Phase (2): US06 drive cycle.

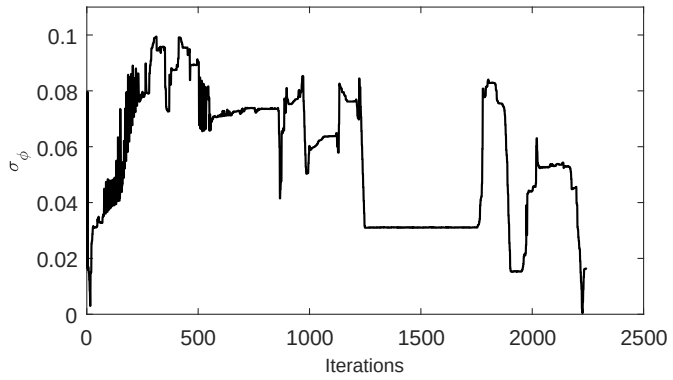

Figure 6.5: Reduction in the standard deviation of the objective function in R-MDSDO iterations.

6.5 Reliability-based MDSDO of HEV powertrain

R-MDSDO and RB-MDSDO approaches are both effective methods in dealing with uncertainties in co-design problem formulations. However, RB-MDSDO provides a more rigorous evaluation of the probabilistic constraints—resulting in a more reliable solution. Although the single-loop RB-MDSDO formulations are superior in terms of computational cost, in this chapter, we use a double-loop RB-MDSDO because of their simple implementation. Here, we examine the application and impact of the proposed double-loop RB-MDSDO approach on the co-design of HEV powertrain problem.

6.5.1 RB-MDSDO of HEV powertrain

The RB-MDSDO HEV powertrain co-design problem formulation is based on the nominal problem formulation shown in Eqn. (4.1). In this section, we assume that the sources of uncertainty are from random plant design variables D_b, and L_{st}, as well as random problem parameters C_{fuel}, average annual mileage S, and average vehicle lifetime y_v. For simplicity, all random variables are assumed to be Gaussian. Because the random design variables are all geometric, they are assumed to have uncertainty due to machining variations, and their standard deviations were obtained or estimated from the literature as appropriate [104]. The standard deviation/variance information for fixed problem parameters C_{fuel}, S, and y_v are similar to those introduced in Chapter 6.4. With all the uncertainties now defined, the objective function for the RB-MDSDO problem formulation of the HEV powertrain co-design problem can be shown as

$$\min_{\mathbf{d},\boldsymbol{\mu}_D,\boldsymbol{\mu}_X(t),\boldsymbol{x}^*_{MPP}(t),\mathbf{u}(t)} \quad \phi = \left[\int_0^{t_f=596} \left[\mu_{C_{fuel}} \dot{m}_{fuel}(\boldsymbol{\mu}_D, \boldsymbol{\mu}_X(t), \mathbf{u}(t), t; \boldsymbol{\mu}_P) \right] dt + C_{cap}(\mathbf{d}, \boldsymbol{\mu}_D; \boldsymbol{\mu}_P) \right] \tag{6.89}$$

Here, $\mathbf{d} = [N_s, N_p, L_{mgi}, D_{mgi}, I_{mgi,max}, CR, FDR]$, $\boldsymbol{\mu}_D = [\mu_{L_{st}}, \mu_{D_b}]$, $\boldsymbol{\mu}_P = [\mu_{C_{fuel}}, and \mu_{d_{yr}}, \mu_{y_v}]$. Defining $\mathbf{S} = (\mathbf{d}, \boldsymbol{\mu}_D, \boldsymbol{\mu}_X(t), \mathbf{u}(t), t; \boldsymbol{\mu}_P)$, the constraints are:

$$\tau_e - \tau_{e,max}(\mathbf{d}, \boldsymbol{\mu}_D, \boldsymbol{\mu}_X(t), \boldsymbol{x}^*_{MPP}(t), \mathbf{u}(t), t; \boldsymbol{\mu}_P) \leq \mathbf{0} \tag{6.90}$$

$$0 \leq \mu_{\omega_e} \leq \omega_{e,max} \tag{6.91}$$

$$\dot{\omega}^*_{e,MPP} - \dot{\omega}_{e,max} \leq 0 \tag{6.92}$$

$$-\tau_{mg1,max}(\mathbf{d},\boldsymbol{\mu}_X(t),\mathbf{u}(t),t;\boldsymbol{\mu}_P) \leq \tau_{mg1} \leq \tau_{mg1,max}(\mathbf{d},\boldsymbol{\mu}_X(t),\mathbf{u}(t),t;\boldsymbol{\mu}_P) \tag{6.93}$$

$$-\omega_{mg1,max}(\mathbf{d};\boldsymbol{\mu}_P) \leq \mu_{\omega_{mg1}} \leq \omega_{mg1,max}(\mathbf{d};\boldsymbol{\mu}_P) \tag{6.94}$$

$$\tau_{mg1}\mu_{\omega_{mg1}} \leq 0 \tag{6.95}$$

$$-\tau_{mg1}\mu_{\omega_{mg1}} - \tau_e\mu_{\omega_e} \leq 0 \tag{6.96}$$

$$-\tau_{mg2,max}(\mathbf{d},\boldsymbol{\mu}_D,\boldsymbol{\mu}_X(t),\mathbf{u}(t),t;\boldsymbol{\mu}_P) \leq \tau_{mg2} \leq \tau_{mg2,max}(\mathbf{d},\boldsymbol{\mu}_D,\boldsymbol{\mu}_X(t),\mathbf{u}(t),t;\boldsymbol{\mu}_P) \tag{6.97}$$

$$0 \leq \mu_{\omega_{mg2}} \leq \omega_{mg2,max}(\mathbf{d};\boldsymbol{\mu}_P) \tag{6.98}$$

$$SOC_{min} \leq \mu_{SOC} \leq SOC_{max} \tag{6.99}$$

$$\mu_{SOC}(t_0) = \mu_{SOC}(t_f) = 0.8 \tag{6.100}$$

$$P_{lim,min}(\mathbf{d},\boldsymbol{\mu}_X,t) \leq P_{batt}(\mathbf{d},\boldsymbol{\mu}_D,\boldsymbol{\mu}_X(t),\mathbf{u}(t),t;\boldsymbol{\mu}_P) \leq P_{lim,max}(\mathbf{d},\boldsymbol{\mu}_X,t) \tag{6.101}$$

$$E_{batt,min} \leq E_{batt}(\mathbf{d}) \leq E_{batt,max} \tag{6.102}$$

$$V_{veh,min}(t) \leq \frac{\mu_{\omega_{mg2}} r_{tire}}{FDR} \leq V_{veh,max}(t) \tag{6.103}$$

$$\mathbf{d}_{min} \leq \mathbf{d} \leq \mathbf{d}_{max} \tag{6.104}$$

$$\boldsymbol{\mu}_{D_{min}} + k_D\boldsymbol{\sigma}_D \leq \boldsymbol{\mu}_D \leq \boldsymbol{\mu}_{D_{max}} - k_D\boldsymbol{\sigma}_D \tag{6.105}$$

$$\dot{\boldsymbol{\mu}}_x(t) - \mathbf{f}(\mathbf{d},\boldsymbol{\mu}_D,\boldsymbol{\mu}_X(t),\mathbf{u}(t),t;\boldsymbol{\mu}_P) = \mathbf{0} \tag{6.106}$$

$$\dot{\mathbf{x}}^*_{MPP,i}(t) - \mathbf{f}(\mathbf{d},\boldsymbol{\mu}_D,\boldsymbol{\mu}_X(t),\mathbf{u}(t),t;\boldsymbol{\mu}_P) = \mathbf{0} \qquad i = 1,2 \tag{6.107}$$

This formulation entails two stochastic inequality constraints: Eqns. (6.90) and (6.92). These constraints are reliably satisfied at their MPPs, which are obtained for the reliability of $\beta = 3$. Note that since Eqns. (6.72) and (6.73) are functionality constraints of the generator, they are treated deterministically to allow for real-world operation of these machines. Also, note that boundary conditions are assumed to be of Type (i) equality constraints [50], and thus are only satisfied at their expected value.

6.5.2 Results and Discussion

Similar to the previous problems, the solution to the RB-MDSDO was obtained using the commercially-available MATLAB®-based software, GPOPS−II [55], with the same setting introduces in Table 6.4.

Table 6.6: Numerical Results for Deterministic and RB-MDSDO HEV Powertrain Co-Design Problem Formulations.

Component	Quantity	MDSDO	RB-MDSDO	Unit
Battry Pack	N_s	66	74	-
	N_p	32	27	-
	m_{batt}	153.54	145.25	kg
	Rated Capacity	16.03	15.17	kWh
Generator	D_{mg1}	156.45	145.04	mm
	L_{mg1}	32.96	33.55	mm
	$I_{mg1,max}$	67.56	67.56	A
	m_{mg1}	14.37	12.9	kg
	Rated Power	31.93	31.95	kW
Electric Motor	D_{mg2}	131	129.52	mm
	L_{mg2}	100.02	86.93	mm
	$I_{mg2,max}$	98.08	120.88	A
	m_{mg2}	29.5	29.5	kg
	Rated Power	45.98	56.43	kW
Engine	D_b	67.98	76.5	mm
	L_{st}	76.27	86.07	mm
	CR	12.99	13	-
	m_e	110.18	157.46	kg
	Rated Power	39.63	56.63	kW
Transmission	FDR	2.7	2.7	-
Operational Cost		0.165	0.223	$
Capital Cost		1.119	1.117	$
Total Cost		1.28	1.34	$
Run Time		12,964	135,190	s

The optimal design variables from the RB-MDSDO problem formulation are compared with the deterministic case in Table 6.6. As expected, uncertainties in **d** and **p** significantly affect several component designs of the HEV powertrain. In particular, N_s and N_p have changed by 12.12% and 15.63%, respectively, resulting in 5.4% and 5.37% variations in m_{batt} and rated battery capacity, respectively. Although the rated generator capacity remains relatively flat, D_{mg1} has decreased dramatically, resulting in a 10.23% reduction in m_{mg1}. For the electric motor, L_{mg2} and $I_{mg2,max}$ has increased by 13.09% and 23.25%, respectively, which in turn boosts the rated power by 22.73%. The engine design variables D_b and L_{st} have changed dramatically by 12.5% and 12.85%, respectively, resulting in an increase in m_e and rated power by 42.9%, and 42.9%, respectively. The only component design that remain relatively unaffected by uncertainties in **d** and **p** in this study is the transmission final drive.

Optimal state and control decision trajectories from the deterministic and RB-MDSDO formulations are compared in Figs. 6.6 and 6.7. According to these trajectories, the engine runs at higher speeds in RB-MDSDO, which along with higher engine power, allows the reliable satisfaction of Eqn. (6.90). In addition, the motor is pulling more power from the battery during the highway drive portion of the drive cycle, which results in the higher SOC drop in in RB-MDSDO.

The detailed breakdown of cost in each case is also displayed in Table 6.6. As expected, the total cost of the objective function has increased by 4.69% compared to the deterministic case. In the RB-MDSDO solution, the operational cost has increased by 35.15%, while the capital cost has dropped by 0.18%. Finally, the proposed RB-MDSDO approach incurs a higher computational cost that is mainly associated with estimating the reliability of the performance measure functions.

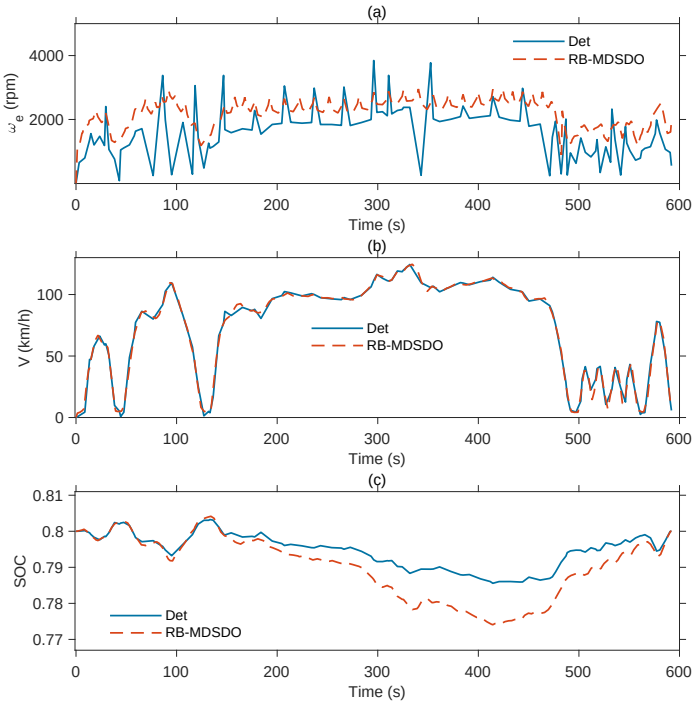

Figure 6.6: State trajectories for the US06 drive cycle.

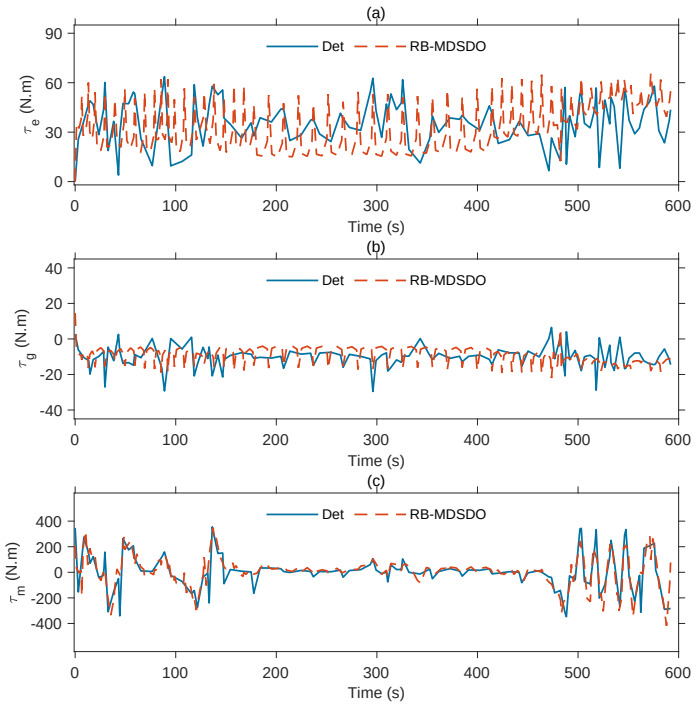

Figure 6.7: Control trajectories for the US06 drive cycle.

Chapter 7

Conclusions and Future work

With the growing complexity of dynamic engineering systems, it is necessary for designers to implement multidisciplinary approaches in developing new artifacts. MDSDO employs techniques from multidisciplinary design optimization and optimal control theory to create a balance formulation for co-design problems. Until recently, these approaches have been limited to the deterministic co-design formulations. However, uncertainties have a significant impact on the integrated solution and performance of dynamic systems. Therefore, in this dissertation, we proposed novel formulations that systematically account for uncertainties within design decision variables and fixed problem parameters.

7.1 R-MDSDO Conclusions

In Chapter 3, we established a robust co-design formulation for stochastic dynamic systems. Using a simultaneous formulation within the balanced framework of MDSDO, we developed the first robust MDSDO problem formulation, known as R-MDSDO. The proposed robust formulation was applied to two case studies and results indicated the significant impact of the robust approach on the overall system solution, as well as its performance. Consequently, this study demonstrated the importance of applying RDO principles to co-design problems.

One unique challenge in the implementation of the proposed methodology was to prescribe the full covariance matrix for the entire set of random variables. Design-related decision variables were assumed to be independent, while the distinct state decision variables were assumed to be independent (having a cross-covariance of zero), unless an algebraic equality constraint defines their statistical dependency. Finally, we assumed that the auto-covariance term associated with state trajectories at different time steps was zero and we only prescribed non-zero values for the variance term. This assumption facilitated the robust

procedure significantly and provided a good approximation. By employing this assumption, we could obtain reasonably meaningful solutions to the robust co-design problems.

Another limitation is imposed due to the inherent nature of RDO problems: the need for numerical differentiation to estimate the variances of functions of random variables. In this study, we obtained the derivatives analytically when possible, and used numerical differentiation for complex problems. This might lead to a computationally expensive problem formulation when applied to RDO-based co-design problems with a large number of variables. A potential remedy for this high computational time would be the usage of automatic differentiation.

7.2 RB-MDSDO Conclusions

Despite the relative simplicity of R-MDSDO, more rigorous techniques are required to reliably satisfy the stochastic inequality constraints. Therefore, we developed and implemented the first known reliability-based MDSDO approach for stochastic co-design problems. Using the robust and efficient PMA along with FORM in an MPP-based formulation, we first developed a double-loop RB-MDSDO algorithm and solved it for a complex automotive active-suspension co-design problem using AMV, CMV, HMV, and a general optimizer such as MATLAB's fmincon.

To improve the computational efficiency of the proposed formulation for the computationally-intensive co-design problems, we used the principles of SORA to develop a single-loop RB-MDSDO problem. By comparing the results for the automotive active-suspension with those obtained from the double-loop formulation, we concluded that in general, despite the advantages of the double-loop formulations in having a smaller MPP optimization subproblem, the decoupled nature of the single-loop SORA algorithm better suits the complexities, as well as the computational time of complex co-design formulations. Among the double-loop RB-MDSDO approaches, AMV is more computationally efficient; however, HMV is generally more numerically stable and thus, is recommended for a larger class of problems.

7.3 HEV application Conclusions

HEVs generally operate under uncertain conditions and are subject to imperfect manufacturing processes. The impact of these uncertainties on powertrain design and energy management strategies of HEVs

was captured within the balanced formulation of R-MDSDO and RB-MDSDO. These formulations account for uncertainty in design variables, and fixed problem parameters; therefore they offer significant improvement over other proposed approaches in the literature. Accounting for these uncertainties results in a system-level optimal solution that generally exhibits large variations compared to the the deterministic case. These variations directly impact vehicle's key characteristics and thus, affect its performance and overall cost. These studies clearly demonstrate the utility of the proposed approaches to real-world co-design problems.

7.4 Future work

Despite the benefits of the proposed formulations, the multidisciplinary nature of stochastic co-design requires methods not only from the design discipline, but also from the stochastic optimal control theory. An important future direction of this research is to implement techniques that capture the impact of uncertainties from state trajectory decision variables and control trajectory decision variables. This future research direction addresses one of the limitations of this study: the assumption that the uncertainty in the state trajectory decision variables is only a result of uncertainties from design decision variables and problem parameters. In reality, the states are directly subject to external noise that affects their auto-covariance and/or cross-covariance characteristics. In addition, since any practical implementation of co-design problems requires a closed-loop control structure, an important future direction for this research would be to close the control loop in the co-design problem. For the current study, this structure results in stochastic optimal control trajectory decisions. This issue needs to be addressed in the future research.

Another direction of this research is to ease the computational expense of the proposed problem formulations. Both R-MDSDO and RB-MDSDO formulations require the estimation of gradient information to perform the reliability analysis or estimate the variance/covariance information. Techniques such as automatic differentiation, along with more advanced reliability approaches could reduce the computational burden of stochastic co-design problems.

A more accurate evaluation os the probabilistic constraint within RB-MDSDO formulations requires a second-order reliability method (SORM). Specifically, since a lot of real-world engineering problems entail nonlinear dynamics and performance measure functions, the usage of SORM within RB-MDSDO can improve the accuracy of their final solution. In addition, implementing more advanced stochastic methods

such as a simultaneous robust and reliable MDSDO formulation, known as $R^2 - \text{MDSDO}$ could further advance the state of the art formulations for stochastic co-design.

Finally, with the availability of large amounts of data through sensor deployment in many engineering applications, including electrified vehicles, and the current attempts in the literature to utilize this data for design or control purposes, a certain future direction of the deterministic and stochastic co-design approaches is to investigate the utility and application of artificial intelligence to the simultaneous design and control optimization problem of dynamic systems. Specifically, this data can be used to capture the uncertainties that are present in the environment in order to create models that adapt to variations in the environmental conditions.

References

[1] James T Allison, Tinghao Guo, and Zhi Han. Co-design of an Active Suspension Using Simultaneous Dynamic Optimization. *Journal of Mechanical Design*, 136(8):081003, 2014.

[2] Anand P Deshmukh and James T Allison. Multidisciplinary Dynamic Optimization of Horizontal Axis Wind Turbine Design. *Structural and Multidisciplinary Optimization*, 53(1):15–27, 2016.

[3] Diane L Peters, PY Papalambros, and AG Ulsoy. Control Proxy Functions for Sequential Design and Control Optimization. *Journal of Mechanical Design*, 133(9), 2011.

[4] Hosam K Fathy, Julie A Reyer, Panos Y Papalambros, and AG Ulsov. On the Coupling Between the Plant and Controller Optimization Problems. In *Proceedings of American control conference, 2001.*, volume 3, pages 1864–1869. IEEE, 2001.

[5] Julie A Reyer and Panos Y Papalambros. Optimal Design and Control of an Electric DC Motor. In *Proceedings of the 1999 ASME Design Engineering Technical Conferences*, pages 85–96. Citeseer, 1999.

[6] H Fathy, PY Papalambros, and AG Ulsoy. On Combined Plant and Control Optimization. In *8th Cairo University international conference on mechanical design and production*. Cairo University Cairo, Egypt, 2004.

[7] Julie A Reyer and Panos Y Papalambros. Combined Optimal Design and Control with Application to an Electric DC Motor. *Journal of Mechanical Design*, 124(2):183–191, 2002.

[8] Dennis Assanis, G Delagrammatikas, R Fellini, Z Filipi, J Liedtke, N Michelena, P Papalambros, D Reyes, D Rosenbaum, A Sales, et al. Optimization Approach to Hybrid Electric Propulsion System Design. *Journal of Structural Mechanics*, 27(4):393–421, 1999.

[9] Vincenzo Galdi, Lucio Ippolito, Antonio Piccolo, and Alfredo Vaccaro. A Genetic-based Methodology for Hybrid Electric Vehicles Sizing. *Soft Computing*, 5(6):451–457, 2001.

[10] James T Allison and Daniel R Herber. Special Section on Multidisciplinary Design Optimization: Multidisciplinary Design Optimization of Dynamic Engineering Systems. *AIAA Journal*, 52(4):691–710, 2014.

[11] Hosam K Fathy, Panos Y Papalambros, A Galip Ulsoy, and Davor Hrovat. Nested Plant/Controller Optimization with Application to Combined Passive/Active Automotive Suspensions. In *Proceedings of the 2003 American Control Conference, 2003.*, volume 4, pages 3375–3380. IEEE, 2003.

[12] Daniel R Herber and James T Allison. Nested and Simultaneous Solution Strategies for General Combined Plant and Controller Design Problems. In *International Design Engineering Technical Conferences and Computers and Information in Engineering Conference*, volume 2A of *43rd Design Automation Conference*. American Society of Mechanical Engineers, 2017.

[13] Nikolce Murgovski, Xiaosong Hu, Lars Johannesson, and Bo Egardt. Combined Design and Control Optimization of Hybrid Vehicles. *Handbook of clean energy systems*, pages 1–14, 2015.

[14] Saeed Azad, Mohammad Behtash, Arian Houshmand, and Michael Alexander-Ramos. Comprehensive PHEV Powertrain Co-design Performance Studies Using MDSDO. In *World Congress of Structural and Multidisciplinary Optimisation*, pages 83–97. Springer, 2017.

[15] Diane L Peters, Panos Y Papalambros, and A Galip Ulsoy. On Measures of Coupling Between the Artifact and Controller Optimal Design Problems. In *Proceedings of the 2009 ASME design engineering technical conference*, 2009.

[16] Julie A. Reyer. *Combined Embodiment Design and Control Optimization: Effects of Cross-disciplinary Coupling*. PhD thesis, The University of Michigan, 2000.

[17] Ricardo M Paiva, Curran Crawford, and Afzal Suleman. Robust and Reliability-based Design Optimization Framework for Wing Design. *AIAA Journal*, 52(4):711–724, 2014.

[18] Richard F Gunst. Response Surface Methodology: Process and Product Optimization Using Designed Experiments. *Technometrics*, 38(3):284–286, 1996.

[19] Om Prakash Yadav, Sunil S Bhamare, and Ajay Rathore. Reliability-based Robust Design Optimization: A Multi-objective Framework Using Hybrid Quality Loss Function. *Quality and Reliability Engineering International*, 26(1):27–41, 2010.

[20] Genichi Taguchi. Introduction to Quality Engineering: Designing Quality into Products and Processes. *Quality and Reliability Engineering International*, 4(2):198, 1988.

[21] C Zang, MI Friswell, and JE Mottershead. A Review of Robust Optimal Design and its Application in Dynamics. *Computers & structures*, 83(4-5):315–326, 2005.

[22] Gyung-Jin Park, Tae-Hee Lee, Kwon Hee Lee, and Kwang-Hyeon Hwang. Robust Design: An Overview. *AIAA journal*, 44(1):181–191, 2006.

[23] Sirisha Rangavajhala, Anoop Mullur, and Achille Messac. The Challenge of Equality Constraints in Robust Design Optimization: Examination and New Approach. *Structural and Multidisciplinary Optimization*, 34(5):381–401, 2007.

[24] Alan Parkinson, Carl Sorensen, and Nader Pourhassan. A General Approach for Robust Optimal Dsign. *Journal of mechanical design*, 115(1):74–80, 1993.

[25] Achintya Haldar and Sankaran Mahadevan. Probability, Reliability, and Statistical Methods in Engineering Design. *Bautechbik*, 77(5):379, 2000.

[26] R Timothy Marler and Jasbir S Arora. Survey of Multi-objective Optimization Methods for Engineering. *Structural and multidisciplinary optimization*, 26(6):369–395, 2004.

[27] Ikjin Lee, KK Choi, Liu Du, and David Gorsich. Dimension Reduction Method for Reliability-based Robust Design Optimization. *Computers & Structures*, 86(13-14):1550–1562, 2008.

[28] Christopher Mattson and Achille Messac. Handling Equality Constraints in Robust Design Optimization. In *44th AIAA/ASME/ASCE/AHS/ASC Structures, Structural Dynamics, and Materials Conference*, page 1780, 2003.

[29] Xiaoping Du, Agus Sudjianto, and Wei Chen. An Integrated Framework for Optimization Under Uncertainty Using Inverse Reliability Strategy. *Journal of Mechanical Design*, 126(4):562–570, 2004.

[30] Byungsu Kang, Dong-Wook Kim, KK Choi, and Dong-Hun Kim. Enriched Performance Measure Approach for Efficient Reliability-based Electromagnetic Designs. *IEEE Transactions on Magnetics*, 53(6):1–4, 2017.

[31] Jeongwoo Han. Sequential Linear Programming Coordination Strategy for Deterministic and Probabilistic Analytical Target Cascading. 2008.

[32] Dhanesh Padmanabhan, Ravindra Tappeta, and Stephen Batill. Monte Carlo Simulation in Reliability-based Optimization Applied to Multidisciplinary System Design. In *44th AIAA/ASME/ASCE/AHS/ASC Structures, Structural Dynamics, and Materials Conference*, page 1503, 2003.

[33] Sang Hoon Lee and Wei Chen. A Comparative Study of Uncertainty Propagation Methods for Black-box-type Problems. *Structural and Multidisciplinary Optimization*, 37(3):239, 2009.

[34] Dongbin Xiu and George Em Karniadakis. The Wiener–Askey Polynomial Chaos for Stochastic Differential Equations. *SIAM journal on scientific computing*, 24(2):619–644, 2002.

[35] Kyung Choi and Byeng Youn. On Probabilistic Approaches for Reliability-based Design Optimization (RBDO). In *9th AIAA/ISSMO Symposium on Multidisciplinary Analysis and Optimization*, page 5472, 2002.

[36] Byeng D Youn, Kyung K Choi, and Young H Park. Hybrid Analysis Method for Reliability-based Design Optimization. *Journal of Mechanical Design*, 125(2):221–232, 2003.

[37] Jian Tu, Kyung K Choi, and Young H Park. A New Study on Reliability-based Design Optimization. *Journal of mechanical design*, 121(4):557–564, 1999.

[38] Byeng D Youn and Kyung K Choi. An Investigation of Nonlinearity of Reliability-based Design Optimization Approaches. *Journal of mechanical design*, 126(3):403–411, 2004.

[39] Y-T Wu, HR Millwater, and TA Cruse. Advanced Probabilistic Structural Analysis Method for Implicit Performance Functions. *AIAA journal*, 28(9):1663–1669, 1990.

[40] Y-T Wu. Computational Methods for Efficient Structural Reliability and Reliability Sensitivity Analysis. *AIAA journal*, 32(8):1717–1723, 1994.

[41] KK Choi, Byeng D Youn, and Ren-Jye Yang. Moving Least Square Method for Reliability-based Design Optimization. *Proc. 4th World Cong. Structural & Multidisciplinary Optimization*, 2001.

[42] Rafael Holdorf Lopez and André Teófilo Beck. Reliability-based Design Optimization Strategies based on FORM: a Review. *Journal of the Brazilian Society of Mechanical Sciences and Engineering*, 34(4):506–514, 2012.

[43] Byeng D Youn and Kyung K Choi. Selecting Probabilistic Approaches for Reliability-based Design Optimization. *AIAA journal*, 42(1):124–131, 2004.

[44] Sankaran Mahadevan. *Probability, Reliability, and Statistical Methods in Engineering Design*. Wiley, 2000.

[45] Marcos A Valdebenito and Gerhart I Schuëller. A Survey on Approaches for Reliability-based Optimization. *Structural and Multidisciplinary Optimization*, 42(5):645–663, 2010.

[46] Rüdiger Rackwitz. Reliability Analysis—a Review and Some Perspectives. *Structural safety*, 23(4):365–395, 2001.

[47] Murray Rosenblatt. Remarks on a Multivariate Transformation. *The annals of mathematical statistics*, 23(3):470–472, 1952.

[48] Xiaoping Du and Beiqing Huang. Reliability-based Design Optimization with Equality Constraints. *International journal for numerical methods in engineering*, 72(11):1314–1331, 2007.

[49] Xiang Li, Prasanth B Nair, ZhiGang Zhang, Lin Gao, and Chen Gao. Aircraft Robust Trajectory Optimization Using Nonintrusive Polynomial Chaos. *Journal of Aircraft*, 51(5):1592–1603, 2014.

[50] Saeed Azad and Michael J Alexander-Ramos. Robust MDSDO for Co-design of Stochastic Dynamic Systems. *Journal of Mechanical design*, 142(1), 2019.

[51] Saeed Azad and Michael J. Alexander-Ramos. Robust MDSDO for Co-design of Stochastic Dynamic Systems. volume Volume 2A: 44th Design Automation Conference of *International Design Engineering Technical Conferences and Computers and Information in Engineering Conference*, 08 2018. V02AT03A002.

[52] F Topputo and C Zhang. Survey of Direct Transcription for Low-thrust Space Trajectory Optimization with Applications. In *Abstract and Applied Analysis*, volume 2014. Hindawi, 2014.

[53] Diego Pardo, Lukas Möller, Michael Neunert, Alexander W Winkler, and Jonas Buchli. Evaluating Direct Transcription and Nonlinear Optimization Methods for Robot Motion Planning. *IEEE Robotics and Automation Letters*, 1(2):946–953, 2016.

[54] John T Betts and William P Huffman. Mesh Refinement in Direct Transcription Methods for Optimal Control. *Optimal Control Applications and Methods*, 19(1):1–21, 1998.

[55] Michael A Patterson and Anil V Rao. GPOPS-II: A MATLAB Software for Solving Multiple-phase Optimal Control Problems Using Hp-adaptive Gaussian Quadrature Collocation Methods and Sparse Nonlinear Programming. *ACM Transactions on Mathematical Software (TOMS)*, 41(1):1, 2014.

[56] Gerald C Cottrill. *Hybrid Solution of Stochastic Optimal Control Problems Using Gauss Pseudospectral Method and Generalized Polynomial Chaos Algorithms*. PhD Thesis, Air Force Institute of Technology, Wright-Patterson Air Force Base, OH, March 2012.

[57] Andreas Wächter and Lorenz T Biegler. On the Implementation of an Interior-Point Filter Line-Search Algorithm for Large-Scale Nonlinear Programming. *Mathematical programming*, 106(1):25–57, 2006.

[58] R. Bulirsch, E. Nerz, H. J. Pesch, and O. von Stryk. Combining Direct and Indirect Methods in Optimal Control: Range Maximization of a Hang Glider. In R. Bulirsch, A.Miele, J. Stoer, and K.H. Well, editors, *Optimal Control Calculus of Variations, Optimal Control Theory and Numerical Methods*, volume 111 of *International series of numerical mathematics*, pages 273–288. Publisher Name, Berlin, Germany, 1993.

[59] Jürgen Lorenz. Numerical Solution of the Minimum-time Flight of a Glider Through a Thermal by Use of Multiple Shooting Methods. *Optimal Control Applications and Methods*, 6(2):125–140, 1985.

[60] Xiao Huang, Kiran Pippalapalli, and Bernd Chudoba. Aerodynamic Analysis of a Class II High Performance Hang Glider- The ATOS. In *44th AIAA Aerospace Sciences Meeting and Exhibit*, page 446, 2006.

[61] Saeed Azad and Michael J Alexander-Ramos. Reliability-based MDSDO for Co-design of Stochastic Dynamic Systems. In *ASME International Mechanical Engineering Congress and Exposition*, volume 83518, page V014T14A018. American Society of Mechanical Engineers, 2019.

[62] James T Allison, Michael Kokkolaras, and Panos Y Papalambros. Optimal Partitioning and Coordination Decisions in Decomposition-based Design Optimization. *Journal of Mechanical Design*, 131(8):081008, 2009.

[63] Michael W Sayers. The Little Book of Profiling: Basic Information About Measuring and Interpreting Road Profiles. 1998.

[64] Joseph Edward Shigley, Charles R Mischke, and R. Budynas. Mechanical Engineering Design. *New York*, 2003.

[65] Christian H. Bischof, H. Martin Bücker, Bruno Lang, Arno Rasch, and Andre Vehreschild. Combining Source Transformation and Operator Overloading Techniques to Compute Derivatives for MATLAB Programs. In *Proceedings of the Second IEEE International Workshop on Source Code Analysis and Manipulation (SCAM 2002)*, pages 65–72, Los Alamitos, CA, USA, 2002. IEEE Computer Society.

[66] Xiaoping Du and Wei Chen. Sequential Optimization and Reliability Assessment Method for Efficient Probabilistic Design. *Journal of Mechanical Design*, 126(2):225–233, 2004.

[67] Xiaoping Du and Wei Chen. Sequential Optimization and Reliability Assessment Method for Efficient Probabilistic Pesign. In *ASME 2002 International Design Engineering Technical Conferences and Computers and Information in Engineering Conference*, pages 871–880. American Society of Mechanical Engineers, 2002.

[68] Xiaoping Du and Wei Chen. Sequential Optimization and Reliability Assessment for Multidisciplinary Systems Design. *Journal of Mechanical Design*, 126(2):225–233, 2004.

[69] Xiaoping Du, Jia Guo, and Harish Beeram. Sequential Optimization and Reliability Assessment for Multidisciplinary Systems Design. *Structural and Multidisciplinary Optimization*, 35(2):117–130, 2008.

[70] Chen Jiang, Haobo Qiu, Xiaoke Li, Ning Ma, Liang Gao, and Xiwen Cai. Datp-based Sequential Optimization and Reliability Assessment for RBDO. In *2016 International Conference on Probabilistic Methods Applied to Power Systems (PMAPS)*, pages 1–6. IEEE, 2016.

[71] VS Vassiliadis, RWH Sargent, and CC Pantelides. Solution of a Class of Multistage Dynamic Optimization Problems. 1. Problems Without Path Constraints. *Industrial & Engineering Chemistry Research*, 33(9):2111–2122, 1994.

[72] Fenfen Xiong, Shishi Chen, and Ying Xiong. Dynamic System Uncertainty Propagation Using Polynomial Chaos. *Chinese Journal of Aeronautics*, 27(5):1156–1170, 2014.

[73] Lianghong Wu, Yaonan Wang, Xiaofang Yuan, and Zhenlong Chen. Multiobjective Optimization of HEV Fuel Economy and Emissions Using the Self-Adaptive Differential Evolution Algorithm. *IEEE Transactions on vehicular technology*, 60(6):2458–2470, 2011.

[74] R. M. Patil. *Combined Design and Control Optimization: Application to Optimal PHEV Design and Control for Multiple Objectives*. PhD thesis, University of Michigan, Ann Arbor (MI), 2012.

[75] Alparslan Emrah Bayrak, Yi Ren, and Panos Y Papalambros. Design of Hybrid-electric Vehicle Architectures Using Auto-generation of Feasible Driving Modes. In *ASME 2013 international design engineering technical conferences and computers and information in engineering conference*, pages V001T01A005–V001T01A005. American Society of Mechanical Engineers, 2013.

[76] Alparslan Emrah Bayrak, Yi Ren, and Panos Papalambros. Optimal Dual-mode Hybrid Electric Vehicle Powertrain Architecture Aesign for a Variety of Loading Scenarios. In *ASME 2014 International Design Engineering Technical Conferences and Computers and Information in Engineering Conference*, pages V003T01A005–V003T01A005. American Society of Mechanical Engineers, 2014.

[77] Bo Egardt, Nikolce Murgovski, Mitra Pourabdollah, and Lars Johannesson Mardh. Electromobility Studies Based on Convex Optimization: Design and Control Issues Regarding Vehicle Electrification. *IEEE Control Systems*, 34(2):32–49, 2014.

[78] Arian Houshmand. *Multidisciplinary Dynamic System Design Optimization of Hybrid Electric Vehicle Powertrains*. PhD thesis, University of Cincinnati, 2016.

[79] Alparslan Emrah Bayrak, Namwoo Kang, and Panos Y Papalambros. Decomposition-based Design Optimization of Hybrid Electric Powertrain Architectures: Simultaneous Configuration and Sizing Design. *Journal of Mechanical Design*, 138(7):071405, 2016.

[80] Emilia Silvas, Theo Hofman, Nikolce Murgovski, LF Pascal Etman, and Maarten Steinbuch. Review of Optimization Strategies for System-level Design in Hybrid Electric Vehicles. *IEEE Transactions on Vehicular Technology*, 66(1):57–70, 2017.

[81] Saeed Azad, Mohammad Behtash, Arian Houshmand, and Michael J Alexander-Ramos. PHEV Powertrain Co-design with Vehicle Performance Considerations Using MDSDO. *Structural and Multidisciplinary Optimization*, pages 1–15, 2019.

[82] Jinming Liu and Huei Peng. Modeling and Control of a Power-split Hybrid Vehicle. *IEEE Transactions on Control Systems Technology*, 16(6):1242–1251, 2008.

[83] Edward K. Nam and Robert Giannelli. Fuel Consumption Modeling of Conventional and Advanced Technology Vehicles in the Physical Emission Rate Estimator (PERE). Technical report, US Environmental Protection Agency, 2005.

[84] John B. Heywood et al. *Internal Combustion Engine Fundamentals*. Mcgraw-hill New York, 1988.

[85] W. L. Soong. *Design and Modeling of Axially-laminated Interior Permanent Magnet Motor Drives for Field-weakening Applications*. PhD thesis, University of Glasgow, 1993.

[86] Fabrice Le Berr, Abdenour Abdelli, D-M Postariu, and R Benlamine. Design and Optimization of Future Hybrid and Electric Propulsion Systems: An Advanced Tool Integrated in a Complete Workflow to Study Electric Devices. *Oil & Gas Science and Technology*, 67(4):547–562, 2012.

[87] T A Burress, C L Coomer, S L Campbell, L E Seiber, L D Marlino, R H Staunton, and J P Cunningham. Evaluation of the 2007 Toyota Camry Hybrid Synergy Drive System.

[88] Timothy A Burress, Steven L Campbell, Chester Coomer, Curtis William Ayers, Andrew A Wereszczak, Joseph Philip Cunningham, Laura D Marlino, Larry Eugene Seiber, and Hua-Tay Lin. Evaluation of the 2010 Toyota Prius Hybrid Synergy Drive System. Technical report, Oak Ridge National Lab.(ORNL), Oak Ridge, TN (United States)., 2011.

[89] Joeri Van Mierlo, Peter Van den Bossche, and Gaston Maggetto. Models of Energy Sources for EV and HEV: Fuel Cells, Batteries, Ultracapacitors, Flywheels and Engine-generators. *Journal of Power Sources*, 128(1):76–89, 2004.

[90] Scott J Moura. *Techniques for Battery Health Conscious Power Management Via Electrochemical Modeling and Optimal Control*. PhD thesis, University of Michigan, 2011.

[91] Scott Jason Moura, Hosam K Fathy, Duncan S Callaway, and Jeffrey L Stein. A Stochastic Optimal Control Approach for Power Management in Plug-in Hybrid Electric Vehicles. *IEEE Transactions on control systems technology*, 19(3):545–555, 2011.

[92] ANDREW Simpson. Cost-benefit Analysis of Plug-in Hybrid electric vehicle technology. In *Presented at the 22nd International Battery, Hybrid and Fuel Cell Electric Vehicle Symposium and Exhibition*, Yokohama, Japan, oct 2006.

[93] Gopalakrishnan Duleep, Huib van Essen, Bettina Kampman, and Max Grünig. Impacts of Electric Eehicles - Deliverable 2, Assessment of Electric Vehicle and Battery Technology. Technical report, CE Delft, ICF, Ecologic, apr 2011.

[94] Aaron David Brooker, Jacob Ward, and Lijuan Wang. Light-weighting Impacts on Fuel Economy, Cost, and Component Losses. Technical report, SAE Technical Paper, 2013.

[95] SE Plotkin, MK Singh, et al. Multi-path Transportation Futures Study: Vehicle Characterization and Scenario Analyses. Technical report, Argonne National Laboratory (ANL), 2009.

[96] Celine Cluzel, Craig Douglas, et al. Cost and Performance of EV Patteries. *Element Energy, Final Report for the Committee on Climate Change*, 2012.

[97] John Maples Maples. Vehicle Choice Modeling and Projections for the Annual Energy Outlook, howpublished = "https://www.eia.gov/outlooks/aeo/pdf/0383(2017).pdf", year = 2013, note = "Accessed 10-June-2018".

[98] Marcello Contestabile, GJ Offer, Raphael Slade, F Jaeger, and M Thoennes. Battery Electric Vehicles, Hydrogen Fuel Cells and Biofuels. Which Will be the Winner? *Energy & Environmental Science*, 4(10):3754–3772, 2011.

[99] McKinsey. Electric Vehicles in Europe: Gearing up for a New Phase? Technical report, Amsterdam Roundtable Foundation and McKinsey & Company., 2014.

[100] Mitra Pourabdollah, Nikolce Murgovski, Anders Grauers, and Bo Egardt. Optimal Sizing of a Parallel PHEV Powertrain. *IEEE Transactions on Vehicular Technology*, 62(6):2469–2480, 2013.

[101] U.S. Department of Transportation, Federal Highway Administration. National Household Travel Survey website. https://www.energy.gov/eere/vehicles/articles/fotw-1046-september-10-2018-average-household-vehicle-was-driven-10200-miles, 2018.

[102] Stefano Lucidi and Francesco Rinaldi. Exact Penalty Functions for Nonlinear Integer Programming Problems. *Journal of optimization theory and applications*, 145(3):479–488, 2010.

[103] Madabhushi Raghavachari. On Connections Between Zero-one Integer Programming and Concave Programming Under Linear Constraints. *Operations Research*, 17(4):680–684, 1969.

[104] Charles D McAllister and Timothy W Simpson. Multidisciplinary Robust Design Optimization of an Internal Combustion Engine. *Journal of mechanical design*, 125(1):124–130, 2003.

[105] C-Y Cynthia Lin and Lea Prince. Gasoline Price Volatility and the Elasticity of Demand for Gasoline. *Energy Economics*, 38:111–117, 2013.

[106] Cheryl D. Fryar, Deanna Kruszon-Moran, Qiuping Gu, and Cynthia L. Ogden. National Health Statistics Report. Technical report, National Center for Health Statistics, Hyattsville, MD, 2018.

[107] Shiva Kumar, P Dinesha, and Marc A Rosen. Effect of Injection Pressure on the Combustion, Performance and Emission Characteristics of a Biodiesel Engine With Cerium Oxide Nanoparticle additive. *Energy*, 185:1163–1173, 2019.